

Syracuse University

SURFACE

Theses - ALL

December 2018

INTERPOLATION AND EXTRAPOLATION OF MISSING ANTENNA MEASUREMENT DATASETS USING THE CAUCHY METHOD AND MATRIX PENCIL METHOD

Nicolas Reginelli
Syracuse University

Follow this and additional works at: <https://surface.syr.edu/thesis>



Part of the [Engineering Commons](#)

Recommended Citation

Reginelli, Nicolas, "INTERPOLATION AND EXTRAPOLATION OF MISSING ANTENNA MEASUREMENT DATASETS USING THE CAUCHY METHOD AND MATRIX PENCIL METHOD" (2018). *Theses - ALL*. 283.
<https://surface.syr.edu/thesis/283>

This is brought to you for free and open access by SURFACE. It has been accepted for inclusion in Theses - ALL by an authorized administrator of SURFACE. For more information, please contact surface@syr.edu.

Abstract

As electromagnetic systems become more complex, the computational time and power required to solve these large problems will also increase. It is thus of practical interest to apply methods of interpolation and extrapolation to reduce the amount of data required for accurate computation. Two such approaches of the implementation of interpolation and extrapolation examined in this thesis are the Cauchy method and the Matrix Pencil method.

This thesis explores the theory, process, and application of the Cauchy method and Matrix Pencil method in interpolating and extrapolating performance metrics of various electromagnetic systems. The Cauchy method begins by assuming that an approximation can be made by a ratio of two polynomials. The two polynomials represent the poles and zeroes of an electromagnetic system in the s -plane. A Total Least Squares (TLS) implementation of the Singular Value Decomposition (SVD) is used to estimate the dimension of the null space and calculate the coefficients of each polynomial. The QR decomposition is added for further computational stability and accuracy. The Matrix Pencil method is a model-based parameter estimation technique that approximates the poles and residues of a system using a sum of complex exponentials.

Four numerical examples will be presented where both techniques are used to interpolate or extrapolate a parameter of interest. The first two examples deal with the approximation of far-field data of a dipole and dipole array. The last two examples showcase these methods in interpolating and extrapolating the near-fields of a parabolic reflector antenna in two different spatial configurations, pointing towards zenith and rotated 90 degrees from zenith. The interpolated/extrapolated near-field will then be transformed to far-field using a spherical near-field to far-field transformation. The results will be evaluated in terms of mean-squared error and compared.

INTERPOLATION AND EXTRAPOLATION OF MISSING ANTENNA MEASUREMENT
DATASETS USING THE CAUCHY METHOD AND MATRIX PENCIL METHOD

By
Nicolas Reginelli
B.S.E.E, Rochester Institute of Technology, 2015

Thesis
Submitted in partial fulfillment of the requirements for the degree of Master of Science in
Electrical Engineering

Syracuse University
December 2018

Copyright © Nicolas Reginelli 2018
All Right Reserved

Acknowledgements

First, I would like to extend great appreciation and thanks to my advisor, Dr. Tapan Sarkar, for his guidance and support throughout my research. He alone has been an excellent resource and has a near endless supply of knowledge and ideas within the field of electrical engineering, especially electromagnetics. I would also like to thank our post-doctoral researcher, Dr. Ming-Da Zhu, for his simulation of the parabolic reflector antenna near-field and far-field that is featured in this thesis, also for his work on the spherical near-field to far-field transformation code, and for auditing my CM and MPM code. In addition, I would like to extend my appreciation for my thesis defense committee, Dr. Jay K. Lee, Harvey Schuman, and Dr. Qi Wang Song, who took time out of their busy schedules to watch my presentation. I would especially like to express great gratitude to my father and step-mother for offering their home to me for the duration of my graduate studies and also for their continued support. I would also like to thank my mother and step-father for their unwavering support and words of encouragement when I needed them the most. Last but certainly not least, I would like to express my appreciation and gratitude for my grandparents who offered their words of wisdom on several occasions and always support me in whatever I do.

Table of Contents

Acknowledgements.....	iv
Table of Contents.....	v
Table of Figures.....	vi
1. Introduction.....	1
2. An Introduction to the SVD and Theory of TLS.....	4
2.1. Singular Value Decomposition.....	5
2.2. The Theory of Total Least Squares.....	8
3. Overview of the Cauchy Method.....	12
3.1. Theory.....	13
3.2. Procedure for Implementing the Cauchy Method.....	19
4. Overview of the Matrix Pencil Method.....	24
4.1. Theory.....	25
4.2. Procedure for Implementing the Matrix Pencil Method.....	29
5. Numerical Results.....	33
5.1. Cauchy Method.....	34
5.1.1. $\lambda/2$ Dipole Antenna.....	34
5.1.2. 10x10 Linear $\lambda/2$ Dipole Array With λ Spacing.....	37
5.1.3. Near-Field to Far-Field Trans. of a Zenith-Directed Reflector Antenna....	48
5.1.4. Near-Field to Far-Field Trans. of a Rotated Reflector Antenna.....	56
5.2. Matrix Pencil Method.....	65
5.2.1. $\lambda/2$ Dipole Antenna.....	65
5.2.2. 10x10 Linear $\lambda/2$ Dipole Array With λ Spacing.....	67
5.2.3. Near-Field to Far-Field Trans. of a Zenith-Directed Reflector Antenna....	72
5.2.4. Near-Field to Far-Field Trans. of a Rotated Reflector Antenna.....	78
6. Conclusion and Future Research.....	85
6.1. Conclusion.....	86
6.2. Future Research.....	88
References.....	89
Curriculum Vitae.....	91

Table of Figures

Figure 3.1: Normalized singular values from SVD of matrix [C].....	20
Figure 3.2: Comparison between generated data and estimated trans. function.....	22
Figure 4.1: Normalized singular values from SVD of matrix [Y].....	30
Figure 4.2: Comparison between original data and estimated data.....	31
Figure 5.1: $\lambda/2$ dipole designed and simulated in HOBBIES.....	34
Figure 5.2: Distribution of normalized singular values of sampled data.....	35
Figure 5.3: Interpolated far-field of dipole using the Cauchy method.....	36
Figure 5.4: 10x10 linear dipole array designed and simulated in HOBBIES.....	37
Figure 5.5: Magnitude of radiated electric field of 10x10 linear dipole array.....	38
Figure 5.6: Distribution of singular values of the real part of the radiated electric field.....	39
Figure 5.7: Interpolated of the real part of the radiated electric field.....	40
Figure 5.8: Distribution of singular values of the imaginary part of the radiated electric field...	41
Figure 5.9: Interpolated of the imaginary part of the radiated electric field.....	42
Figure 5.10: Resulting interpolation of the magnitude of the mirror far-field.....	43
Figure 5.11: Comparison between original and interpolated far-field.....	43
Figure 5.12: Distribution of the singular values for real part of far-field pattern.....	44
Figure 5.13: Extrapolation of the real part of the far-field pattern.....	45
Figure 5.14: Distribution of the singular values for imaginary part of far-field pattern.....	46
Figure 5.15: Extrapolation of the imaginary part of the far-field radiation pattern.....	47
Figure 5.16: Comparison between original and extrapolated far-field.....	47
Figure 5.17: Zenith-directed parabolic reflector with a spherical near-field boundary.....	48
Figure 5.18: Interpolation of the real part of E_θ at $\varphi = 0$ degrees.....	50
Figure 5.19: Interpolation of the imaginary part of E_θ at $\varphi = 0$ degrees.....	50
Figure 5.20: Interpolation of the real part of E_θ at $\varphi = 90$ degrees.....	51
Figure 5.21: Interpolation of the imaginary part of E_θ at $\varphi = 90$ degrees.....	52
Figure 5.22: Interpolation of the real part of E_φ at $\varphi = 0$ degrees.....	53
Figure 5.23: Interpolation of the imaginary part of E_φ at $\varphi = 0$ degrees.....	53

Figure 5.24: Interpolation of the real part of E_φ at $\varphi = 90$ degrees.....	54
Figure 5.25: Interpolation of the imaginary part of E_φ at $\varphi = 90$ degrees.....	55
Figure 5.26: Comparison between original far-field and interpolated far-field.....	56
Figure 5.27: Rotated parabolic reflector antenna.....	57
Figure 5.28: Interpolation of the real part of E_θ at $\varphi = 0$ degrees.....	58
Figure 5.29: Interpolation of the imaginary part of E_θ at $\varphi = 0$ degrees.....	58
Figure 5.30: Interpolation of the real part of E_θ at $\varphi = 90$ degrees.....	60
Figure 5.31: Interpolation of the imaginary part of E_θ at $\varphi = 90$ degrees.....	60
Figure 5.32: Interpolation of the real part of E_φ at $\varphi = 0$ degrees.....	61
Figure 5.33: Interpolation of the imaginary part of E_φ at $\varphi = 0$ degrees.....	62
Figure 5.34: Interpolation of the real part of E_φ at $\varphi = 90$ degrees.....	63
Figure 5.35: Interpolation of the imaginary part of E_φ at $\varphi = 90$ degrees.....	63
Figure 5.36: Comparison between original far-field and interpolated far-field.....	64
Figure 5.37: Distribution of singular values of the input data matrix $[Y]$	66
Figure 5.38: Result of extrapolating far-field of dipole antenna using MPM.....	67
Figure 5.39: Singular value distribution of dipole array.....	68
Figure 5.40: Comparison between original far-field and extrapolated far-field.....	69
Figure 5.41: Comparison between original far-field and extrapolated far-field (dB).....	70
Figure 5.42: Comparison between original far-field and extrapolated far-field.....	71
Figure 5.43: Comparison between original far-field and extrapolated far-field (dB).....	71
Figure 5.44: Extrapolation of the real part of E_θ at $\varphi = 0$ degrees.....	73
Figure 5.45: Extrapolation of the Imaginary part of E_θ at $\varphi = 0$ degrees.....	73
Figure 5.46: Extrapolation of the real part of E_θ at $\varphi = 90$ degrees.....	74
Figure 5.47: Extrapolation of the imaginary part of E_θ at $\varphi = 90$ degrees.....	74
Figure 5.48: Extrapolation of the real part of E_φ at $\varphi = 0$ degrees.....	75
Figure 5.49: Extrapolation of the imaginary part of E_φ at $\varphi = 0$ degrees.....	75
Figure 5.50: Extrapolation of the real part of E_φ at $\varphi = 90$ degrees.....	76
Figure 5.51: Extrapolation of the imaginary part of E_φ at $\varphi = 90$ degrees.....	76
Figure 5.52: Comparison between the original far-field and extrapolated far-field.....	77
Figure 5.53: Extrapolation of the real part of E_θ at $\varphi = 0$ degrees.....	79

Figure 5.54: Extrapolation of the imaginary part of E_θ at $\varphi = 0$ degrees.....	79
Figure 5.55: Extrapolation of the real part of E_θ at $\varphi = 90$ degrees.....	80
Figure 5.56: Extrapolation of the imaginary part of E_θ at $\varphi = 90$ degrees.....	80
Figure 5.57: Extrapolation of the real part of E_φ at $\varphi = 0$ degrees.....	81
Figure 5.58: Extrapolation of the imaginary part of E_φ at $\varphi = 0$ degrees.....	81
Figure 5.59: Extrapolation of the real part of E_φ at $\varphi = 90$ degrees.....	82
Figure 5.60: Extrapolation of the imaginary part of E_φ at $\varphi = 90$ degrees.....	82
Figure 5.61: Comparison between original and extrapolated far-field.....	83

CHAPTER 1
INTRODUCTION

1. Introduction

In electromagnetic analysis the response of a device, such as an antenna or filter, contains many sharp peaks and nulls. The computation of such a response will usually need to be completed by using a fine frequency or angle step. This implies that it will take a large amount of time to accurately compute the response of the device of interest. We of course would then like to reduce this time and computational power while preserving the accuracy of the computation. The scope of this thesis is to introduce methods to reduce the number of frequency points in the case of a filter, or angle points in the case of an antenna. Two different techniques will be proposed in this thesis that can interpolate or extrapolate the response from sparsely sampled data. These two techniques are the Cauchy method and the Matrix Pencil method. The concern of the thesis will primarily be with the interpolation and extrapolation of antenna near-field data. In many real-world scenarios near-field antenna measurements can be difficult to make in certain locations, such as directly underneath or behind the antenna. Many times, the near-field probe is not able to physically reach underneath the antenna therefore making it difficult to accurately measure the near-field radiated over the entire elevation and azimuth. The near-field data is not only important to understand the characteristics of the antenna under test, but it can also be used to construct the far-field radiation pattern using a near-field to far-field transformation [1]. We will specifically be looking at interpolating and extrapolating this “hole” of missing near-field data of a parabolic reflector antenna in two configurations. The first configuration will be with the antenna pointed towards zenith, that is directly above. The second configuration will be with the same antenna rotated counter-clockwise 90 degrees.

The Cauchy method interpolates/extrapolates data by a ratio of two polynomials. This concept is expanded to interpolate or extrapolate a gap in antenna measurement data using the

available sampled data. Once the coefficients of the polynomials are determined from the sampled data, the response of interest can be interpolated or extrapolated at other angles of interest. A Total Least Squares (TLS) based implementation of the Singular Value Decomposition (SVD) technique will be used to determine the coefficients of the polynomials. The QR decomposition will also be added before applying the SVD to increase the accuracy and numerical stability of the computation.

The Matrix Pencil method is a model-based parameter estimation technique that interpolates and extrapolates sampled data using estimated residues and poles of an exponential signal model. Once the residues and poles are determined from the sampled data, the antenna near-field radiation pattern can be interpolated or extrapolated as a function of theta.

CHAPTER 2

AN INTRODUCTION TO THE SINGULAR VALUE DECOMPOSITION AND THE THEORY OF TOTAL LEAST SQUARES

2. An Introduction to the SVD and the Theory of TLS

2.1 Singular Value Decomposition

First, we will introduce a critical component in solving a Total Least Squares problem called the Singular Value Decomposition (SVD). The singular value decomposition is one of the most important concepts in linear algebra [2]. To start, we first need to understand what eigenvectors and eigenvalues are as related to a dynamic system. If we multiply a vector \mathbf{x} by a matrix $[A]$, we will get a new vector, $A\mathbf{x}$. (2.1) below shows the simple equation relating a matrix $[A]$ and an eigenvector \mathbf{x} to an eigenvalue (just a number) and the original \mathbf{x} .

$$A\mathbf{x} = \lambda\mathbf{x} \quad (2.1)$$

$[A]$ is assumed to be a square matrix, \mathbf{x} is the eigenvector, and λ is a value called the eigenvalue. Normally when any vector \mathbf{x} is multiplied by any matrix $[A]$ a new vector results with components pointing in different directions than the original \mathbf{x} . However, eigenvectors are special vectors that come out in the same direction even after they are multiplied by the matrix $[A]$. From (2.1) we can see that when you multiply an eigenvector by $[A]$, the new vector $A\mathbf{x}$ is just the eigenvalue λ times the original \mathbf{x} . This eigenvalue determines whether the vector \mathbf{x} is shrunk, stretched, reversed, or unchanged. Eigenvectors and eigenvalues play crucial roles in linear algebra ranging from simplifying matrix algebra such as taking the 500th power of $[A]$ to solving differential equations. To take the 500th power of $[A]$, one only needs to find the eigenvalues and eigenvectors of $[A]$ and take the 500th power of the eigenvalues. The eigenvectors will not change direction and the multiplication of the 500th power of the eigenvalues and the eigenvectors will result in $[A]^{500}$. As we will see in later sections, the

eigenvalues can also provide important parameters of a system transfer function such as the poles.

One way to characterize and extract the eigenvalues of a matrix $[A]$ is to diagonalize it. Diagonalizing a matrix not only provides a quick way to extract eigenvalues but important parameters such as the rank and dimension of a matrix can be found easily once a matrix is diagonalized. To diagonalize matrix $[A]$, the eigenvalues of $[A]$ must first be placed in a diagonal matrix, $[\Lambda]$. This is completed by forming an eigenvector matrix $[S]$ with the eigenvectors of $[A]$ put into the columns of $[S]$ and multiplying as such

$$[S]^{-1}[A][S] = [\Lambda] = \begin{bmatrix} \lambda_1 & & \\ & \ddots & \\ & & \lambda_n \end{bmatrix} \quad (2.2)$$

(2.2) can be rearranged and $[A]$ can also be written as

$$[A] = [S][\Lambda][S]^{-1} \quad (2.3)$$

We start to encounter problems when matrices are not only square but also rectangular. Previously we assumed that $[A]$ was an n by n square matrix. Now we will assume $[A]$ is any m by n rectangular matrix. We would still like to simplify the matrix or “diagonalize” it but using $[S]^{-1}[A][S]$ is no longer ideal for a few reasons; the eigenvectors of $[S]$ are not always orthogonal, there are sometimes not enough eigenvectors, and using $Ax = \lambda x$ requires $[A]$ to be a square matrix. However, this problem can be solved with the singular value decomposition but of course at a cost. The SVD of $[A]$ results in the following

$$[A]_{(m \times n)} = [U][\Sigma][V]^T = \begin{bmatrix} \mathbf{u}_1 & \cdots & \mathbf{u}_r \end{bmatrix}_{(m \times r)} \begin{bmatrix} \sigma_1 & & \\ & \ddots & \\ & & \sigma_r \end{bmatrix}_{(r \times r)} \begin{bmatrix} \mathbf{v}_1 & \cdots & \mathbf{v}_r \end{bmatrix}_{(n \times r)} \quad (2.4)$$

where m is the number of rows of $[A]$, n is the number of columns of $[A]$, and r is the rank of $[A]$. The SVD of $[A]$, which can now be rectangular or square, will have two sets of singular vectors, \mathbf{u} 's and \mathbf{v} 's. The \mathbf{u} 's are the eigenvectors of $[A][A]^T$ and the \mathbf{v} 's are the eigenvectors of $[A]^T[A]$. $[U]$ and $[V]$ are also unitary matrices which means that $[U]^T[U] = I$ and $[V]^T[V] = I$. In other words, they are orthogonal. The σ 's are the singular values which also so happen to be the square roots of the eigenvalues of both $[A][A]^T$ and $[A]^T[A]$. We are not totally finished however because $[U]$ and $[V]$ are not square matrices. While (2.4) is the diagonalization of $[A]$, the matrix equation is technically not valid since we cannot multiply these rectangular matrices of different sizes. To make them square we will need $n - r$ more \mathbf{v} 's and $m - r$ more \mathbf{u} 's. We can get these required \mathbf{u} 's and \mathbf{v} 's from the nullspace $N(A)$ and the left nullspace $N(A^T)$. Once the new \mathbf{u} 's and \mathbf{v} 's are added, the matrices are square and $[A]$ will still equal $[U][\Sigma][V]^T$. The true SVD of $[A]$ will now be

$$[A]_{(m \times n)} = [U]_{(m \times m)}[\Sigma]_{(m \times n)}[V]^T_{(n \times n)} = \begin{bmatrix} \mathbf{u}_1 & \cdots & \mathbf{u}_r & \cdots & \mathbf{u}_m \end{bmatrix}_{(m \times m)} \begin{bmatrix} \sigma_1 & & & & \\ & \ddots & & & \\ & & \sigma_r & & \\ & & & 0 & \\ & & & & 0 \end{bmatrix}_{(m \times n)} \begin{bmatrix} \mathbf{v}_1 & \cdots & \mathbf{v}_r & \cdots & \mathbf{v}_n \end{bmatrix}_{(n \times n)} \quad (2.5)$$

The new singular value matrix $[\Sigma]$ is the same matrix as the old $r \times r$ matrix but with $m - r$ new zero rows and $n - r$ new zero columns added. The theory of total least squares (TLS) heavily utilizes the SVD as will be seen in the next section.

2.2 The Theory of Total Least Squares

The method of total least squares (TLS) is a linear parameter estimation technique and is used in wide variety of disciplines such as signal processing, general engineering, statistics, physics, etc. We start out with a set of m measured data points $\{(x_1, y_1), \dots, (x_m, y_m)\}$, and a set of n linear coefficients (a_1, \dots, a_n) that describe a model, $\hat{y}(x; a)$ where $m > n$ [3]. The objective of total least squares is to find the linear coefficients that best approximate the model in the scenario that there is missing data or errors in the measurements. We can describe the approximation by a simple linear expression

$$y \approx Xa \quad (2.5)$$

Since $m > n$, there are more equations than unknowns and therefore (2.5) has an overdetermined set of equations. The best approximation according to total least squares minimizes the norm of the difference between the approximated data and the model $\hat{y}(x; a)$ as well as the independent variables X . Considering the errors of the measured data vector, y , and the independent variables, X , (2.5) can be re-written as

$$y + \tilde{y} = [X + \tilde{X}]a \quad (2.6)$$

where \tilde{y} and \tilde{X} are the errors in both the dependent variable measurements and independent variable measurements, respectively. We then want to approximate in a way that minimizes these errors in the dependent and independent variables. This can be expressed by,

$$\min \|[\tilde{X} \ \tilde{y}]\|_F^2 \quad (2.7)$$

where $[\tilde{X} \ \tilde{y}]$ is an augmented matrix with the columns of error matrix \tilde{X} concatenated with the error vector \tilde{y} . The operator $\|\bullet\|_F$ represents the Frobenius norm of the augmented matrix. The

Frobenius norm is defined as the square root of the sum of the absolute squares of all of the elements in a matrix. This can be expressed in equation form as the following, where A is any matrix,

$$\|A\|_F^2 = \sum_{i=1}^m \sum_{j=1}^n A_{ij}^2 = \text{trace}(A^T A) = \sum_{i=1}^n \sigma_i^2 \quad (2.8)$$

and where σ_i is the i -th singular value of matrix A .

We will now bring the right-hand side of (2.6) over to the left side of the equation and equate it to zero as such

$$[X + \tilde{X}; \quad y + \tilde{y}] \begin{bmatrix} a \\ -1 \end{bmatrix} = 0 \quad (2.9)$$

If the concatenated matrix $[X \ y]$ has a rank of $n + 1$, the $n + 1$ columns of the matrix are linearly independent and the $n + 1$, m -dimensional columns of the matrix span the same n -dimensional space as X . In order to have a unique solution for the coefficients, a , the matrix $[X + \tilde{X}; \ y + \tilde{y}]$ must have n linearly independent columns. However, this matrix has $n + 1$ columns in total and therefore is rank deficient by 1. We then must find the smallest matrix $[\tilde{X} \ \tilde{y}]$ that changes matrix $[X \ y]$ with a rank of $n + 1$, to a matrix $\{[X \ y] + [\tilde{X} \ \tilde{y}]\}$ with rank n . According to the Eckart-Young theorem we can achieve this by defining $\{[X \ y] + [\tilde{X} \ \tilde{y}]\}$ as the best rank- n approximation to $[X \ y]$ and by eliminating the last singular value of $[X \ y]$ which contains the least amount of system information and provides a unique solution.

First, we will take the SVD of $[X \ y]$ as follows

$$[X \ y] = [U_x \quad u_y] \begin{bmatrix} \Sigma_x & \\ & \sigma_y \end{bmatrix} \begin{bmatrix} V_{xx} & v_{xy} \\ v_{yx} & v_{yy} \end{bmatrix}^T \quad (2.10)$$

where U_x has n columns, u_y is a column vector, Σ_x contains the n largest singular values diagonally, σ_y is the smallest singular value, V_{xx} is a $n \times n$ matrix, and v_{yy} is scalar. Let us multiple both sides by matrix V .

$$[X \quad y] \begin{bmatrix} V_{xx} & v_{xy} \\ v_{yx} & v_{yy} \end{bmatrix} = [U_x \quad u_y] \begin{bmatrix} \Sigma_x & \\ & \sigma_y \end{bmatrix} \quad (2.11)$$

Next, we will equate just the last columns of the matrix multiplication occurring in (2.11).

$$[X \quad y] \begin{bmatrix} v_{xy} \\ v_{yy} \end{bmatrix} = u_y \sigma_y \quad (2.12)$$

From the Eckart-Young theorem, we know that $\{[X \quad y] + [\tilde{X} \quad \tilde{y}]\}$ is the closest rank- n approximation to $[X \quad y]$. Matrix $\{[X \quad y] + [\tilde{X} \quad \tilde{y}]\}$ has the same singular values contained in Σ_x above with σ_y equal to zero. We can then write the SVD of $\{[X \quad y] + [\tilde{X} \quad \tilde{y}]\}$ as such

$$[X + \tilde{X}; \quad y + \tilde{y}] = [U_x \quad u_y] \begin{bmatrix} \Sigma_x & \\ & 0 \end{bmatrix} \begin{bmatrix} V_{xx} & v_{xy} \\ v_{yx} & v_{yy} \end{bmatrix}^T \quad (2.13)$$

To obtain $[\tilde{X} \quad \tilde{y}]$ we must solve the following

$$[\tilde{X} \quad \tilde{y}] = [X \quad y] + [\tilde{X} \quad \tilde{y}] - [X \quad y] \quad (2.14)$$

(2.14) can be solved by first using (2.10) and (2.13) which results in

$$\begin{aligned} [\tilde{X} \quad \tilde{y}] &= -[U_x \quad u_y] \begin{bmatrix} 0 & \\ & \sigma_y \end{bmatrix} \begin{bmatrix} V_{xx} & v_{xy} \\ v_{yx} & v_{yy} \end{bmatrix}^T \\ &= -[0 \quad u_y \sigma_y] \begin{bmatrix} V_{xx} & v_{xy} \\ v_{yx} & v_{yy} \end{bmatrix}^T \\ &= -u_y \sigma_y \begin{bmatrix} v_{xy} \\ v_{yy} \end{bmatrix}^T \end{aligned} \quad (2.15)$$

Then, from (2.12) we can rewrite (2.15) as

$$[\tilde{X} \quad \tilde{y}] = -[X \quad y] \begin{bmatrix} v_{xy} \\ v_{yy} \end{bmatrix} \begin{bmatrix} v_{xy} \\ v_{yy} \end{bmatrix}^T \quad (2.16)$$

Finally, $\{[X \quad y] + [\tilde{X} \quad \tilde{y}]\}$ can be defined as

$$[X + \tilde{X}; \quad y + \tilde{y}] = [X \quad y] - [X \quad y] \begin{bmatrix} v_{xy} \\ v_{yy} \end{bmatrix} \begin{bmatrix} v_{xy} \\ v_{yy} \end{bmatrix}^T \quad (2.17)$$

After multiplying each term in (2.17) by $\begin{bmatrix} v_{xy} \\ v_{yy} \end{bmatrix}$ we get the following

$$[X + \tilde{X}; \quad y + \tilde{y}] \begin{bmatrix} v_{xy} \\ v_{yy} \end{bmatrix} = [X \quad y] \begin{bmatrix} v_{xy} \\ v_{yy} \end{bmatrix} - [X \quad y] \begin{bmatrix} v_{xy} \\ v_{yy} \end{bmatrix} \quad (2.18)$$

The right-hand side cancels and we are left with

$$[X + \tilde{X}; \quad y + \tilde{y}] \begin{bmatrix} v_{xy} \\ v_{yy} \end{bmatrix} = 0 \quad (2.19)$$

From (2.9) and (2.19) we can solve for the model coefficient a .

$$a = -v_{xy}v_{yy}^{-1} \quad (2.20)$$

The vector v_{xy} is the first n elements of the $n + 1$ -th columns of the right singular matrix V , of $[X \quad y]$ and v_{yy} is the $n + 1$ -th element of the $n + 1$ columns of V . The best approximation of the model is then given by

$$\hat{y} = [X + \tilde{X}]a \quad (2.21)$$

CHAPTER 3

OVERVIEW OF THE CAUCHY METHOD

3. Overview of the Cauchy Method

3.1 Theory

The Cauchy method starts by assuming that a parameter of interest can be interpolated or extrapolated by a ratio of two polynomials [4]. For electromagnetic systems, this means that narrow-band data can be sampled and interpolated or extrapolated to obtain the wide-band response [5]-[9]. This is particularly useful in simulation where fast numerical computation time is desired without compromising accuracy. A few parameters of interest that may be interpolated or extrapolated using the Cauchy method include input impedance, currents, scattering data, and radiation patterns. The only requirement for the electromagnetic system being approximated is that it is a Linear Time Invariant (LTI) system.

As we know, the Cauchy method assumes that the system of interest that is to be interpolated or extrapolated can be performed using a ratio of two polynomials. We also must assume that the EM system has a system response that is LTI [10]. The transfer function, $H(f)$ of any LTI system as a function of frequency can be written as

$$H(f_i) \approx \frac{A(f_i)}{B(f_i)} = \frac{\sum_{k=0}^P a_k f_i^k}{\sum_{k=0}^Q b_k f_i^k}, \quad i = 1, 2, \dots, N \quad (3.1)$$

The numerator and denominator polynomials are given by $A(f_i)$ and $B(f_i)$ respectively. The zeroes and poles are contained within these polynomials. One novelty of this thesis is the application of the Cauchy method to antenna near-field and far-field patterns. For this case, the system transfer function is no longer a function of frequency but of space, particularly of the angle theta or phi depending on the cut of the radiation pattern. Therefore, the transfer function in 2.1 can be re-written as

$$H(\sin \theta) \approx \frac{A(\sin \theta)}{B(\sin \theta)} = \frac{\sum_{k=0}^P a_k \sin \theta_i^k}{\sum_{k=0}^Q b_k \sin \theta_i^k}, \quad i = 1, 2, \dots, N \quad (3.2)$$

For the approximation, P is the order of the numerator polynomial and Q is the order of the denominator polynomial. An initial “guess” must be made for the orders, P and Q . The initial guess of P is given by

$$P = \frac{N-3}{2} \quad (3.3)$$

Q is then found by the following assumption

$$Q = P + 1 \quad (3.4)$$

Rearranging (3.2) will result in the following

$$\sum_{k=0}^Q b_k \sin \theta_i^k H(\sin \theta_i) = \sum_{k=0}^P a_k \sin \theta_i^k, \quad i = 1, 2, \dots, N \quad (3.5)$$

From (3.1) or (3.2) depending on whether the system is frequency or space dependent, and from (3.5) the coefficients a_k and b_k are placed into column vector format, the polynomials A and B are put into matrix form and a matrix equation can be created as such

$$[A]_{Nx(P+1)} a_{(P+1) \times 1} = [B]_{Nx(Q+1)} b_{(Q+1) \times 1} \quad (3.6)$$

We can simplify (3.6) by moving the matrix $[B]$ and the vector b over to the left-hand side. This essentially creates a null space problem where the left-hand side of the equation is equal to zero and to solve for the coefficients a and b , one must solve for the null space of the system (i.e. $Ax = 0$). (3.6) then becomes

$$[A \quad -B]_{Nx(P+Q+2)} \begin{bmatrix} a \\ b \end{bmatrix}_{(P+Q+2) \times 1} = 0 \quad (3.7)$$

For conciseness and to simplify (3.7) even further, a new matrix C can be set equal to an augmented matrix containing A and B and (3.6) can be re-written as

$$[C]_{Nx(P+Q+2)} \begin{bmatrix} a \\ b \end{bmatrix}_{(P+Q+2) \times 1} = 0 \quad (3.8)$$

Where the vectors a and b are

$$[a] = [a_0, a_1, a_2, \dots, a_P]^T \quad (3.9)$$

$$[b] = [b_0, b_1, b_2, \dots, b_Q]^T \quad (3.10)$$

Note that $[a]$ and $[b]$ are written as transposed column vectors, denoted by the superscript T, instead of regular column vectors. The matrix $[C]$ can be represented by the following

$$[C] = \begin{bmatrix} \boxed{1 \quad \sin \theta_1 \quad \cdots \quad (\sin \theta_1)^P} & \boxed{-H(\sin \theta_1) \quad -H(\sin \theta_1) \sin \theta_1 \quad \cdots \quad -H(\sin \theta_1)(\sin \theta_1)^Q} \\ \boxed{1 \quad \sin \theta_2 \quad \cdots \quad (\sin \theta_2)^P} & \boxed{-H(\sin \theta_2) \quad -H(\sin \theta_2) \sin \theta_2 \quad \cdots \quad -H(\sin \theta_2)(\sin \theta_2)^Q} \\ \vdots & \vdots \\ \boxed{1 \quad \sin \theta_N \quad \cdots \quad (\sin \theta_N)^P} & \boxed{-H(\sin \theta_N) \quad -H(\sin \theta_N) \sin \theta_N \quad \cdots \quad -H(\sin \theta_N)(\sin \theta_N)^Q} \end{bmatrix} \quad (3.11)$$

[A] [B]

Matrix $[C]$ has a size of $N \times (P+Q+2)$. The solution to the coefficients $[a]$ and $[b]$ are unique only if the total number of sample points N , are greater than or equal to the number of unknown coefficients. This can be summarized as such

$$N \geq P + Q + 2 \quad (3.12)$$

To obtain a better estimate for the required values of the orders P and Q , the singular value decomposition (SVD) [11] of matrix $[C]$ must be computed. The SVD of $[C]$ will result in the following

$$[U][\Sigma][V]^H \begin{bmatrix} a \\ b \end{bmatrix} = 0 \quad (3.13)$$

The matrix $[\Sigma]$ is a diagonal matrix and contains the singular values of the matrix $[C]$ in descending order.

$$\Sigma = \begin{bmatrix} \sigma_1 & & & & & \\ & \sigma_2 & & & & \\ & & \ddots & & & \\ & & & \sigma_R & & \\ & & & & 0 & \\ & & & & & \ddots \end{bmatrix}, \quad \sigma_1 \geq \sigma_2 \geq \cdots \sigma_R \geq 0 \quad (3.14)$$

Matrices $[U]$ and $[V]$ are both unitary matrixes where when multiplied by their Hermitian transpose, denoted by superscript H , are equal to the identity matrix $[I]$.

$$[U]^H[U] = [I] \quad (3.15)$$

$$[V]^H[V] = [I] \quad (3.16)$$

The columns of matrix $[U]$ are the left singular vectors of the matrix $[C]$ and the eigenvectors of the matrix $[C][C]^H$. The columns of matrix $[V]$ are the right singular vectors of the matrix $[C]$ and the eigenvectors of the matrix $[C]^H[C]$. The singular values contained in $[\Sigma]$ are the square roots of the eigenvalues of the matrix $[C]^H[C]$. Therefore, the singular values of any matrix must be real and positive. The number of nonzero singular values are eventually used to estimate the order of the approximation. They also contain the information content of the system transfer function $H(\sin\theta)$. The rank (R) of matrix $[C]$ corresponds to the number of nonzero singular values of the matrix.

To validate the approximation and to properly estimate the rank of matrix $[C]$ and therefore the order of the numerator and denominator polynomials, the smallest singular value must be less than or equal to the number of accurate significant digits. The orders P and Q can be estimated by normalizing each singular value to the largest singular value like so [12]

$$\frac{\sigma_R}{\sigma_{max}} \approx 10^{-w} \quad (3.17)$$

where w is equal to the number of accurate significant digits (i.e. using double precision, w would equal 16). To make the data interpretation of the singular values simple, one can convert (3.17) into the dB scale as shown in the equation below

$$10 * \log_{10} \left(\frac{\sigma_R}{\sigma_{max}} \right) (dB) \approx -10w (dB) \quad (3.18)$$

So, for example if we are dealing with double precision data, the number of singular values less than or equal to -160 dB will equal the rank (R) of the matrix $[C]$. From the rank (R) of the matrix $[C]$, the orders P and Q can be better estimated in the presence of additive noise which could corrupt the data. Since we know that the rank (R) is equal to the number of non-zero singular values, the dimension of the right null space of $[C]$ is equal to $P+Q+2-R$. We also know that the solution vector belongs to this null space so to make the solution unique, the dimension of this null

space must be set to one so that only one vector defines this space. Therefore, P and Q must satisfy the following relationship

$$1 = P + Q + 2 - R \quad (3.19)$$

$$R + 1 = P + Q + 2 \quad (3.20)$$

Since $Q = P + 1$, we can estimate the order P by the following

$$R + 1 = 2P + 3 \quad (3.21)$$

$$P = \frac{R-2}{2} \quad (3.22)$$

(3.20) and (3.22) provide better estimates for the parameters P and Q . Once P and Q are known, the matrix $[C]$ can be regenerated using (3.11), and then (3.8) essentially becomes a system of simultaneous equations. Setting P and Q to the new estimates of the numerator and denominator polynomial orders respectively, the newly re-formed matrix $[C]$ results in the following

$$[C]_{N \times (P+Q+2)} \begin{bmatrix} a \\ b \end{bmatrix}_{(P+Q+2) \times 1} = [A \quad -B]_{N \times (P+Q+2)} \begin{bmatrix} a \\ b \end{bmatrix}_{(P+Q+2) \times 1} = 0 \quad (3.23)$$

Matrix $[C]$ is a rectangular matrix that must have more rows than columns to satisfy (3.12).

The equation in (3.23) can be solved by the way of the total least squares (TLS) method [3]. Submatrix $[A]$ in (3.23) is a function of space only and is therefore not corrupted by the measurement data in submatrix $[B]$. Submatrix $[B]$ contains the sampled data, $H(\sin\theta)$, of the system measured and can be affected by any measurement or computational errors in the evaluation of the transfer function. Since there is some noise non-uniformity in matrix $[C]$, a QR decomposition [8] must be performed up to the first $P+1$ columns of matrix $[C]$. In other words, the QR decomposition is only computed on submatrix $[A]$. This prevents any noise due to measurement and computation error from propagating through the computations and further corrupting the interpolation or extrapolation. A QR decomposition on submatrix $[A]$ results in the following

$$[A] = [Q][R] \quad (3.24)$$

The matrix $[Q]$ is a n-by-n orthogonal matrix and matrix $[R]$ is a n-by-m upper triangular matrix.

Applying (3.24) to (3.23) results in the following

$$[A \quad -B] = [Q]^T [A \quad -B] = [R \quad -Q^T B] \quad (3.25)$$

$$[R \quad -Q^T B] \begin{bmatrix} a \\ b \end{bmatrix} = \begin{bmatrix} R_{11} & R_{12} \\ 0 & R_{22} \end{bmatrix} \begin{bmatrix} a \\ b \end{bmatrix} = 0 \quad (3.26)$$

Submatrix $[R_{11}]$ is an upper triangular matrix containing only values resulting in the matrix multiplication of $[Q]^T$ and $[A]$. Submatrices $[R_{12}]$ and $[R_{22}]$ contain values resulting in the matrix multiplication of $-[Q]^T$ and $[B]$ so therefore they are affected by any noise resulting from measurement or computational error. From (3.26) we can apply matrix multiplication and form the following equations to solve for coefficients a and b , and then compute the resulting polynomials to complete the interpolation or extrapolation.

$$[R_{11}][a] + [R_{12}][b] = 0 \quad (3.27)$$

$$[R_{22}][b] = 0 \quad (3.28)$$

To solve for $[b]$ in (3.28), the SVD must be applied to submatrix $[R_{22}]$ which results in

$$[U'][\Sigma'][V']^H [b] = 0 \quad (3.29)$$

By the theory of Total Least Squares, the solution vector $[b]$ is proportional to the last column of the matrix $[V']$ in (3.29), as shown below

$$[b] = [V']_{q+1} \quad (3.30)$$

Once the values of b are found, (3.27) can be rearranged to solve for a .

$$[a] = -[R_{11}]^{-1}[R_{12}][b] \quad (3.31)$$

With the coefficients a and b determined, the optimal solution of the numerator and denominator polynomials is found. Using (3.30) and (3.31) one can interpolate or extrapolate the

system response from the numerator and denominator polynomials. The transfer function $H(\sin\theta)$ can be rewritten using the newly computed coefficients as such

$$H(\sin\theta) \approx \frac{A(\sin\theta)}{B(\sin\theta)} = \frac{\sum_{k=0}^P a_k \sin^k \theta}{\sum_{k=0}^Q b_k \sin^k \theta} \approx \sum_{m=1}^M \left(\frac{R_m}{f - \left(\frac{\sigma_m}{j2\pi} + f_m\right)} + \frac{R_m^*}{f - \left(\frac{\sigma_m}{j2\pi} - f_m\right)} \right) \quad (3.32)$$

where R_m is the residue, R_m^* is the complex conjugate of R_m , σ_m is the damping factor, and f_m is the natural frequency of the m th pole.

3.2 Procedure for Implementing the Cauchy Method

The process of implementing the Cauchy method is quite straight forward. We will illustrate the procedure using a simple example. We will first generate a system transfer function $H(u)$ using a ratio of two polynomials as shown below.

$$H(u) = \frac{5u^2 + 7u + 33}{5u^3 - 2u^2 - 16u - 15} \quad (3.33)$$

Where u is equal to $\sin(\theta)$ and θ is varied from -90 degrees to +90 degrees. In total, 181 samples of u and $H(u)$ are taken. The following example will outline the process of extrapolating the above transfer function by the Cauchy method using only a few samples.

Step 1. The first step is to choose the samples of u and $H(u)$ that will be used for the extrapolation. We will choose 9 samples among the 181 total samples so $N=9$ as such:

$$u = -1, -0.9925, -0.9703, -0.9336, -0.8829, -0.8129, -0.7431, -0.6561, -0.5592$$

$$H(u) = -5.1667, -5.1815, -5.2171, -5.2471, -5.2296, -5.1172, -4.8768, -4.5101, -4.0581$$

Step 2. Next, the optimal orders of the numerator and denominator polynomials must be determined. The order of the numerator polynomials, P , is determined to be 3 by using (3.22). Q is therefore equal to 4 since Q is equal to $P+1$. We can now generate the matrix $[C]$ from (3.11).

$[C] =$	<table style="border-collapse: collapse; width: 100%; text-align: center;"> <tr><td style="border: none;">1</td><td style="border: none;">-1</td><td style="border: none;">1</td><td style="border: none;">-1</td></tr> <tr><td style="border: none;">1</td><td style="border: none;">-0.9925</td><td style="border: none;">0.9851</td><td style="border: none;">-0.9778</td></tr> <tr><td style="border: none;">1</td><td style="border: none;">-0.9703</td><td style="border: none;">0.9415</td><td style="border: none;">-0.9135</td></tr> <tr><td style="border: none;">1</td><td style="border: none;">-0.9336</td><td style="border: none;">0.8716</td><td style="border: none;">-0.8137</td></tr> <tr><td style="border: none;">1</td><td style="border: none;">-0.8829</td><td style="border: none;">0.7796</td><td style="border: none;">-0.6883</td></tr> <tr><td style="border: none;">1</td><td style="border: none;">-0.8192</td><td style="border: none;">0.6710</td><td style="border: none;">-0.5497</td></tr> <tr><td style="border: none;">1</td><td style="border: none;">-0.7431</td><td style="border: none;">0.5523</td><td style="border: none;">-0.4104</td></tr> <tr><td style="border: none;">1</td><td style="border: none;">-0.6561</td><td style="border: none;">0.4304</td><td style="border: none;">-0.2824</td></tr> <tr><td style="border: none;">1</td><td style="border: none;">-0.5592</td><td style="border: none;">0.3127</td><td style="border: none;">-0.1749</td></tr> </table>	1	-1	1	-1	1	-0.9925	0.9851	-0.9778	1	-0.9703	0.9415	-0.9135	1	-0.9336	0.8716	-0.8137	1	-0.8829	0.7796	-0.6883	1	-0.8192	0.6710	-0.5497	1	-0.7431	0.5523	-0.4104	1	-0.6561	0.4304	-0.2824	1	-0.5592	0.3127	-0.1749	<table style="border-collapse: collapse; width: 100%; text-align: center;"> <tr><td style="border: none;">5.1667</td><td style="border: none;">-5.1667</td><td style="border: none;">5.1667</td><td style="border: none;">-5.1667</td><td style="border: none;">5.1667</td></tr> <tr><td style="border: none;">5.1815</td><td style="border: none;">-5.1429</td><td style="border: none;">5.1045</td><td style="border: none;">-5.0665</td><td style="border: none;">5.0287</td></tr> <tr><td style="border: none;">5.2171</td><td style="border: none;">-5.0621</td><td style="border: none;">4.9118</td><td style="border: none;">-4.7659</td><td style="border: none;">4.6243</td></tr> <tr><td style="border: none;">5.2471</td><td style="border: none;">-4.8986</td><td style="border: none;">4.5732</td><td style="border: none;">-4.2695</td><td style="border: none;">3.9859</td></tr> <tr><td style="border: none;">5.2296</td><td style="border: none;">-4.6175</td><td style="border: none;">4.0770</td><td style="border: none;">-3.5998</td><td style="border: none;">3.1784</td></tr> <tr><td style="border: none;">5.1172</td><td style="border: none;">-4.1918</td><td style="border: none;">3.4337</td><td style="border: none;">-2.8127</td><td style="border: none;">2.3041</td></tr> <tr><td style="border: none;">4.8768</td><td style="border: none;">-3.6242</td><td style="border: none;">2.6933</td><td style="border: none;">-2.0015</td><td style="border: none;">1.4874</td></tr> <tr><td style="border: none;">4.5101</td><td style="border: none;">-2.9589</td><td style="border: none;">1.9412</td><td style="border: none;">-1.2736</td><td style="border: none;">0.8355</td></tr> <tr><td style="border: none;">4.0581</td><td style="border: none;">-2.2693</td><td style="border: none;">1.2690</td><td style="border: none;">-0.7096</td><td style="border: none;">0.3968</td></tr> </table>	5.1667	-5.1667	5.1667	-5.1667	5.1667	5.1815	-5.1429	5.1045	-5.0665	5.0287	5.2171	-5.0621	4.9118	-4.7659	4.6243	5.2471	-4.8986	4.5732	-4.2695	3.9859	5.2296	-4.6175	4.0770	-3.5998	3.1784	5.1172	-4.1918	3.4337	-2.8127	2.3041	4.8768	-3.6242	2.6933	-2.0015	1.4874	4.5101	-2.9589	1.9412	-1.2736	0.8355	4.0581	-2.2693	1.2690	-0.7096	0.3968	(9x9)
1	-1	1	-1																																																																																	
1	-0.9925	0.9851	-0.9778																																																																																	
1	-0.9703	0.9415	-0.9135																																																																																	
1	-0.9336	0.8716	-0.8137																																																																																	
1	-0.8829	0.7796	-0.6883																																																																																	
1	-0.8192	0.6710	-0.5497																																																																																	
1	-0.7431	0.5523	-0.4104																																																																																	
1	-0.6561	0.4304	-0.2824																																																																																	
1	-0.5592	0.3127	-0.1749																																																																																	
5.1667	-5.1667	5.1667	-5.1667	5.1667																																																																																
5.1815	-5.1429	5.1045	-5.0665	5.0287																																																																																
5.2171	-5.0621	4.9118	-4.7659	4.6243																																																																																
5.2471	-4.8986	4.5732	-4.2695	3.9859																																																																																
5.2296	-4.6175	4.0770	-3.5998	3.1784																																																																																
5.1172	-4.1918	3.4337	-2.8127	2.3041																																																																																
4.8768	-3.6242	2.6933	-2.0015	1.4874																																																																																
4.5101	-2.9589	1.9412	-1.2736	0.8355																																																																																
4.0581	-2.2693	1.2690	-0.7096	0.3968																																																																																
	Matrix [A]	Matrix [B]																																																																																		

The size of matrix $[C]$ is $N \times (P+Q+2)$ so 9×9 in this example. To reduce the size of matrix $[C]$ and find the optimal values of P and Q , the SVD of $[C]$ is taken. Figure 3.1 shows the normalized singular values in dB scale from the SVD of matrix $[C]$.

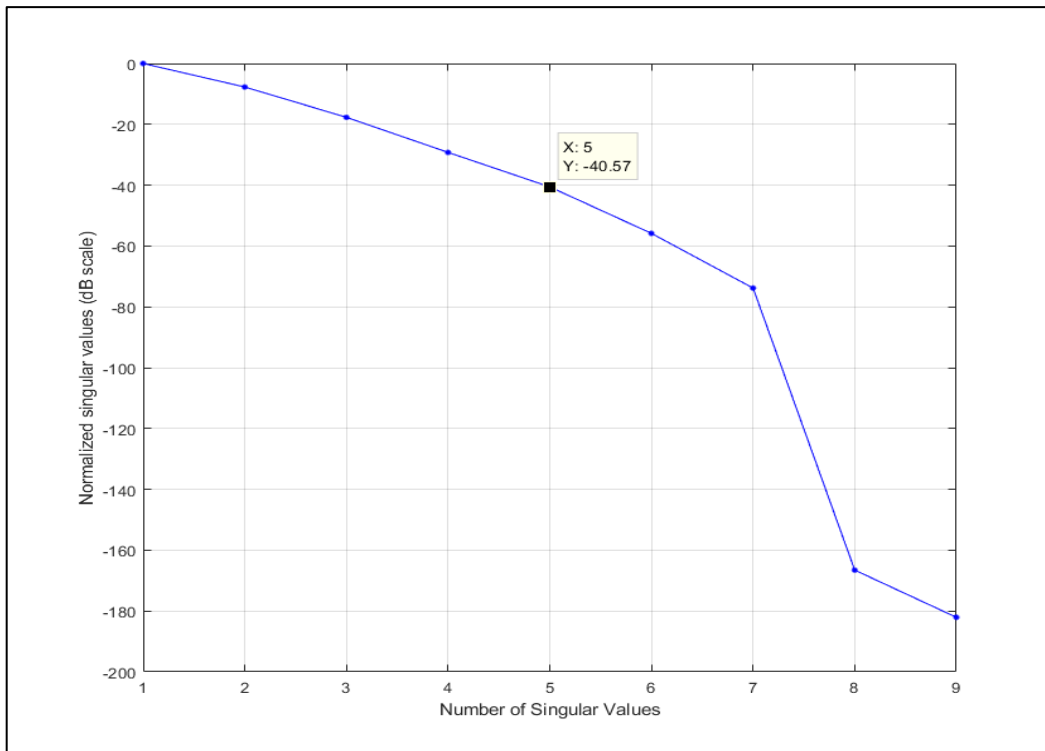


Figure 3.1. Normalized singular values from SVD of matrix $[C]$

Since the number of accurate significant digits used for this example is 5, the equivalent number of normalized singular values should be less than or equal to -50 dB. The number of singular values that are less than or equal to -50 dB is equal to 5 and therefore the optimal rank (R) of the

matrix $[C]$ is also equal to 5. We then use (3.22) to calculate the new value of the numerator order P . The new value of P is calculated to be 2 by rounding up to the nearest integer. The new optimal value of Q is then calculated to be 3.

Step 3. Matrix $[C]$ can now be regenerated with the new optimal orders of P and Q .

$$[C] = \begin{matrix} \begin{matrix} 1 & -1 & 1 & 5.1667 \\ 1 & -0.9925 & 0.9851 & 5.1815 \\ 1 & -0.9703 & 0.9415 & 5.2171 \\ 1 & -0.9336 & 0.8716 & 5.2471 \\ 1 & -0.8829 & 0.7796 & 5.2296 \\ 1 & -0.8192 & 0.6710 & 5.1172 \\ 1 & -0.7431 & 0.5523 & 4.8768 \\ 1 & -0.6561 & 0.4304 & 4.5105 \\ 1 & -0.5592 & 0.3127 & 4.0581 \end{matrix} & \begin{matrix} -5.1667 & 5.1667 & -5.1667 \\ -5.1429 & 5.1045 & -5.0665 \\ -5.0621 & 4.9118 & -4.7659 \\ -4.8986 & 4.5732 & -4.2695 \\ -4.6175 & 4.0770 & -3.5998 \\ -4.1918 & 3.4337 & -2.8127 \\ -3.6242 & 2.6933 & -2.0015 \\ -2.9589 & 1.9412 & -1.2736 \\ -2.2693 & 1.2690 & -0.7096 \end{matrix} \end{matrix} \quad (9 \times 7)$$

Matrix $[A]$ Matrix $[B]$

The size of matrix $[C]$ has been reduced from 9×9 to 9×7 after computing the optimal orders P and Q using the SVD. Coefficients a and b can now be solved for using (3.23) and the TLS method. First, a QR decomposition must be performed on submatrix $[A]$. As discussed in the previous section, submatrix $[A]$ is only a function of space and does not include any noise due to computational or measurement error. From (3.24) through (3.26) the matrix $[A \ -B]$ can be reconstructed as the following

$$\begin{matrix} \begin{matrix} [R_{11}] \\ -3 & 2.5190 & -2.1814 \\ 0 & 0.4460 & -0.7080 \\ 0 & 0 & -0.0539 \\ 0 & 0 & 0 \\ 0 & 0 & 0 \\ 0 & 0 & 0 \\ 0 & 0 & 0 \\ 0 & 0 & 0 \end{matrix} & \begin{matrix} [R_{12}] \\ -14.8681 & 12.6439 & -11.0568 & 9.8885 \\ -1.0752 & 2.9607 & -4.0667 & 4.7054 \\ 0.4442 & -0.2193 & -0.1771 & 0.6140 \\ 0.0358 & -0.0563 & 0.0630 & -0.0476 \\ 0.0460 & -0.0667 & 0.0700 & -0.0476 \\ 0.0271 & -0.0353 & 0.0335 & -0.0183 \\ -0.0167 & 0.0234 & -0.0238 & 0.0153 \\ -0.0439 & 0.0531 & -0.0462 & 0.0196 \\ 0.0246 & -0.0300 & 0.0264 & -0.0116 \end{matrix} \end{matrix}$$

[R_{21}] [R_{22}]

The SVD of submatrix $[R_{22}]$ is computed to solve (3.28) resulting in (3.29). From the TLS method and (3.30), we know that the vector representing coefficient b is equal to the last column of matrix $[V']$ from the resulting SVD of submatrix $[R_{22}]$. Matrix $[V']$ is shown below

$$[V'] = \begin{bmatrix} -0.4190 & -0.5680 & 0.2462 & 0.6642 \\ 0.5827 & 0.2730 & -0.2898 & 0.7085 \\ -0.5886 & 0.2004 & -0.7782 & 0.0886 \\ 0.3772 & -0.7501 & -0.4998 & -0.2214 \end{bmatrix}$$

Solution vector $[b]$ is shown in the highlighted box above in matrix $[V']$. The coefficients of the denominator polynomial are then as follows

$$b_0 = 0.6642, b_1 = 0.7085, b_2 = 0.0886, b_3 = -0.2214 \quad (3.34)$$

Once we know $[b]$, we can use (3.31) to solve for the solution vector $[a]$ and the coefficients of the numerator polynomial which are as follows

$$a_0 = -1.4613, a_1 = -0.3100, a_2 = -0.2214 \quad (3.35)$$

Step 4. We can now estimate the transfer function based on the computed coefficients of the numerator and denominator polynomials. Figure 3.2 shows the actual transfer function, the estimated transfer function using the Cauchy method, and the selected samples.

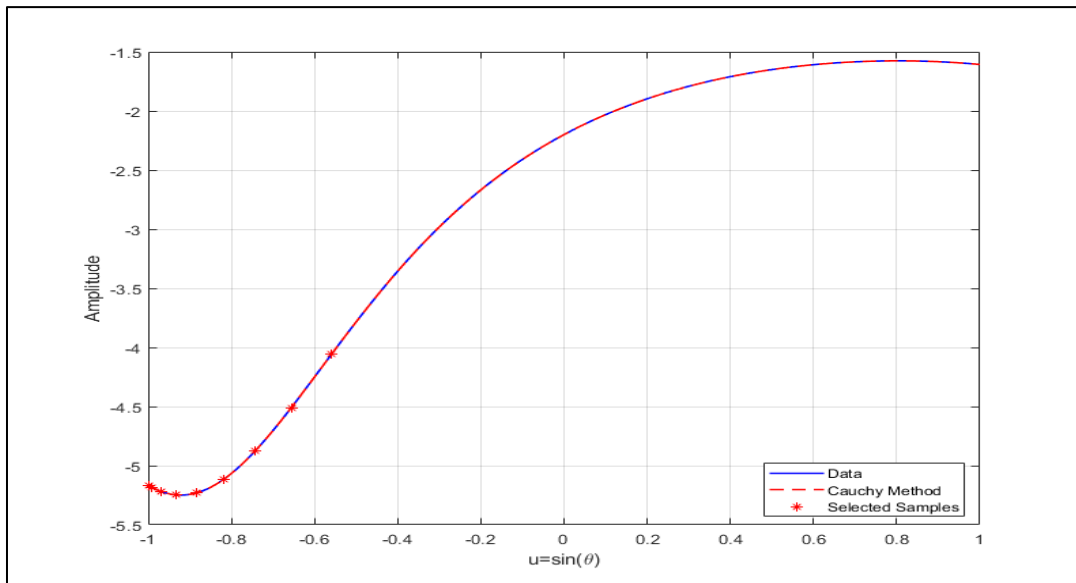


Figure 3.2. Comparison between generated data and estimated transfer function

The performance of the interpolation and extrapolation using the Cauchy method can be quantified by calculating the estimated error. This is completed by computing the mean squared error (MSE) in the frequency domain given as such

$$E_{est} = \frac{\|\hat{H}-H\|_2}{\|H\|_2} \quad (3.36)$$

where $\|\bullet\|_2$ is the L^2 -norm of a vector. \hat{H} contains the estimated space domain data. For this example, using (3.36), the MSE was calculated to be 2.6819e-12.

The transfer function $H(u)$ can also be regenerated with the residues R , and poles P . Therefore, (3.33) can be rewritten as the following

$$H(u) = \frac{1.3646}{u-2.3281} - \frac{0.1823-j1.4416}{u+(0.9640-j0.5994)} - \frac{0.1823+j1.4416}{u+(0.9640+j0.5994)} \quad (3.37)$$

The residues of the transfer function $H(u)$ are 1.3646, $-0.1823 + j1.4416$, and $-0.1823 - j1.4416$ respectively. The poles of $H(u)$ are 2.3281, $-0.9640 + j0.5994$, and $-0.9640 - j0.5994$ respectively. From (3.34) and (3.35), we can calculate the same exact residues and poles by hand as (3.37). The results above show the effectiveness of the Cauchy method in estimating a transfer function with only a few data samples.

CHAPTER 4

OVERVIEW OF THE MATRIX PENCIL METHOD

4. Overview of the Matrix Pencil Method

4.1 Theory

In the previous chapter, the Cauchy method assumed that a parameter of interest could be interpolated or extrapolated using a ratio of two polynomials. The Matrix Pencil method is another method that can achieve the same goal of interpolation or extrapolation. However, instead of using a ratio of two polynomials to interpolate or extrapolate, the Matrix Pencil method estimates the poles and residues using the exponential signal model. Any electromagnetic signal can be described using a summation of complex exponentials as shown below,

$$y_k = \sum_{i=1}^M R_i z_i^k + n_k, \quad \text{for } k = 0, 1, \dots, N - 1 \quad (4.1)$$

where y_k is measured data that has some noise component n_k . For the cases explored in this thesis, we can neglect the noise component since we are dealing with noiseless simulation data. Our goal then is to estimate the parameters M , R_i , and Z_i to interpolate or extrapolate the measurement data. The Matrix Pencil method [13]-[17] is proposed to achieve this goal and the procedure for implementing it to simultaneously estimate these parameters will be discussed.

The Matrix Pencil method works by approximating a function by a sum of complex exponentials. For the duration of this thesis, we will assume that our function is one of space and is dependent on elevation angle θ . An electromagnetic signal can be formulated as

$$y(\theta) = x(\theta) + n(\theta) \approx \sum_{i=1}^M R_i e^{s_i \theta} + n(\theta) \quad (4.2)$$

Once again, we can neglect noise n for the examples discussed in this thesis due to the fact that noiseless simulations were used. This model can be used because for an LTI system [10], the eigenfunctions of the transfer operator are of the form $e^{s_i \theta}$ where s_i are the poles of the system.

Once the data is sampled, θ is replaced by $k\theta_s$, where θ_s is the sample separation between angle measurements. The sequence of (4.2), neglecting noise, can be rewritten as the following

$$y(k\theta_s) = x(k\theta_s) \approx \sum_{i=1}^M R_i z_i^k, \quad \text{for } k = 0, 1, \dots, N-1 \quad (4.3)$$

$$z_i = e^{s_i \theta_s} = e^{(\alpha_i + j\omega_i)\theta_s}, \quad \text{for } i = 1, 2, \dots, M \quad (4.4)$$

where

$y(\theta)$ = approximated radiation pattern

$x(\theta)$ = sampled radiation pattern

R_i = residue or complex amplitudes of the i th pole

$s_i = \alpha_i + j\omega_i$ (i th pole of the system)

α_i = negative damping factor of the i th pole

ω_i = angular frequency of the i th pole

N = number of data samples

M = number of poles of the signal (number of singular values)

We can characterize the response by using the Matrix Pencil method to estimate M , R_i , and Z_i even if the data is corrupted by numerical errors or random noise. Since we are dealing with noiseless data, we can define a matrix $[Y]$ that is of size $(N-L) \times (L+1)$ as

$$[Y] = \begin{bmatrix} y_0 & y_1 & \cdots & y_L \\ y_1 & y_2 & \cdots & y_{L+1} \\ \vdots & \vdots & \ddots & \vdots \\ y_{N-L-1} & y_{N-L} & \cdots & y_{N-1} \end{bmatrix}_{(N-L) \times (L+1)} \quad (4.5)$$

(4.5) can also be defined as

$$[Y] = [c_1, Y_1] = [Y_2, c_{L+1}] \quad (4.6)$$

where c_i represents the i th column of matrix $[Y]$. Matrices $[Y_1]$ and $[Y_2]$ are defined as

$$[Y_1] = [Z_1][R][Z_0][Z_2] \quad (4.7)$$

$$[Y_2] = [Z_1][R][Z_2] \quad (4.8)$$

Matrices $[Z_1]$, $[Z_2]$, $[Z_0]$, and $[R]$ are defined as

$$[Z_1] = \begin{bmatrix} 1 & 1 & \cdots & 1 \\ z_1 & z_2 & \cdots & z_M \\ \vdots & \vdots & \ddots & \vdots \\ z_1^{(N-L-1)} & z_2^{(N-L-1)} & \cdots & z_M^{(N-L-1)} \end{bmatrix}_{(N-L) \times M} \quad (4.9)$$

$$[Z_2] = \begin{bmatrix} 1 & z_1 & \cdots & z_1^{L-1} \\ 1 & z_2 & \cdots & z_2^{L-1} \\ \vdots & \vdots & \ddots & \vdots \\ 1 & z_M & \cdots & z_M^{L-1} \end{bmatrix}_{M \times L} \quad (4.10)$$

$$[Z_0] = \begin{bmatrix} z_1 & 0 & \cdots & 0 \\ 0 & z_2 & \cdots & 0 \\ \vdots & \vdots & \ddots & \vdots \\ 0 & 0 & \cdots & z_M \end{bmatrix}_{M \times M} \quad (4.11)$$

$$[R] = \begin{bmatrix} R_1 & 0 & \cdots & 0 \\ 0 & R_2 & \cdots & 0 \\ \vdots & \vdots & \ddots & \vdots \\ 0 & 0 & \cdots & R_M \end{bmatrix}_{M \times M} \quad (4.12)$$

Let us consider the following matrix pencil

$$[Y_1] - \lambda[Y_2] = [Z_1][R]\{[Z_0] - \lambda[I]\}[Z_2] \quad (4.13)$$

Given that $M \leq L \leq N-M$ where L is the pencil parameter, the matrix $[Y_1] - \lambda[Y_2]$ has rank M . The pencil parameter L should be chosen to be between $N/3$ and $N/2$ for computational efficiency. However, if $\lambda = z_i, i = 1, 2, \dots, M$, the i th row of $[Z_0] - \lambda[I]$ is zero, and the rank of $[Z_0] - \lambda[I]$ will be $M - 1$, where $[I]$ is the identity matrix. If this is the case, then the matrix pencil $[Y_1] - \lambda[Y_2]$ will also be reduced to rank $M - 1$. This implies that the z_i 's are the generalized eigenvalues of the matrix pair $\{[Y_1], [Y_2]\}$. We can then define the following

$$[Y_1][r_i] = z_i[Y_2][r_i] \quad (4.14)$$

Where r_i is the generalized eigenvector corresponding to z_i . We can move the right-hand side over to the left-hand side and set it equal to zero as follows

$$\{[Y_2]^\dagger[Y_1] - z_i[I]\}[r_i] = 0 \quad (4.15)$$

$[Y_2]^\dagger$ signifies the Moore-Penrose pseudo-inverse of $[Y_2]$. (4.15) is now in least squares form and we can use the theory of total least squares to solve the equation. We can obtain the z_i 's from the eigenvalues of $[Y_2]^\dagger[Y_1]$. This suggests that the poles can be determined directly as a one-step process.

We will define the singular value decomposition [11] of matrix $[Y]$ as

$$[Y] = [U][\Sigma][V]^H \quad (4.16)$$

The matrix $[U]$ and $[V]$ are $(N-L) \times (N-L)$ and $(L+1) \times (L+1)$ unitary matrices respectively. The singular values of matrix $[Y]$ are contained in matrix $[\Sigma]$ in descending order which is a $(N-L) \times (L+1)$ diagonal matrix. Since we will be dealing with noiseless data, matrix $[Y]$ should have exactly M nonzero singular values. If there was noise contained within the data, several small nonzero singular values would also be present. We can suppress the error due to noise by eliminating these spurious small nonzero singular values from the matrix $[\Sigma]$. We will define a new singular value matrix $[\Sigma']$ as a $M \times M$ diagonal matrix with the M largest singular values of $[Y]$ on its main diagonal. We will also define $[U']$ and $[V']$ as submatrices of $[U]$ and $[V]$ corresponding to the newly selected singular values

$$[U'] = [U(:, 1:M)] \quad (4.17)$$

$$[V'] = [V(:, 1:M)] \quad (4.18)$$

$$[\Sigma'] = [\Sigma(:, 1:M)] \quad (4.19)$$

$$[Y'] = [U'][\Sigma'][V']^H \quad (4.20)$$

Now instead of using matrix $[Y]$ in (4.6) which could contain noisy data, we are able to use $[Y']$ which will no longer contain noise. The noise in $[Y_1]$ and $[Y_2]$ will essentially be filtered out.

From (4.6) and (4.20) we can write

$$[Y_1] = [U'][\Sigma'][V_1']^H \quad (4.21)$$

$$[Y_2] = [U'][\Sigma'][V_2']^H \quad (4.22)$$

where $[V_1']$ and $[V_2']$ are equal to $[V']$ without the first and last row, respectively. We can now find the poles of the noiseless signal which are given by the nonzero eigenvalues of the following

$$[V_2']^\dagger [V_1'] \quad (4.23)$$

The optimal number of singular values M is chosen by observing the ratio of the various singular values to the largest one [9], similar to the procedure defined in the previous chapter dealing with the Cauchy method. We can write

$$\frac{\sigma_R}{\sigma_{max}} \approx 10^{-w} \quad (4.24)$$

where w is the number of accurate significant digits of the system response data [12]. Once w is determined, we are able to select the proper number of singular values M for the assumed precision. Using this better choice of M , we can then evaluate the poles z_i and the residues R_i using the previously detailed approach. We are therefore able to extract the residues and poles from the data even if it is contaminated by noise using the Matrix Pencil method in conjunction with the SVD [11] and TLS method [3].

4.2 Procedure for Implementing the Matrix Pencil Method

To illustrate how the Matrix Pencil method is implemented, we will go through a simple example of extrapolation. We will consider the following signal as a function of time, t .

$$y(t) = e^{-0.015\pi t} \sin(0.15\pi t) + e^{-0.03\pi t} \sin(0.3\pi t), \quad t = 0, 0.5, 1, \dots, 100 \quad (4.25)$$

The data is sampled at every 0.5 seconds making the total number of samples equal to 201. For this signal $\alpha_1 = -0.015\pi$, $\omega_1 = 0.15\pi$, $\alpha_2 = 0.03\pi$, and $\omega_2 = 0.3\pi$. We will now use very few of the 201 samples to extract the poles and residues of the signal in order to extrapolate the rest of the signal.

Step 1. We will choose 12 samples among the 201 data samples ($N = 12$).

$$t = 0, 3, 6, 9, 12, 15, 18, 21, 24, 27, 30, 33$$

$$y(t) = 0, 1.0904, -0.1010, -0.2366, -0.6408, 0.5920, 0.1720, -0.0570, -0.3681, 0.0681, 0.2432,$$

$$0.0193$$

Step 2. We can now form the $(N - L) \times (L + 1)$ matrix $[Y]$ from the selected time sampling data. For efficient noise filtering, we will use $N/2 - 1$ for the pencil parameter L which will be 5 for this example. Therefore, the size of the matrix $[Y]$ is 7×6 .

$$[Y] = \begin{bmatrix} 0 & 1.0904 & -0.1010 & -0.2366 & -0.6408 & 0.5920 \\ 1.0904 & -0.1010 & -0.2366 & -0.6408 & 0.5920 & 0.1720 \\ -0.1010 & -0.2366 & -0.6408 & 0.5920 & 0.1720 & -0.0570 \\ -0.2366 & -0.6408 & 0.5920 & 0.1720 & -0.0570 & -0.3681 \\ -0.6408 & 0.5920 & 0.1720 & -0.0570 & -0.3681 & 0.0681 \\ 0.5920 & 0.1720 & -0.0570 & -0.3681 & 0.0681 & 0.2432 \\ 0.1720 & -0.0570 & -0.3681 & 0.0681 & 0.2432 & 0.0193 \end{bmatrix}_{(7 \times 6)} \quad (4.26)$$

Step 3. Next, the SVD of matrix $[Y]$ is taken which will give us the optimal number of singular values M . Figure 4.1 shows the normalized singular values in dB scale from the SVD of matrix $[Y]$. We know from (4.24) that if the number of accurate significant digits (w) is 1, then the number of singular values, M , is 4.

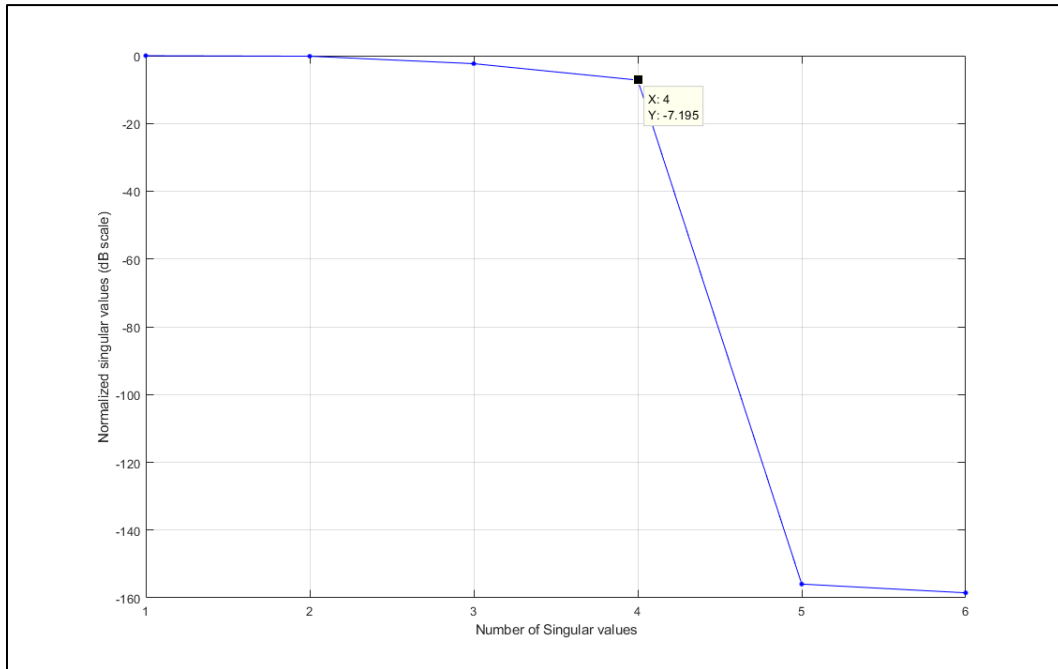


Figure 4.1. Normalized singular values from SVD of matrix $[Y]$

Step 4. Once the number of singular values M , is known, we can obtain matrices $[V_1']$ and $[V_2']$ from $[V']$ as submatrices of $[V]$ corresponding to M .

$$[V'] = \begin{matrix} & & & [V_2'] \\ \begin{matrix} \left[\begin{array}{cccc} -0.6488 & 0.4440 & -0.0979 & 0.4891 \\ 0.4921 & 0.6285 & 0.1139 & -0.2600 \\ 0.1744 & -0.1926 & -0.8324 & 0.1312 \\ 0.1573 & -0.4375 & 0.5082 & 0.4563 \\ -0.5233 & -0.0843 & 0.1220 & -0.6212 \\ 0.0893 & 0.4151 & 0.1066 & 0.2862 \end{array} \right] \\ [V_1'] \end{matrix} & & & \end{matrix} \quad (4.27)$$

We can now compute the poles, z_i , from the nonzero eigenvalues of $[V_2']^\dagger[V_1']$. From (4.4), the poles of the signal can be obtained by

$$s_i = \alpha_i + j\omega_i = \log_e \left(\frac{z_i}{T_s} \right), \quad \text{for } i = 1, 2, \dots, M \quad (4.28)$$

$$s_1 = -0.0471 + j0.4712$$

$$s_2 = -0.0471 - j0.4712$$

$$s_3 = -0.0942 + j0.9425$$

$$s_4 = -0.0942 - j0.9425$$

The poles are the complex conjugate of s_1, s_2 , and s_3, s_4 . From (4.25), the original poles are $\alpha_1 = -0.0471, \omega_1 = 0.4712, \alpha_2 = -0.0942$, and $\omega_2 = 0.9425$. As we can see from our results above, the estimated poles found using the Matrix Pencil method are exactly equal to the original poles.

The residues can also be calculated corresponding to each pole using (4.3)

$$R_1 \approx -j0.5$$

$$R_2 \approx j0.5$$

$$R_3 \approx -j0.5$$

$$R_4 = j0.5$$

Once the poles and residues are calculated, the estimated signal formula can be written and compared to the original signal model. The signal model from (4.25) can be reformulated using the newly determined poles and residues as the following

$$y(t) = e^{-0.015\pi t} (j0.5e^{-0.15\pi t} - j0.5e^{0.15\pi t}) + e^{-0.03\pi t} (j0.5e^{-0.3\pi t} - j0.5e^{0.3\pi t}) \quad (4.29)$$

Thus, it is proved that the Matrix Pencil method is able to obtain the correct poles and residues of the signal.

Step 5. Finally, the poles and residues calculated using the Matrix Pencil method are used to estimate the signal which is shown in figure 4.2. Once again, we will evaluate the performance of the interpolation and extrapolation by determining the mean squared error. For this example, the MSE was calculated to be $3.1314e-15$.

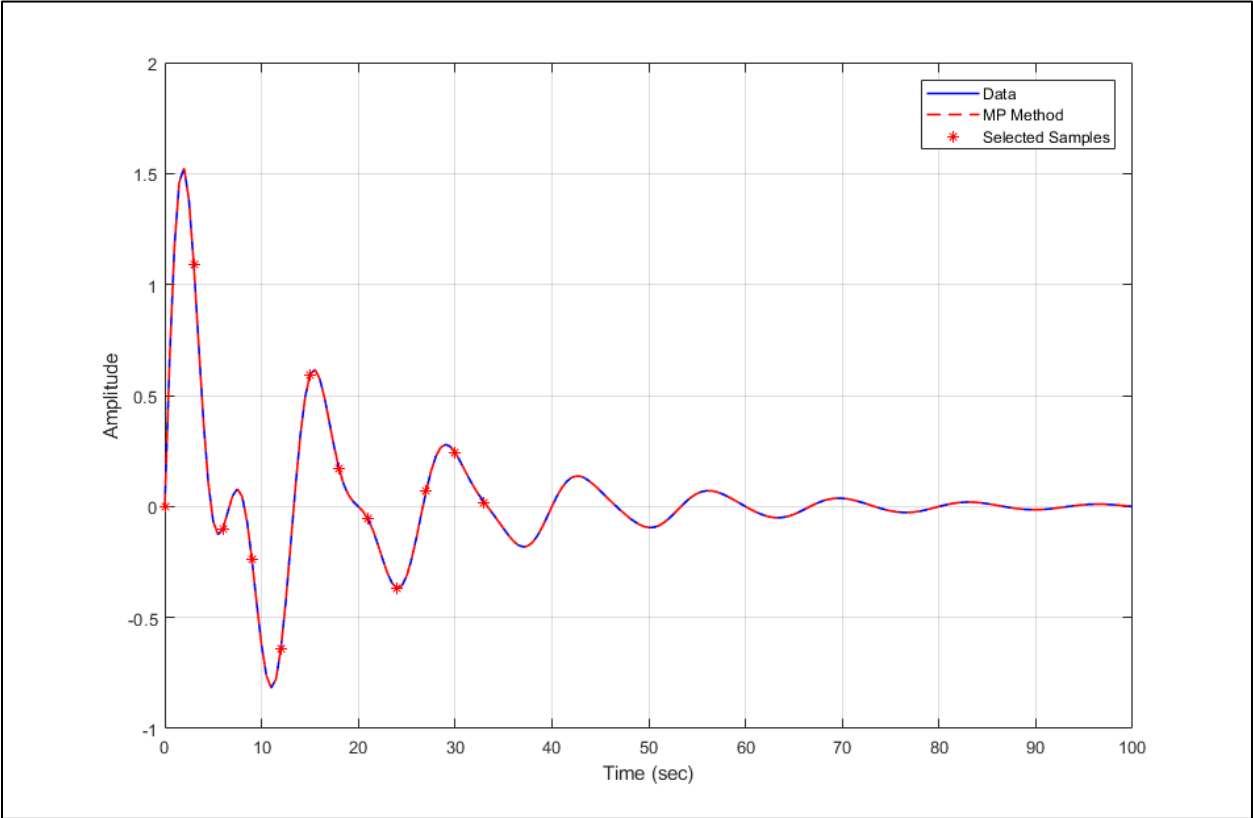


Figure 4.2. Comparison between original data and estimated data

CHAPTER 5
NUMERICAL RESULTS

5. Numerical Results

5.1 Cauchy Method

5.1.1 $\lambda/2$ Dipole Antenna

We will start out by showing how the Cauchy method performs for interpolating the gain pattern of a simple dipole antenna. Once again, the Cauchy method approximates a function by a ratio of two polynomials. The dipole antenna used for this example is a $\lambda/2$ dipole operating at a center frequency of 300MHz. It has a length of 0.5m with a diameter of 0.050m. The dipole was designed and simulated using the HOBBIES [18] electromagnetic simulation software. The far-field of the antenna was sampled every two degrees in theta from -90 to +90 degrees and every ten degrees in phi from 0 to 360 degrees. The far-field pattern is assumed to be symmetrical and therefore only 181 degrees of data in theta is analyzed. The data from the phi-cut of the field was extracted at $\varphi = 0$ degrees with 91 total samples and imported into MATLAB where the Cauchy method code was implemented. Figure 5.1 below shows the dipole antenna designed in HOBBIES.

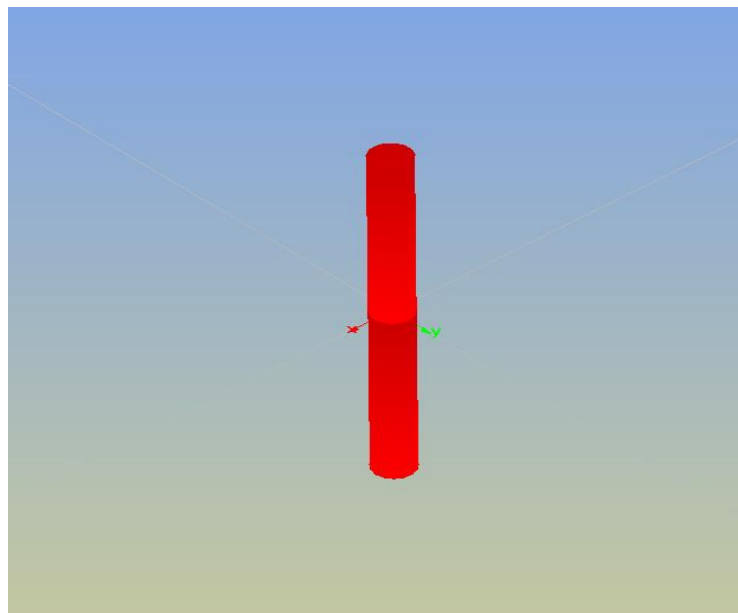


Figure 5.1 $\lambda/2$ dipole designed and simulated in HOBBIES

Once the data was imported into MATLAB, sixteen samples of the data ($N = 16$) were taken from -90 to -76 degrees and $+76$ to $+90$ degrees (two degree increments) and the far-field was interpolated from -76 to $+76$ degrees in theta. To select the optimal polynomial orders, P and Q , a singular value decomposition of the 16 sampled points was taken. Figure 5.2 below shows the distribution of the normalized singular values in the dB scale.

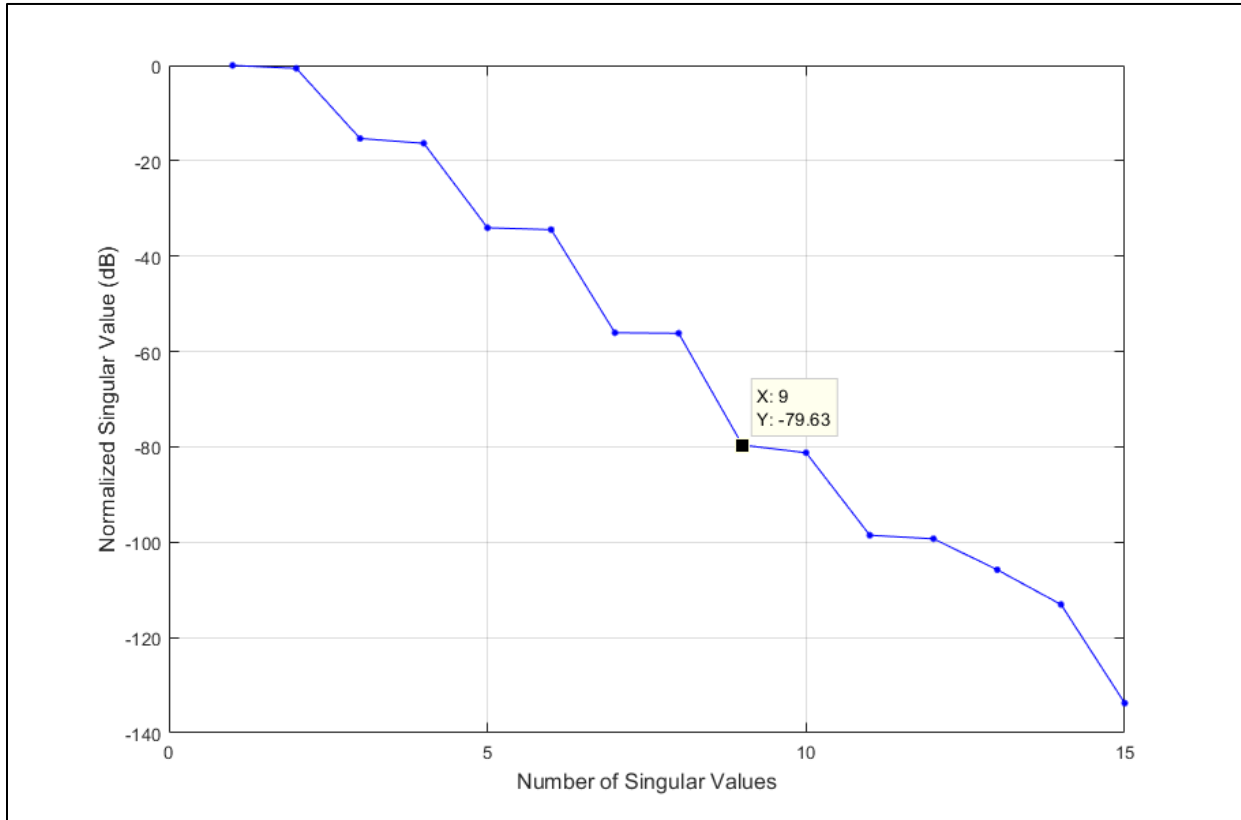


Figure 5.2. Distribution of the normalized singular values of the sampled data

From figure 5.2 and (3.17) we are able to determine the rank (R) of the sampled data matrix and also the optimal polynomial orders P and Q . Since the imported data of the dipole antenna has at least 8 accurate significant digits, the lowest singular value should be closest to -80 dB. For this particular data set, the number of singular values up to that point is equal to 9, therefore the rank (R) of the matrix is also 9. By using (3.21) and (3.3) we determine that the numerator polynomial P is 4 and the denominator polynomial Q is 5. This reduces the size of the

data matrix from 16x15 to 16x11. Using total least squares as discussed in chapter 3, the far-field pattern of the dipole can now be reconstructed using only 9 (down from 16 originally) samples out of the 91 total samples. Figure 5.3 shows the reconstructed far-field gain pattern.

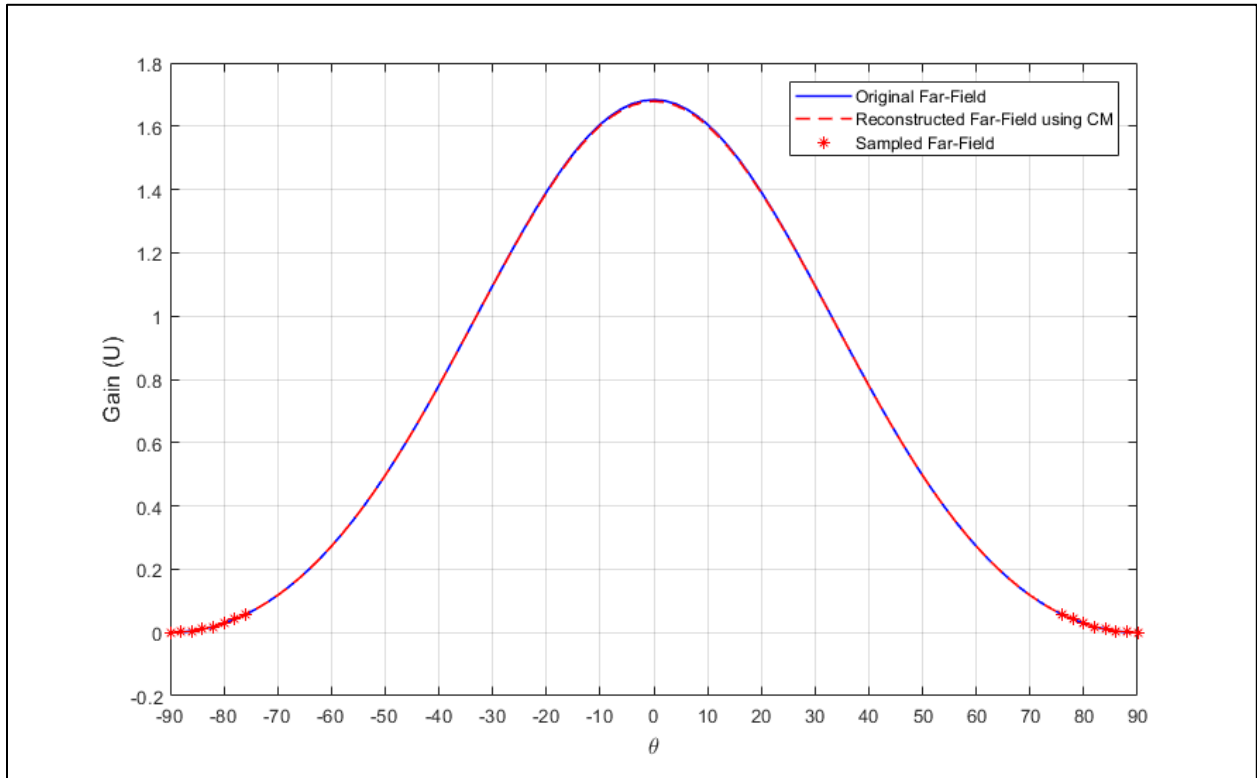


Figure 5.3. Interpolated far-field of dipole using the Cauchy method

Looking at figure 5.3, the red stars represent the 16 sampled data points used as the input to the Cauchy method before data reduction using the SVD, the solid blue line represents the original far-field gain pattern, and the red dashed line represents the reconstructed far-field gain pattern using the 16 samples and the Cauchy method. We can quantify the interpolation performance of the Cauchy method by taking the MSE of the reconstructed far-field and original far-field. Using (3.35) the MSE was calculated to be $2.0087e-03$. Therefore, we were successfully able to interpolate the far-field gain pattern of a dipole antenna using only 9 out of

91 samples of data after optimizing the polynomial orders using the singular value decomposition and then applying Cauchy method.

5.1.2 10x10 Linear $\lambda/2$ Dipole Array With λ Spacing

Next, we will look at a 10x10 linear dipole array with spacing between the elements equal to λ . Each individual dipole is $\lambda/2$ in length and is designed to operate at a center frequency of 600MHz. The length of each dipole is 0.25m with a radius of 0.025m. The dipoles are also all excited with in-phase signals at the center. HOBBIES was once again used for the design and simulation of the array. The simulation was configured to sample -90 to +90 degrees in theta with one degree increments for a total of 181 samples in theta and from 0 to 360 degrees with 10 degree increments in phi for a total of 37 samples in phi. The far-field pattern is assumed to be symmetrical and therefore only 181 degrees of data in theta is analyzed. The phi-cut of the far-field radiation pattern at $\phi = 0$ was taken and exported to MATLAB. Figure 5.4 shows the 10x10 linear dipole array designed and simulated in HOBBIES.

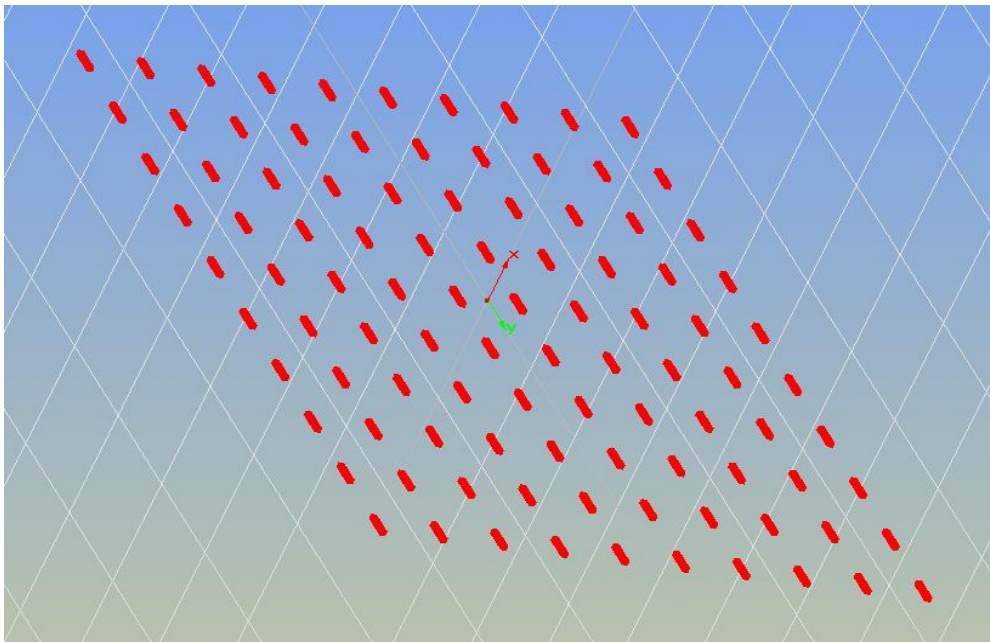


Figure 5.4. 10x10 linear dipole array designed and simulated in HOBBIES

For this example, the main beam is broadside to the array in the $\pm x$ direction at $\theta = 0$ degrees. Since the radiation pattern will be more complex than just a single dipole and contains many localized peaks and nulls, more sample points are needed to successfully interpolate or extrapolate the pattern. Estimation of the main beam is not quite possible because the majority of the information content is contained there. We will be specifically looking at the extrapolation of the pattern from -55 to -90 degrees and $+55$ to $+90$ degrees with the sampled points in between. This is essentially the opposite of what was done in the previous section where the end points were sampled, and the pattern in between was interpolated. Also, the shape of the pattern can be exploited to improve the accuracy of the extrapolation. If we look at the radiation pattern from -90 to 90 degrees in theta, we will see that it is symmetric about 0 degrees. Figure 5.5 shows the magnitude of the radiated electric field in dB.

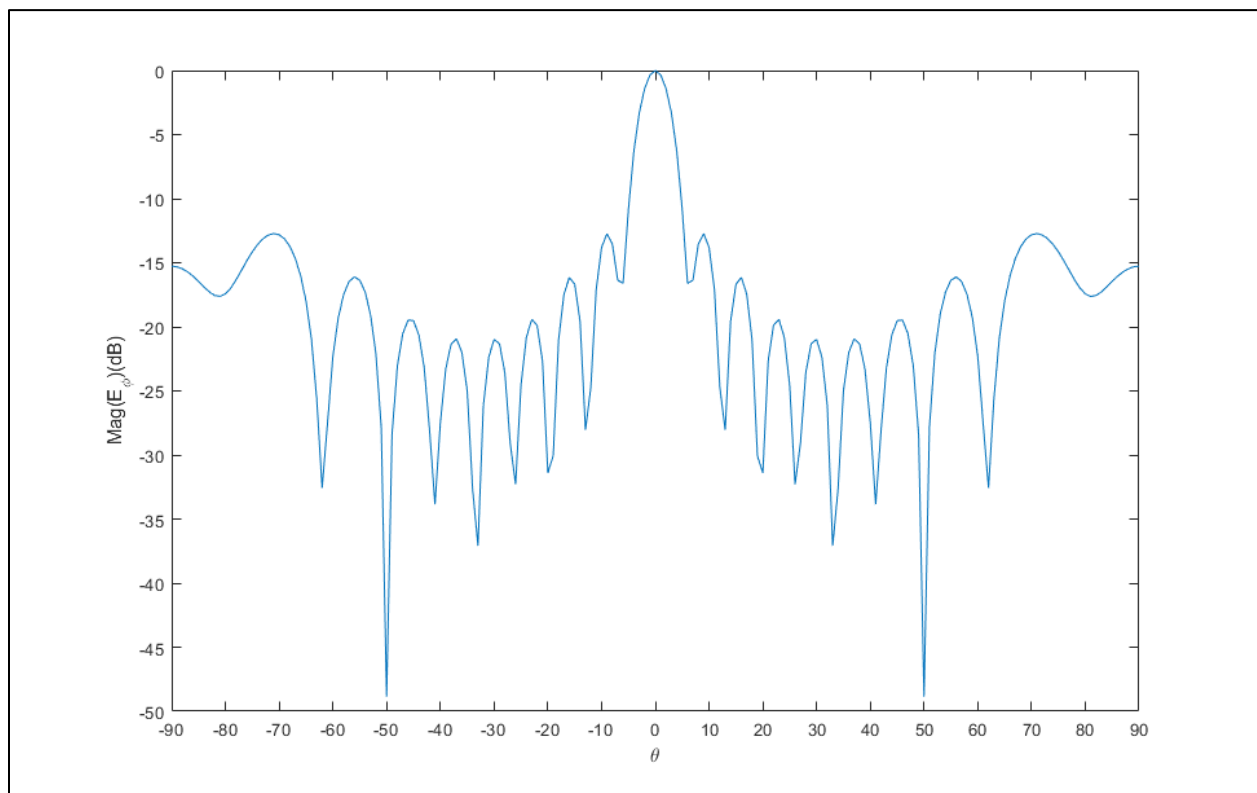


Figure 5.5 Magnitude of radiated electric field of 10x10 linear dipole array

We can therefore turn an extrapolation problem into an interpolation problem by rotating each half of the field so that +/- 90 degrees is the center point. The accuracy of interpolation was improved by interpolating the real and imaginary parts of the electric field pattern separately instead of the complex electric field.

For the real part of the radiated electric field, the data was sampled from -55 to +55 degrees at a one degree increment, for a total of 111 samples ($N = 111$) and interpolated/extrapolated from -55 to -90 degrees and +55 to +90 degrees for a total of 70 degrees. The distribution of the singular values is shown below in figure 5.6.

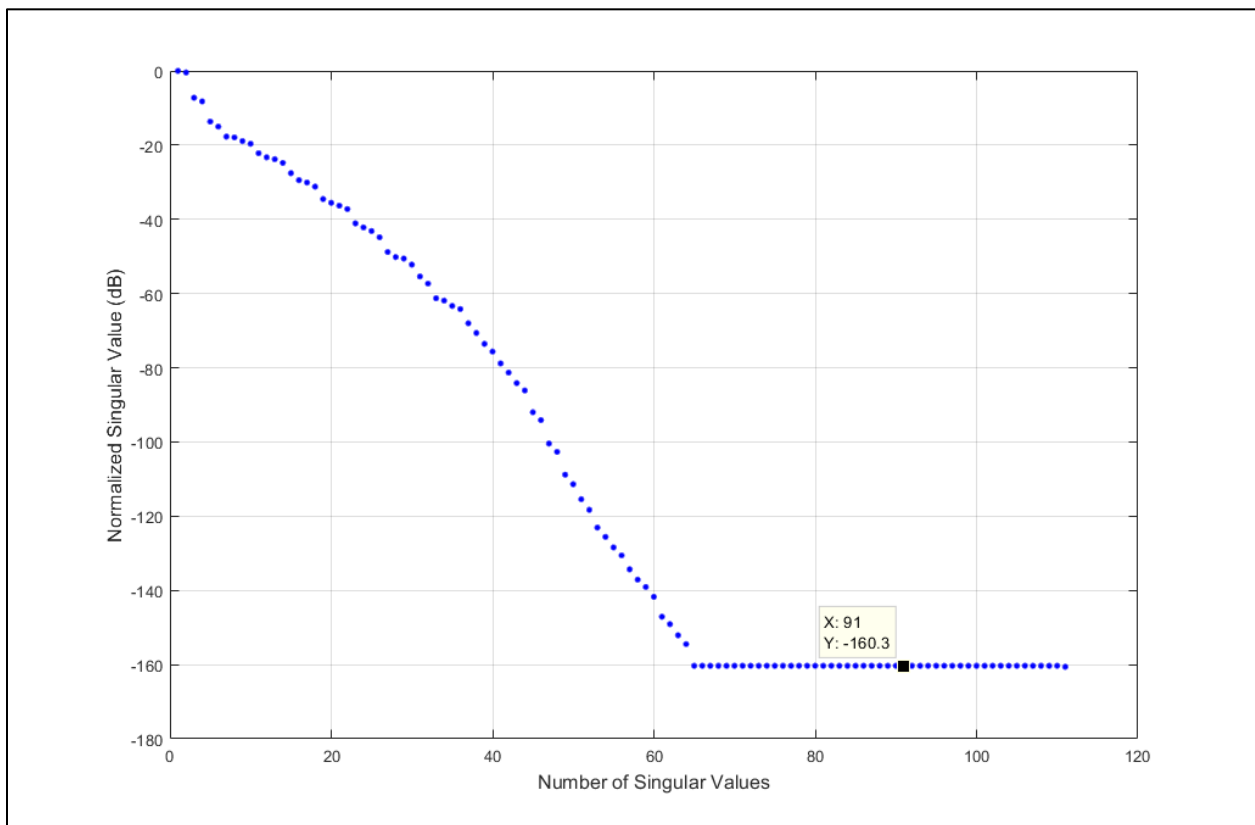


Figure 5.6. Distribution of the singular values of the real part of the radiated electric field

Double precision data was used therefore the number of accurate significant digits is equal to 16.

Using (3.17) we would need a singular value approximately equal to -160 dB. From figure 5.6

we can see that 65 singular values would be closest to -160 dB. However, due to the complexity of this particular radiation pattern and the fact that a unique solution may not always exist, it was determined that more singular values would be needed to accurately interpolate. More singular values means that the rank (R) of the optimal data matrix would be greater therefore leading to higher order polynomials in the numerator and denominator. Using error analysis code, it was determined that 91 singular values would provide optimal orders of the numerator and denominator polynomials. This is still an improvement over the original sampled data matrix which contained 111 samples. We are able to reduce the rank of matrix $[C]$ from 111 to 91 and accurately interpolate/extrapolate the missing data. A rank of 91 leads to a numerator polynomial order of 45 and a denominator order of 46. Figure 5.7 shows the interpolation result for the real part of the radiated electric field of the 10x10 linear dipole array.

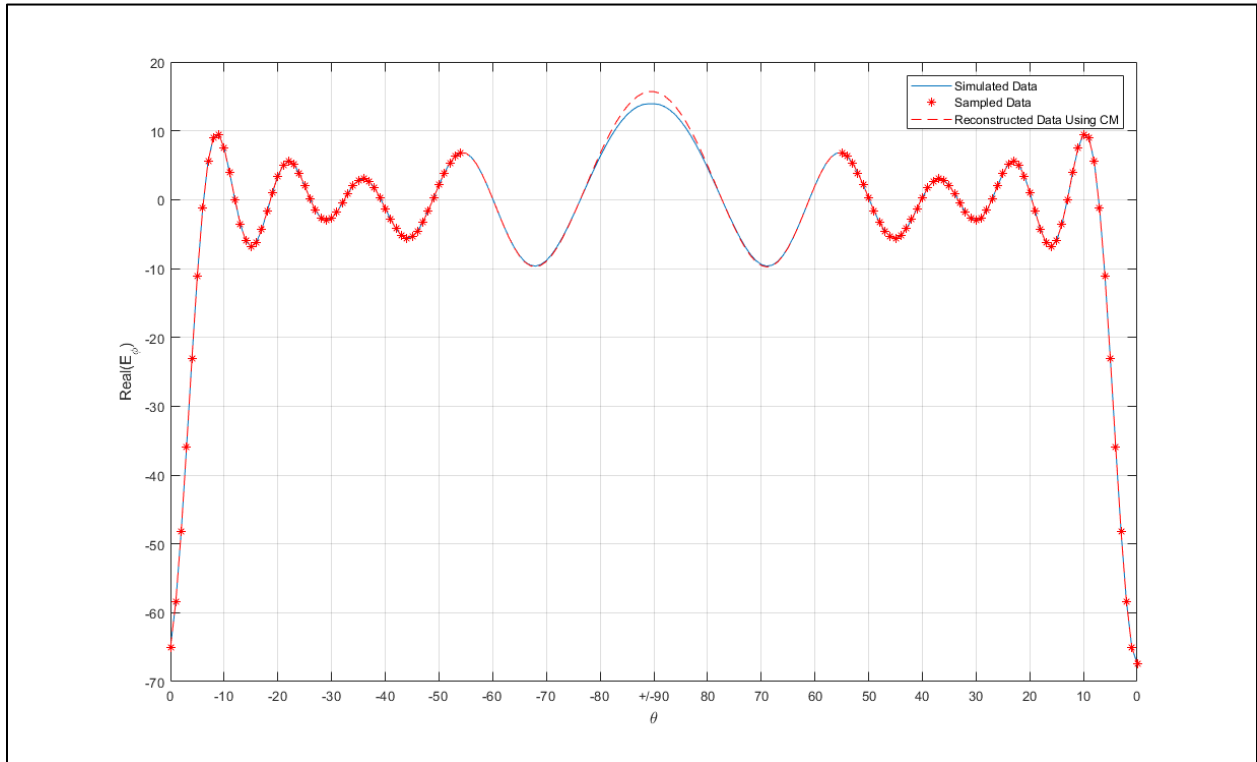


Figure 5.7. Interpolation of the real part of the radiated electric field

Once again, the red stars represent the 111 original samples of the data before reduction using the SVD, the solid blue line is the original simulated real part of the radiated electric field, and the dashed red line is the result of the interpolation using the Cauchy method. The MSE was calculated to be 0.0293.

Next, the imaginary part of the radiated electric far-field was interpolated/extrapolated using the same procedure as above. The same number of samples was used ($N = 111$). The distribution of the singular values is shown in figure 5.8.

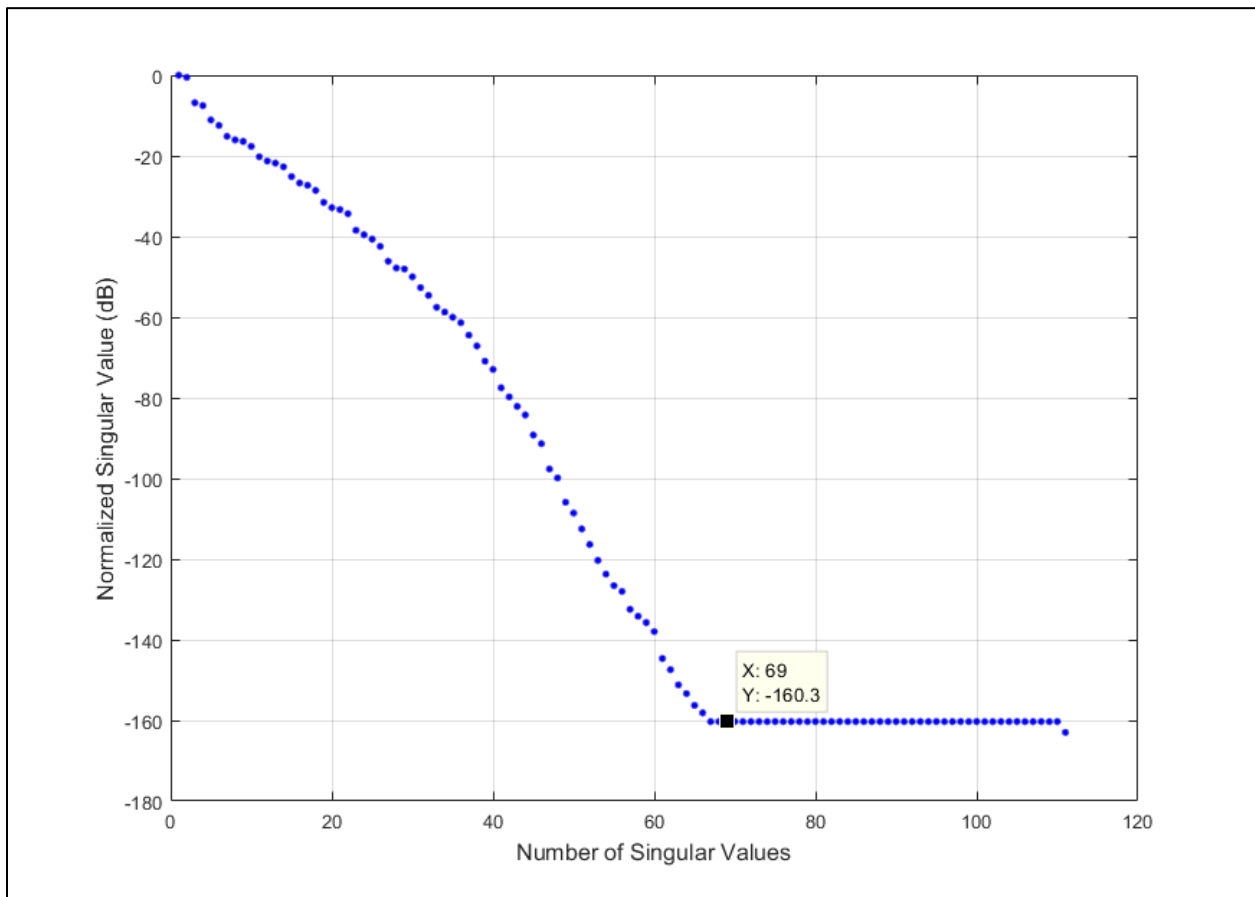


Figure 5.8. Distribution of the singular values of the imaginary part of the radiated electric field

Using the same error analysis, it was determined that 69 singular values were sufficient to accurately interpolate/extrapolate the field. This value is closer to the expected number of 67 singular values. This reduces the final input data matrix $[C]$ rank from 111 to 69. A rank of 69

leads to a numerator polynomial order of 34 and denominator polynomial order of 35. Figure 5.9 shows the resulting interpolation of the imaginary part of the radiated electric field.

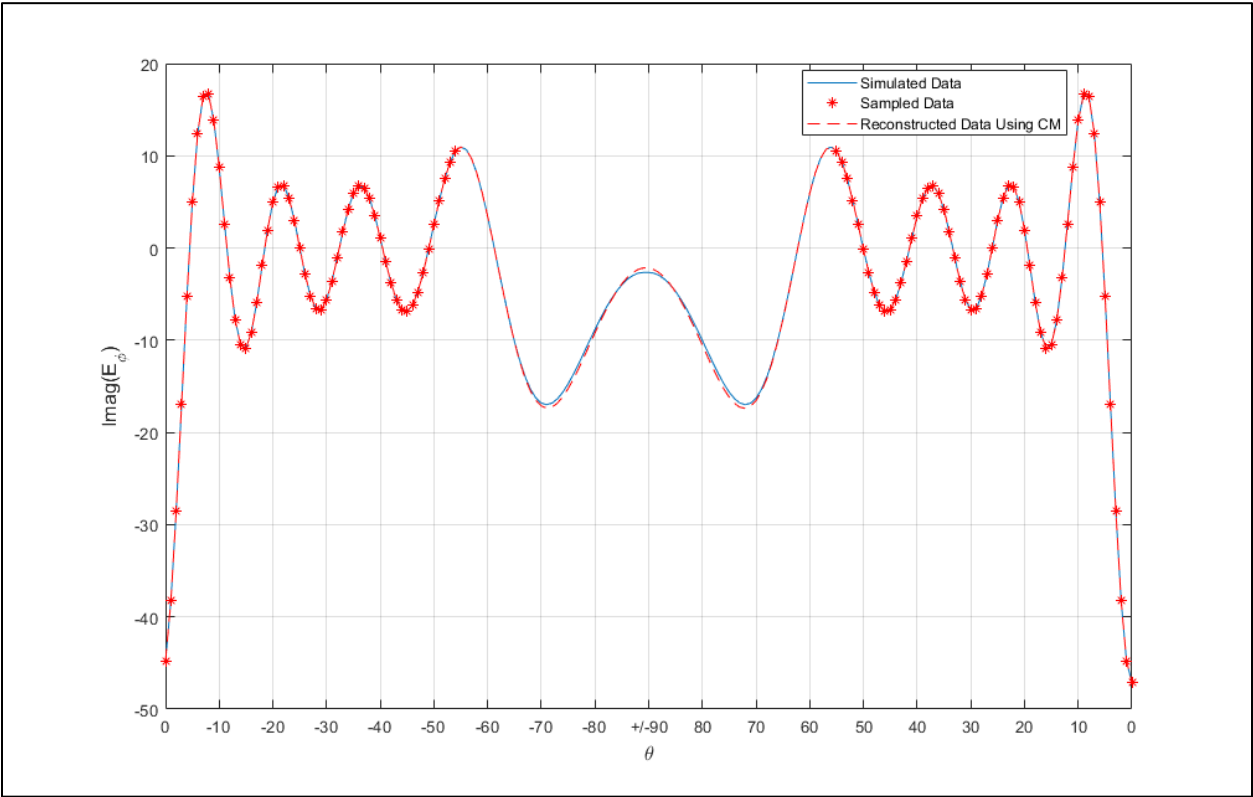


Figure 5.9. Interpolation of the imaginary part of the radiated electric field

The MSE for the interpolation of the imaginary part of the radiated electric far-field was calculated to be 0.0169.

From the interpolated real and imaginary part of the electric far-field, the magnitude of the interpolated far-field could be calculated in the dB scale. Figure 5.10 shows the resulting magnitude of the far-field.

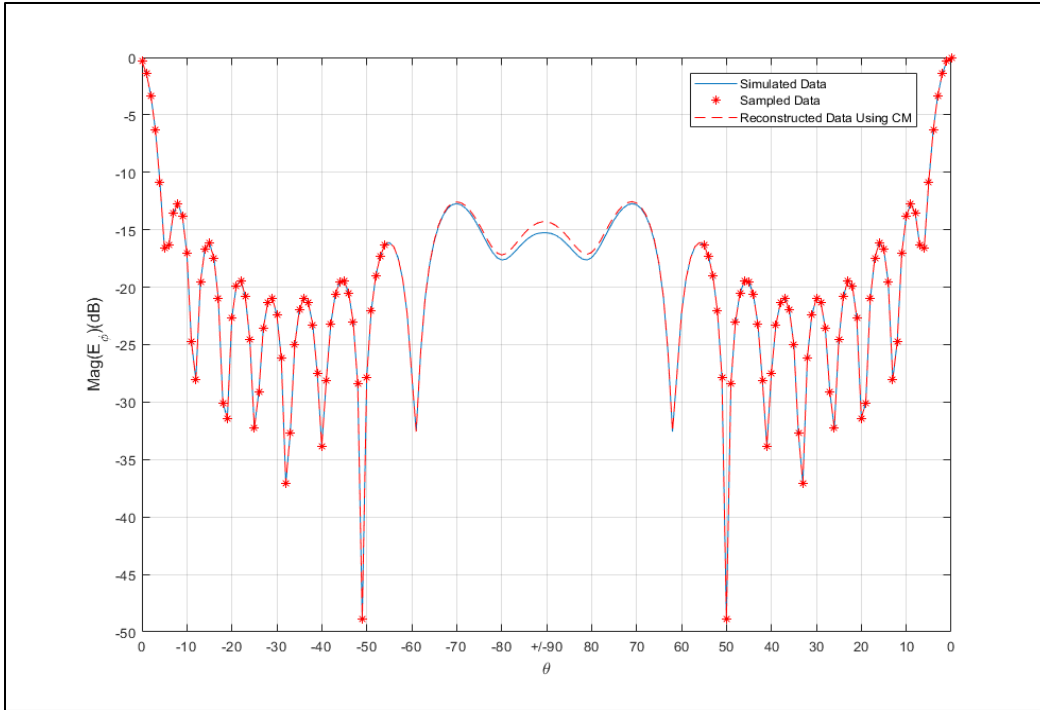


Figure 5.10. Resulting interpolation of the magnitude of the mirrored far-field

We can now rotate each half of the far-field to reconstruct the far-field that was originally simulated and imported into MATLAB that was shown in figure 5.5. Figure 5.11 below shows this.

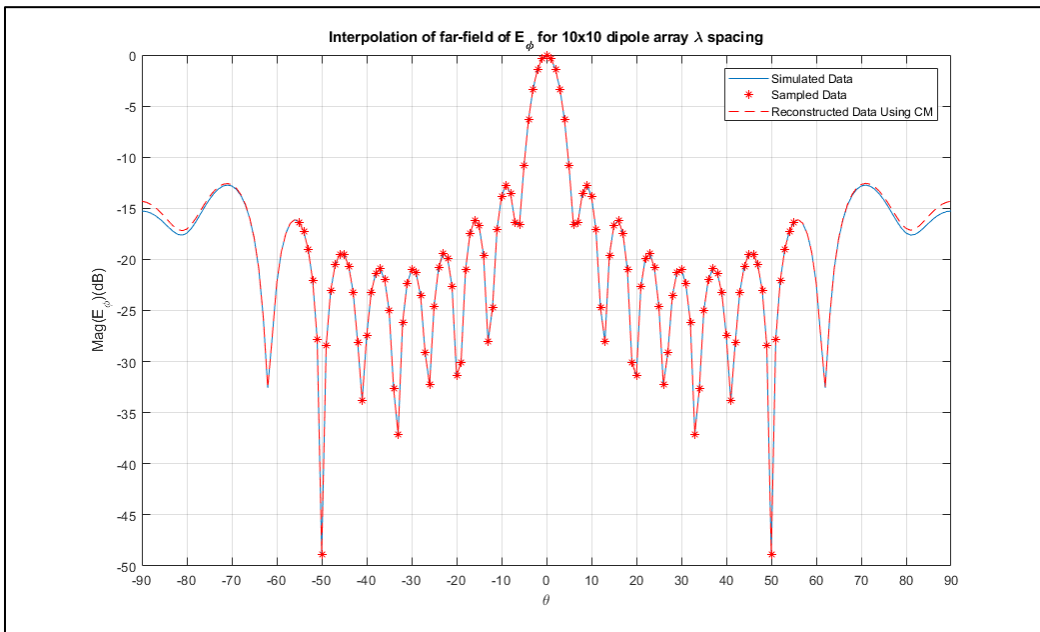


Figure 5.11. Comparison between original and interpolated far-field

From figure 5.10 and 5.11, we can see that by rotating each half of a symmetrical pattern one can turn an extrapolation problem into an interpolation problem to increase the accuracy of an estimation. The MSE of the interpolation of the magnitude of the far-field was calculated to be 0.0126.

To illustrate how interpolation can be more accurate than extrapolation using the Cauchy method, we will now attempt to extrapolate the same far-field pattern. The extrapolation will also be from -55 to -90 degrees and +55 to +90 degrees, but we will no longer be rotating each half of the pattern. The distribution of the singular values of the real part of the far-field is shown in figure 5.12.

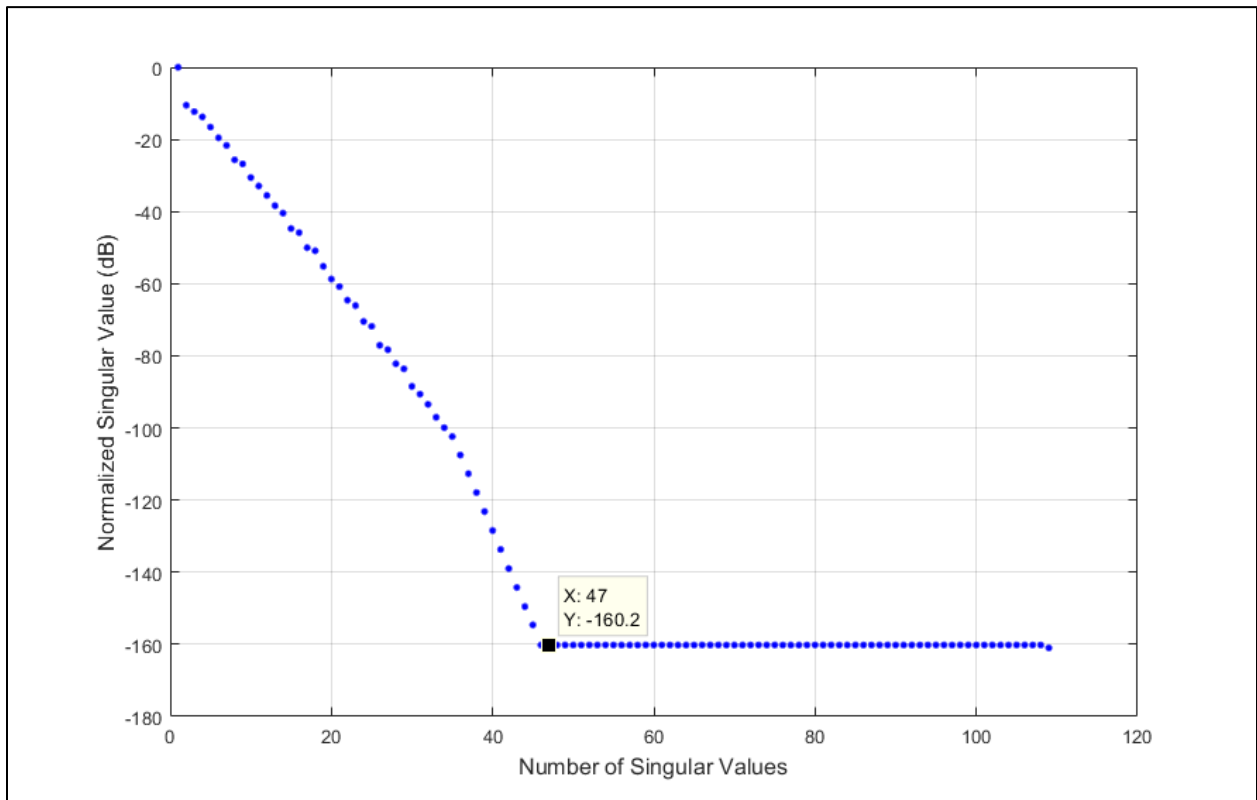


Figure 5.12. Distribution of the singular values for the real part of the far-field pattern

From figure 5.12 the number of singular values that is closest to -160 dB and also produces the least amount of error is 47. This leads to a numerator polynomial order of 24 and a denominator

polynomial order of 25. The resulting extrapolation of the real part of the radiating electric far-field pattern is shown in figure 5.13.

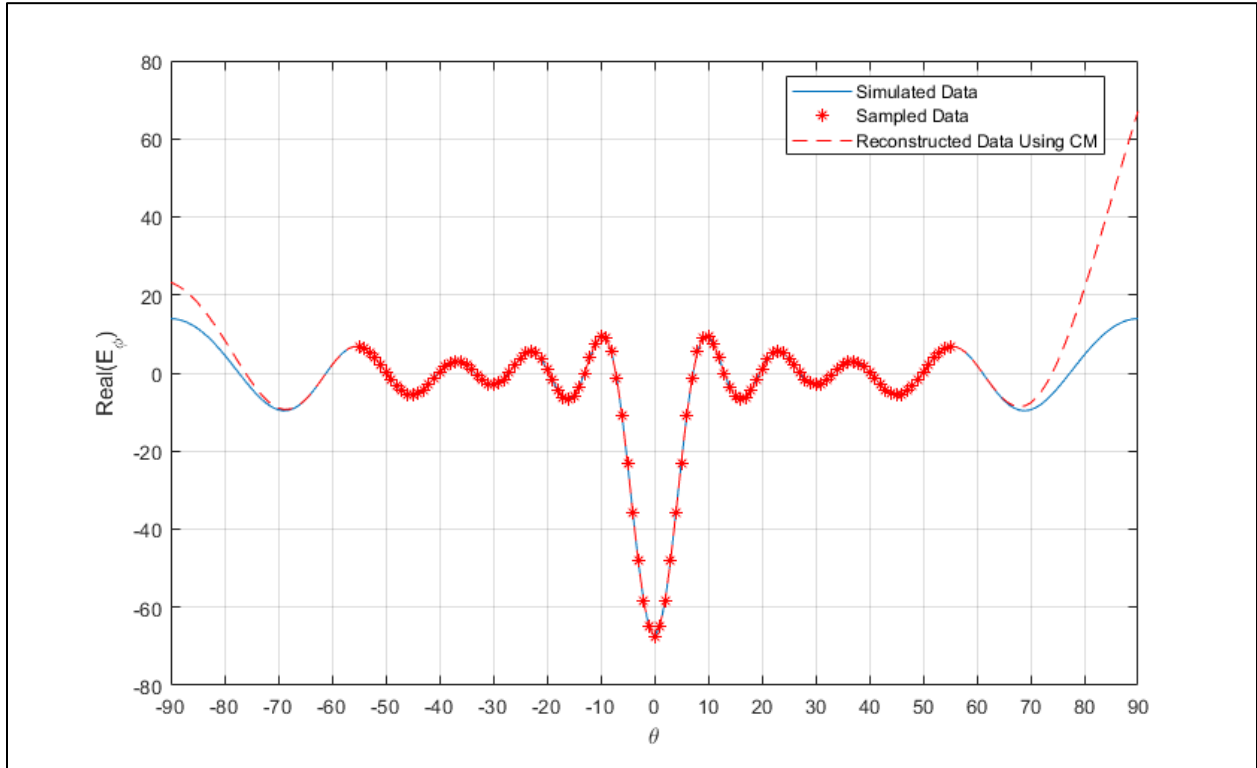


Figure 5.13. Extrapolation of the real part of the far-field radiation pattern

The MSE of the extrapolation of the real part of the far-field radiation pattern was calculated to be 0.6619. This is a significant increase in error of approximately 2159% over the interpolation of the same pattern which had an MSE of 0.0293.

The imaginary part of the far-field radiation pattern was extrapolated next. The singular values were once again evaluated to determine the optimal rank of the data matrix and the orders of the numerator and denominator polynomials. The distribution of the singular values is shown in figure 5.14.

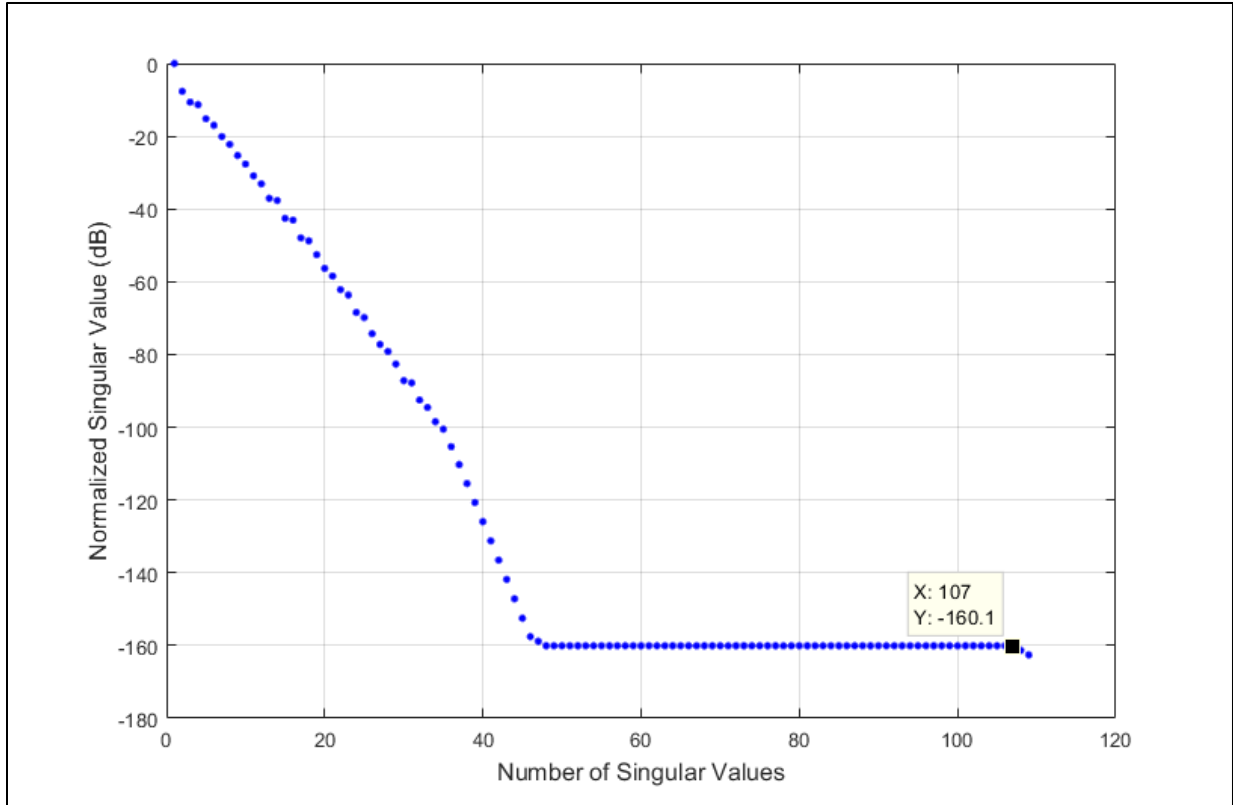


Figure 5.14. Distribution of the singular values for the imaginary part of the far-field pattern

From figure 5.14 and the error analysis code it was determined that 107 singular values were needed for the best accuracy of the extrapolation. A rank of 107 leads to a numerator polynomial order of 54 and a denominator polynomial order of 55. The resulting extrapolation of the imaginary part of the far-field is shown in figure 5.15.

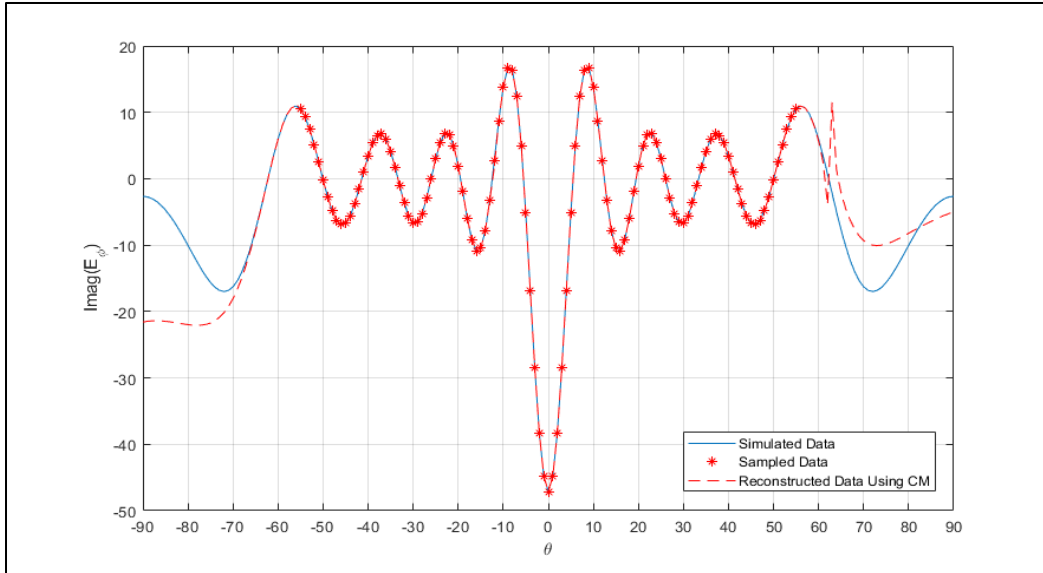


Figure 5.15. Extrapolation of the imaginary part of the far-field radiation pattern

The MSE of the extrapolation of the imaginary part of the far-field radiation pattern was calculated to be 0.4149. Extrapolating the imaginary part of the far-field instead of interpolating led to an increase in error of approximately 2355%. Next, the extrapolated real and imaginary parts were combined to plot the magnitude of the far-field radiation pattern. Figure 5.16 shows the extrapolated normalized magnitude of the far-field pattern.

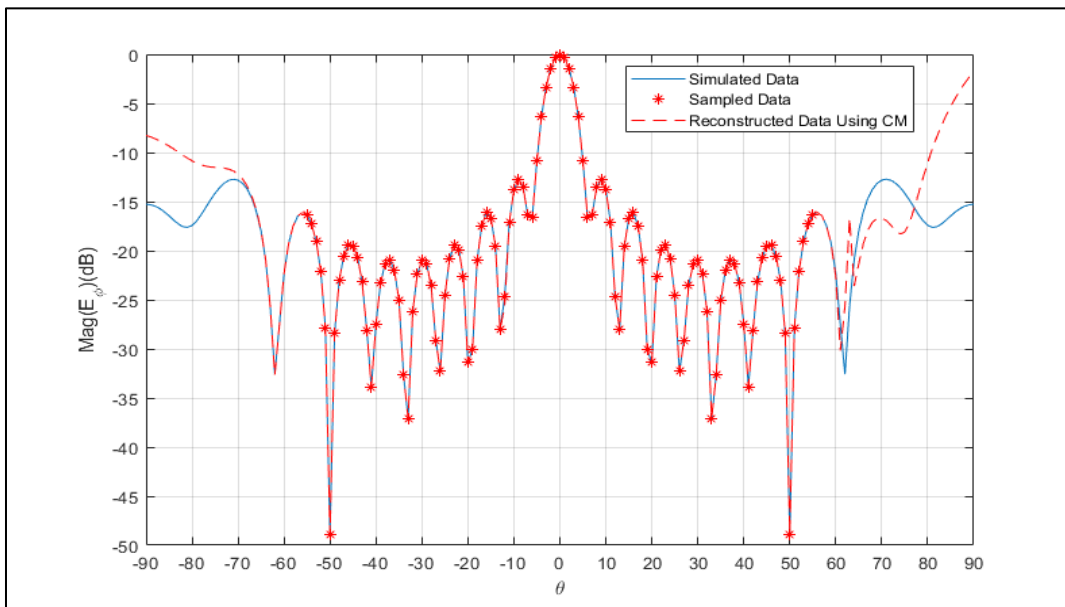


Figure 5.16. Comparison between original and extrapolated far-field

From figure 5.11 and figure 5.16, it is very easy to see that interpolation with the Cauchy method provides much better accuracy in reconstructing the missing far-field data than extrapolation. The MSE of the extrapolation was determined to be 0.1700 which is approximately a 1249% increase in error compared to the interpolation of the far-field radiation pattern.

5.1.3 Near-Field to Far-Field Transformation of a Zenith-Directed Parabolic Reflector

The next two examples showcase the real-world applications of the Cauchy method. For the first example, the goal was to interpolate the “hole” of the near-field measurement of a parabolic reflector antenna. The “hole” that is being referred to is a spherical area where a near-field probe is unable to reach to accurately obtain antenna measurements. The parabolic reflector antenna was simulated using FEKO, a Method of Moments software package. This particular example had the hole placed at 65 degrees below the horizon (155 degrees from zenith) and extending to 180 degrees from zenith in theta and swept 360 degrees in phi. Figure 5.17 below illustrates the design and orientation of the zenith-directed parabolic reflector along with the spherical near-field boundaries.

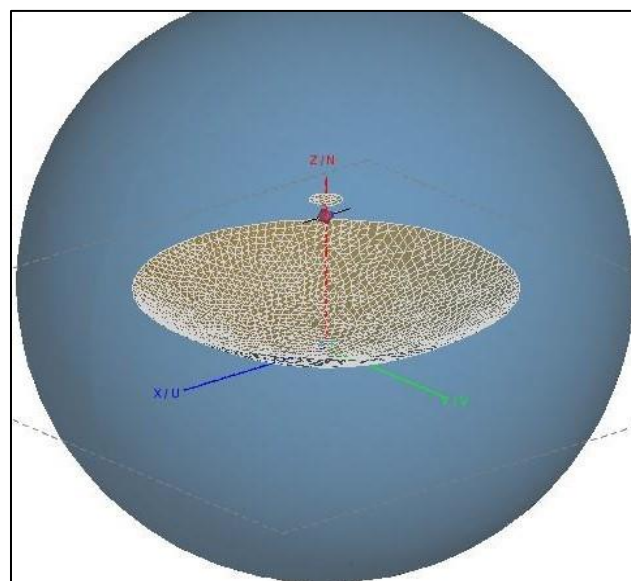


Figure 5.17. Zenith-directed parabolic reflector with a spherical near-field boundary

The blue sphere in figure 5.17 represents the near-field boundary where simulation measurements were taken. The theta and phi component of the electric near-field was sampled at 1 degree increments in theta for a total of 181 samples and at 1 degree increments in phi for a total of 361 samples. After simulation, the data was exported to MATLAB to be interpolated using the Cauchy method. In MATLAB the near-field data was re-organized so that at each cut of phi, 360 degrees of data in theta was available. For example, the near-field data at $\varphi = 0$ degrees and $\varphi = 180$ degrees was concatenated together to produce a full 360 degree circular cut of near-field data in theta. The data from +155 degrees to +180 degrees and -155 degrees to -180 degrees was removed to create the hole of missing data. The data from 0 degrees (zenith) to +154 degrees and from 0 degrees to -154 degrees was sampled ($N = 310$ samples). After interpolation, the estimated near-field data was re-assembled to match the form and organization of the original data and then it was transformed to the far-field using a spherical near-field to far-field transformation code written in FORTRAN.

There were four components of the near-field that were interpolated, the real and imaginary parts of the theta component and the real and imaginary parts of the phi component. In total 720 near-field vectors were interpolated; four component near-fields with 180 cuts in phi. For conciseness, we will only present eight of the 720 total results. We will look at the interpolation of the real and imaginary parts of the theta and phi components of the near field at the phi cuts of $\varphi = 0$ and $\varphi = 90$. In addition to those eight plots, we will also present the far-field that results from the spherical near-field to far-field transformation.

We will first look at the real and imaginary parts of the theta component of the near-field (E_θ) at $\varphi = 0$ degrees. From their singular value distributions and the error analysis code, it was determined that 45 and 65 singular values were needed to sufficiently interpolate the real and

imaginary parts respectively. This leads to a polynomial order of 22 and 23 for the numerator and denominator respectively for the real part, and a numerator and denominator polynomial order of 32 and 33 for the imaginary part. Figure 5.18 and 5.19 shows the result of the interpolation of the real and imaginary parts of E_θ at $\varphi = 0$ degrees.

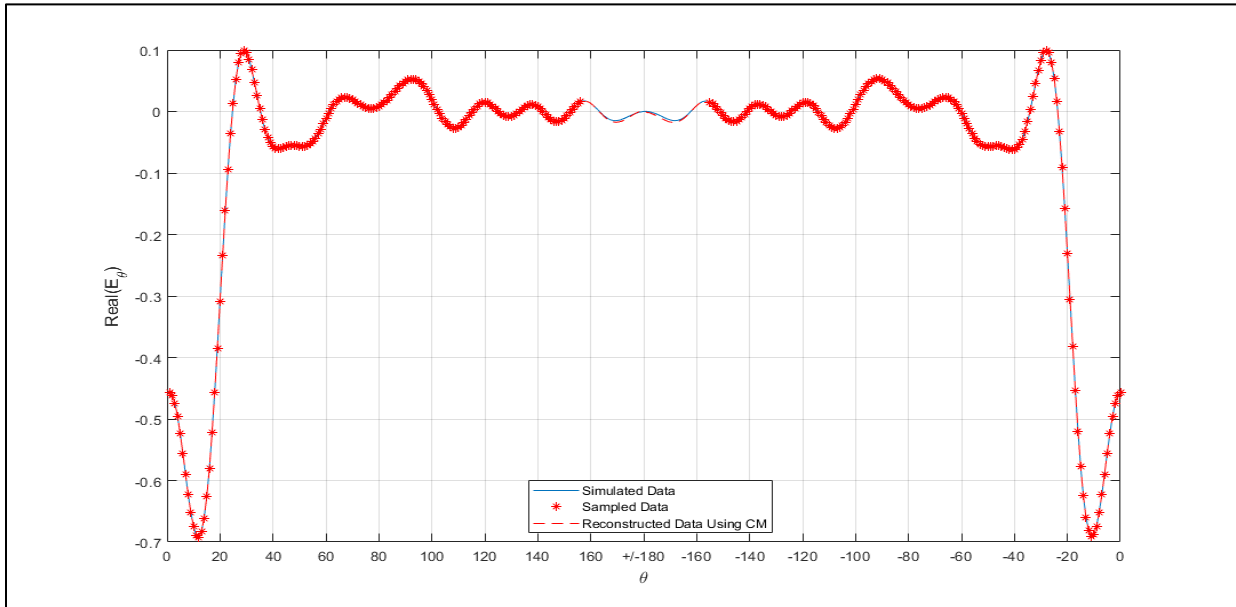


Figure 5.18. Interpolation of the real part of E_θ at $\varphi = 0$ degrees

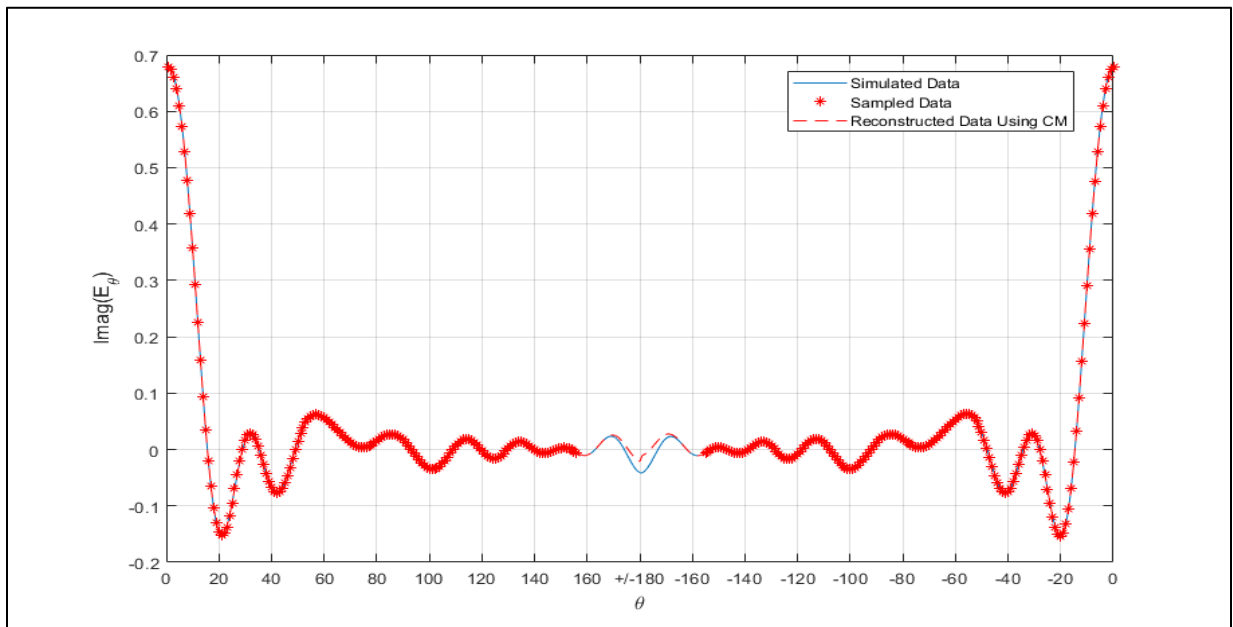


Figure 5.19. Interpolation of the imaginary part of E_θ at $\varphi = 0$ degrees

The MSE of the interpolation of the real part of E_θ was calculated to be 0.0036 and for the imaginary part it was 0.0392.

Next, will look at the real and imaginary parts of E_θ at $\varphi = 90$ degrees. The number of singular values needed to accurately interpolate the real and imaginary parts was determined to be 71 and 61 respectively. Once again, these values correlate to the optimal rank of the input data matrix and are used to determine the optimal orders of the numerator and denominator polynomials. The order of the numerator and denominator polynomials for the real part of E_θ was calculated to be 35 and 36 respectively and for the imaginary part they were determined to be 30 and 31 respectively. Figures 5.20 and 5.21 show the results of the interpolation using the Cauchy method for the real and imaginary parts of E_θ at $\varphi = 90$ degrees respectively.

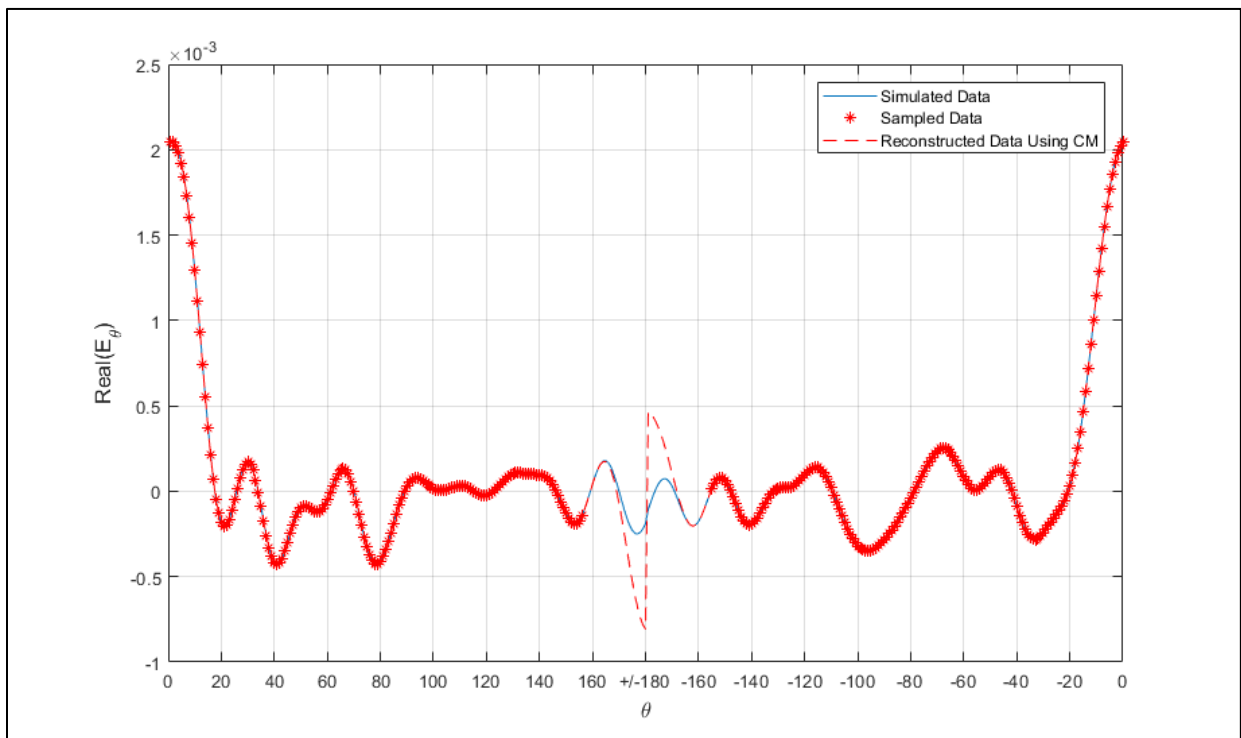


Figure 5.20. Interpolation of the real part of E_θ at $\varphi = 90$ degrees

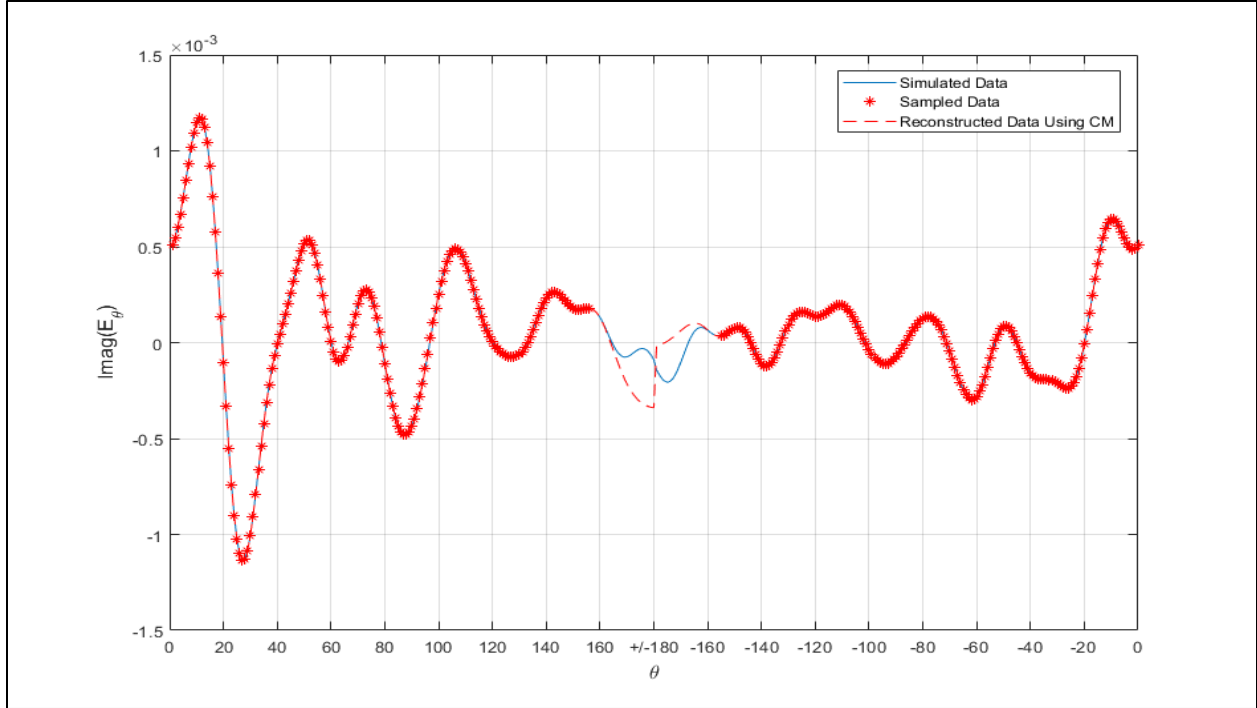


Figure 5.21. Interpolation of the imaginary part of E_θ at $\varphi = 90$ degrees

By inspection, it is easy to see that the interpolation performance is worse for the $\varphi = 90$ degree cut. This is due to the fact that the amplitude of the near-field is on the order of 10^{-3} and interpolating at those levels is less accurate. Also, the fields are not symmetric. As we will see, this error does not contribute much to the final far-field result after the spherical near-field to far-field transformation. The MSE of the interpolation of the real part of E_θ was calculated to be 0.1835 and for the imaginary part it was 0.2024.

The real and imaginary parts of the phi component of the near-field (E_φ) at $\varphi = 0$ degrees will be presented next. Once again, the number of singular values needed to sufficiently interpolate the real and imaginary parts was determined to be 53 and 35 respectively. From these values the numerator and denominator polynomial orders for the real part of E_φ was calculated to be 26 and 27 respectively and for the imaginary part they were calculated to be 17 and 18

respectively. Figure 5.22 and 5.23 show the results of the interpolation for the real and imaginary parts of E_φ respectively.

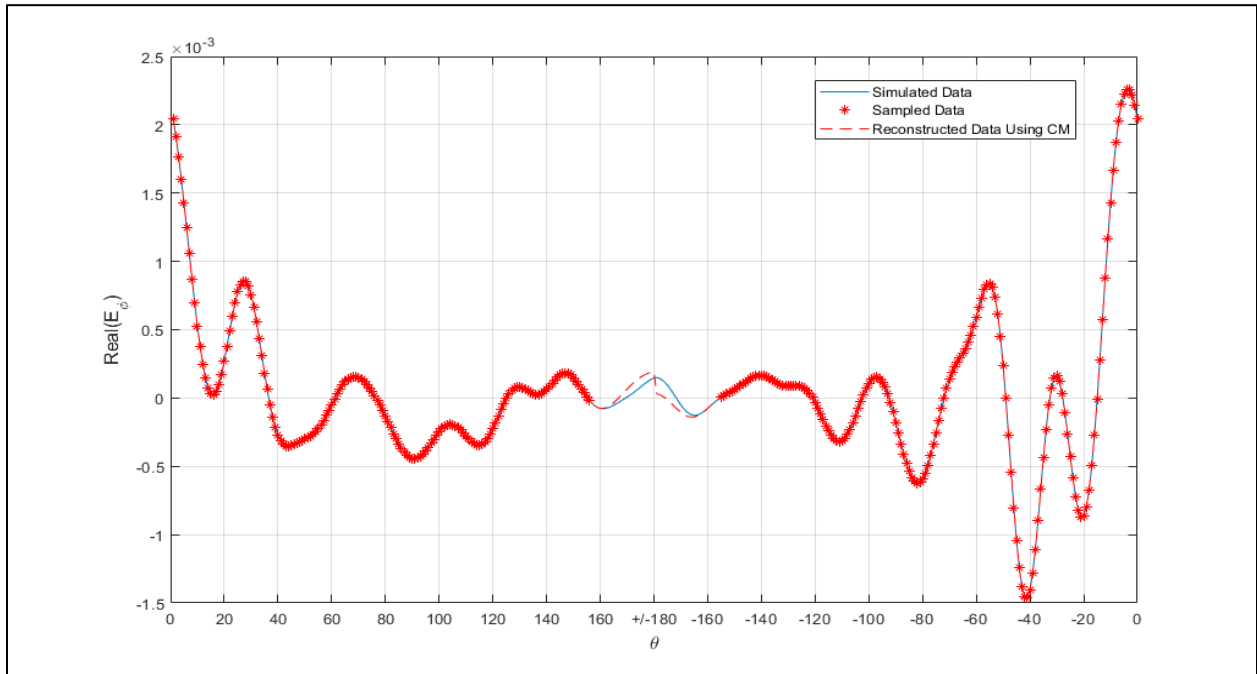


Figure 5.22. Interpolation of the real part of E_φ at $\varphi = 0$ degrees

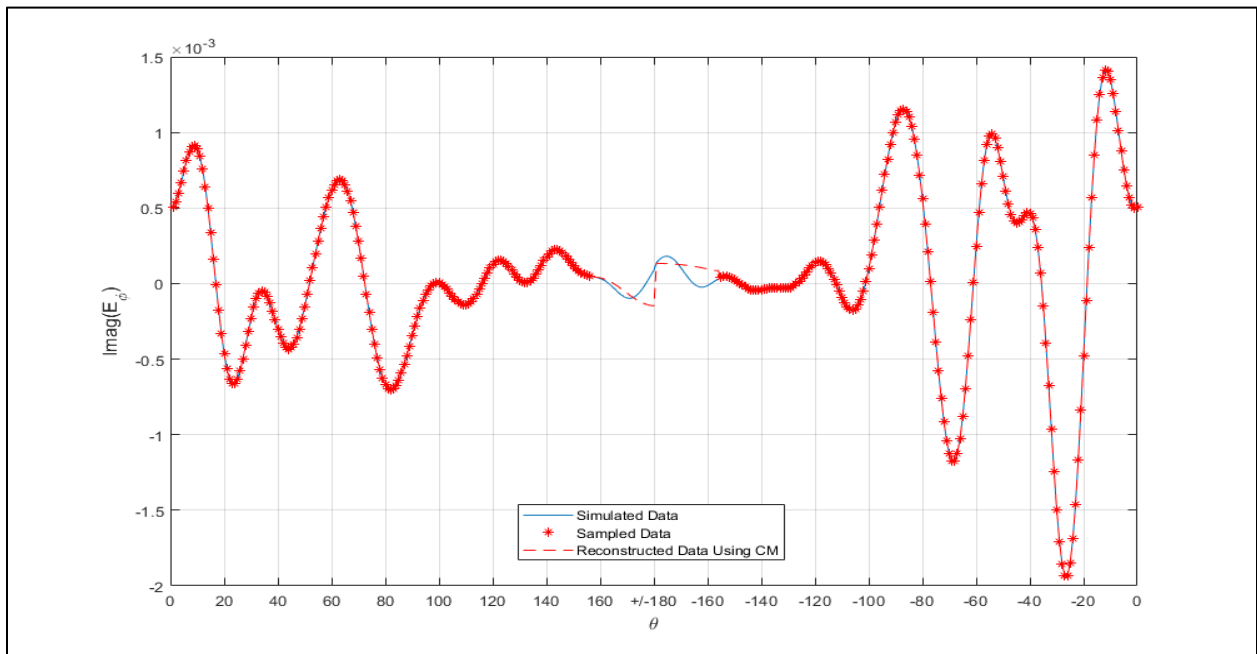


Figure 5.23. Interpolation of the imaginary part of E_φ at $\varphi = 0$ degrees

The MSE's of the interpolation of the real and imaginary parts of E_φ at $\varphi = 0$ degrees were found to be 0.0377 and 0.0663 respectively.

Finally, we will look at the interpolation of the real and imaginary parts of E_φ at $\varphi = 90$ degrees. The optimal number of singular values was determined to be 57 for the real part and 67 for the imaginary part. This led to numerator and denominator polynomial orders of 28 and 29 for the real part of E_φ , and orders of 33 and 34 for the imaginary part. Figures 5.24 and 5.25 shows the results of the interpolation respectively.

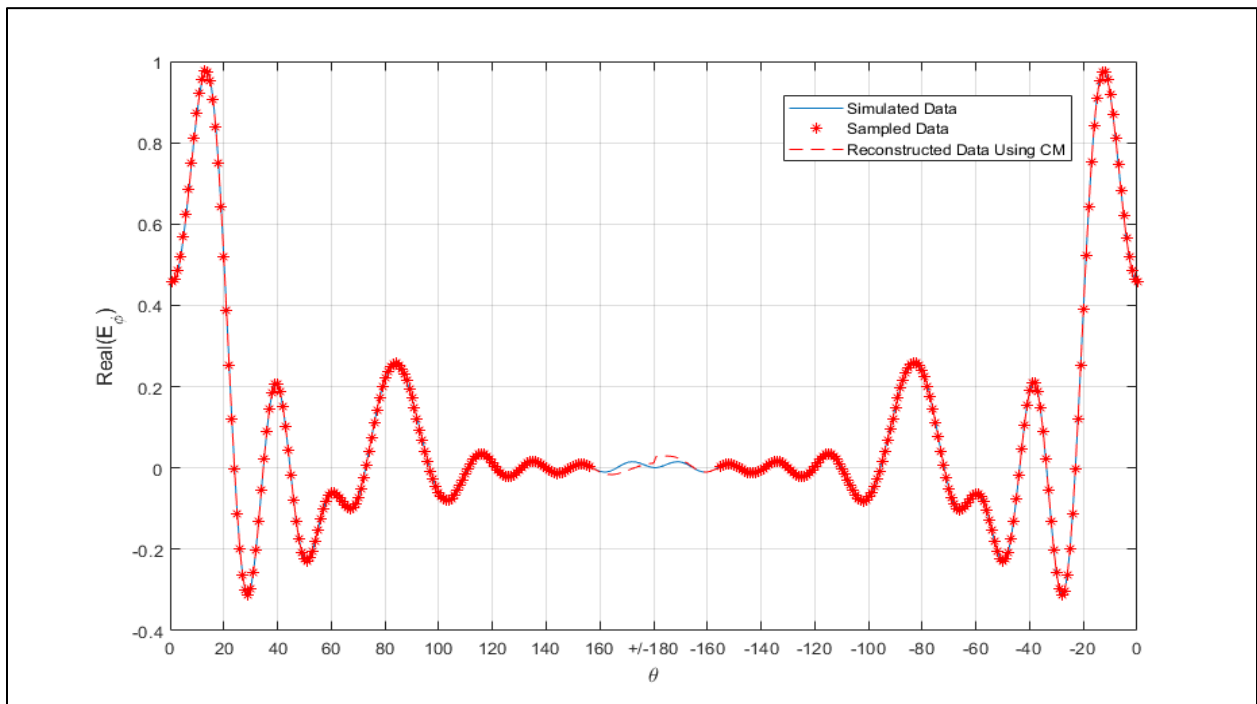


Figure 5.24. Interpolation of the real part of E_φ at $\varphi = 90$ degrees

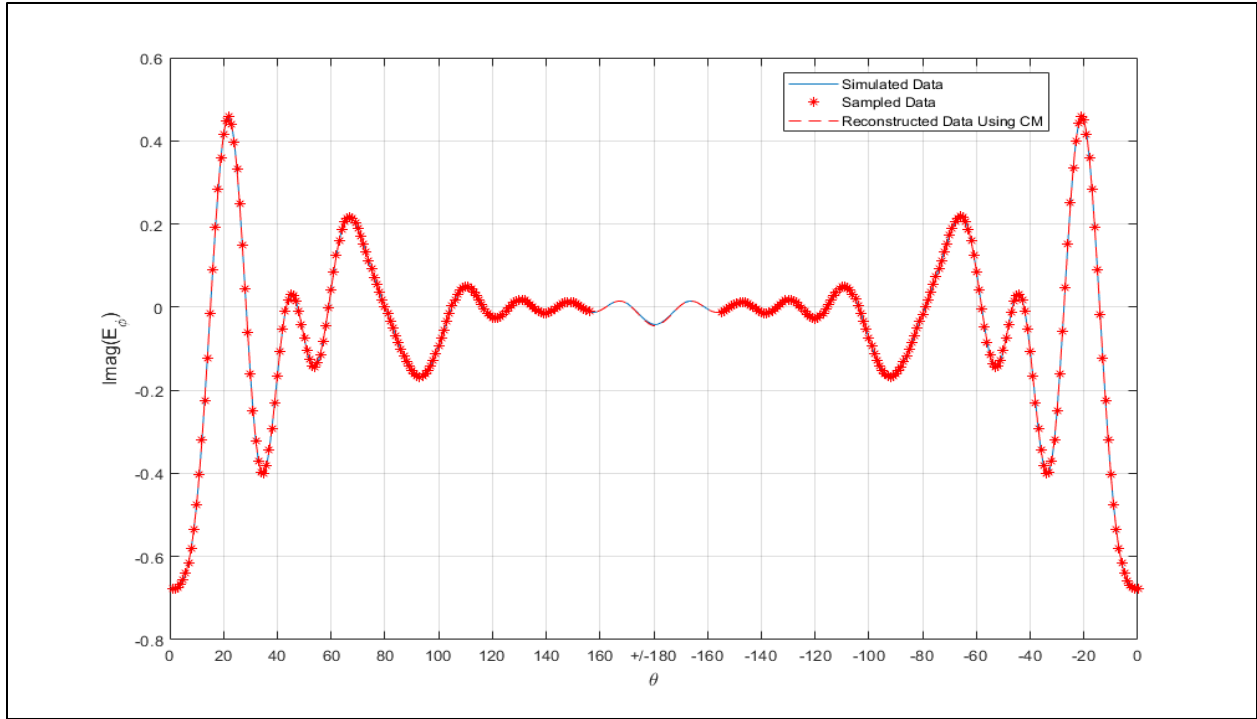


Figure 5.25. Interpolation of the imaginary part of E_ϕ at $\phi = 90$ degrees

The MSE was calculated to be 0.0161 for the interpolation of the real part and 0.0030 for the imaginary part.

After all 720 components of the near-field were interpolated, the data was then used in a spherical near-field to far-field transformation. Figure 5.26 shows the resulting far-field ($\phi = 0$ cut) with the “hole” interpolated including a comparison to the simulated far-field without the hole.

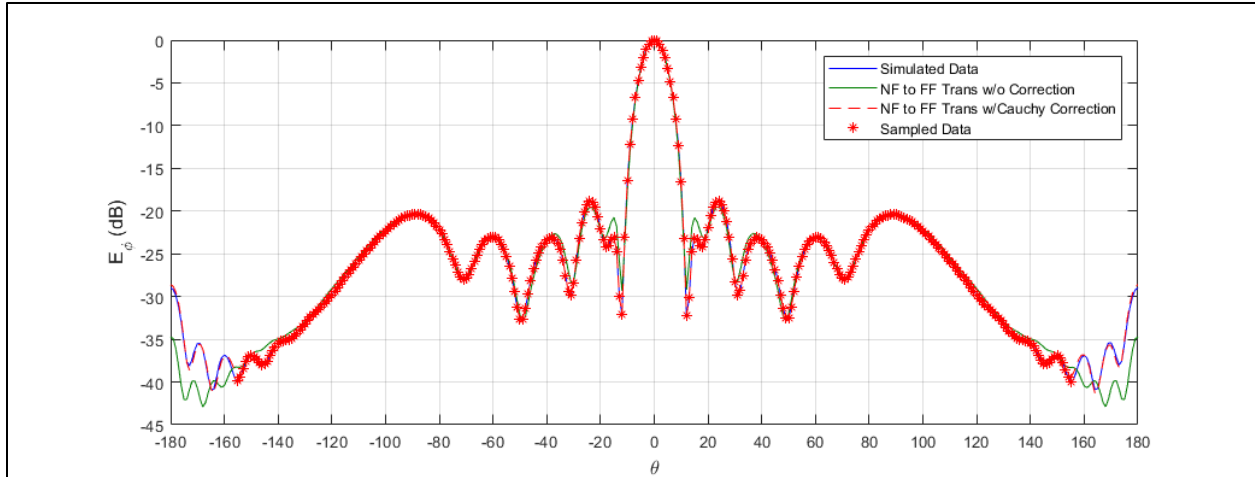


Figure 5.26. Comparison between original far-field and interpolated far-field

From figure 5.26, we can say that it is possible to interpolate the missing data of near-field measurements spanning 50 degrees using the Cauchy method and then construct an accurate representation of the far-field using a spherical near-field to far-field transformation. The MSE of the resulting far-field was calculated to be 0.0070. If we were to replace the hole of missing near-field data with zeroes, then the MSE would increase to 0.0644.

5.1.4 Near-Field to Far-Field Transformation of a Rotated Parabolic Reflector

For the final example, the zenith-directed reflector antenna introduced in the previous section was rotated clockwise 90 degrees. The location of the hole of missing data was kept the same. However, an interesting result of this antenna configuration is that the hole was able to be expanded significantly without increasing the error of interpolation. Instead of the missing data spanning 50 degrees like in the previous example, the hole of missing data was able to be expanded to 90 degrees with sufficient performance of interpolation. Figure 5.27 shows the rotated parabolic reflector antenna with the spherical near-field boundary where measurements were taken.

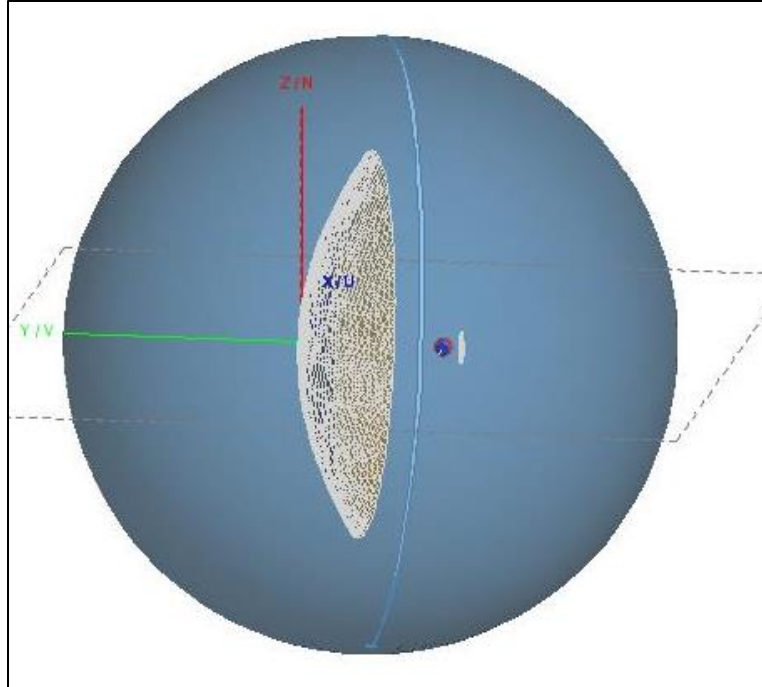


Figure 5.27. Rotated parabolic reflector antenna

Eight plots will be shown just like in the previous example; the real and imaginary parts of the theta and phi components of the near field (E_θ and E_ϕ) at $\varphi = 0$ and 90 degrees.

We will first look at the real and imaginary parts of E_θ at the cut of $\varphi = 0$ degrees. From the distribution of the singular values in conjunction with error analysis, it was determined that the optimal rank of the matrix $[C]$ is 55 for the real part and 27 for imaginary part. This leads to a numerator polynomial order of 27 and a denominator polynomial order of 28 for the real part. For the imaginary part, the numerator polynomial order was 13 and the denominator polynomial was 14. Figure 5.27 and 5.28 show the result of the interpolation of real and imaginary part of E_θ at $\varphi = 0$ degrees respectively.

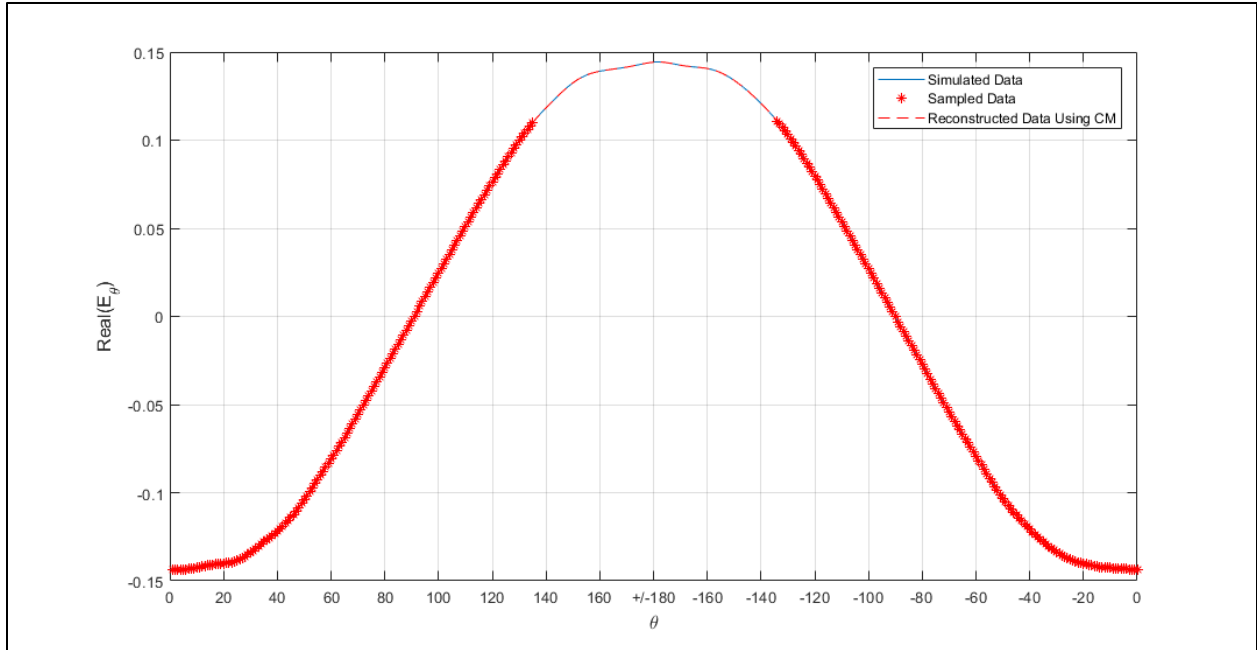


Figure 5.28. Interpolation of the real part of E_θ at $\varphi = 0$ degrees

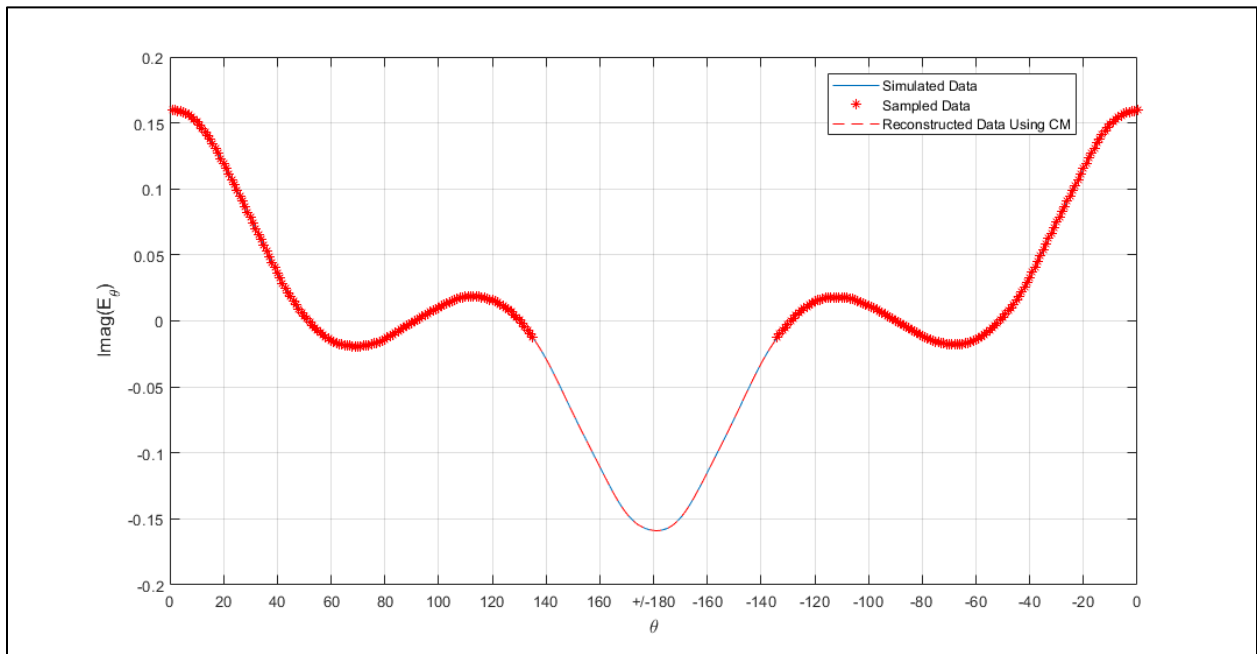


Figure 5.29. Interpolation of the imaginary part of E_θ at $\varphi = 0$ degrees

Comparing figures 5.28 and 5.29 to figures 5.18 and 5.19 we can see by inspection that the error of the interpolation is much less for the rotated case versus the zenith-directed case. The near-fields of the rotated antenna at this cut of φ are not as complex and are very nicely symmetric

which improves the accuracy of the Cauchy method greatly when interpolating. The MSE of interpolating the real part of E_θ was calculated to be 0.0036 and for the imaginary part it was calculated to be 0.0079.

Next, we will look at the interpolation of the real and imaginary parts of E_θ at the $\varphi = 90$ degree cut. This cut showed the worst performance of the Cauchy method out of all of the cuts of φ that were interpolated. We are dealing with very low amplitudes as well as near-field patterns that are not symmetric and for these reasons the Cauchy method did not perform well. Due to these reasons, the optimal number of singular values for the real part of E_θ was only 2. With an optimal rank of 2, this led to an interesting result for the optimal orders of the numerator and denominator polynomial. The order of the numerator polynomial was found to be 0 and the order of the denominator polynomial was found to be 1, therefore an approximate solution was unable to be found. For the interpolation of the imaginary part which performed slightly better, the optimal number of singular values was 65. With a rank of 65, the optimal orders of the numerator and denominator polynomial were calculated to be 32 and 33. Figures 5.30 and 5.31 show the result of interpolating the real and imaginary part of E_θ at $\varphi = 90$ degrees respectively.

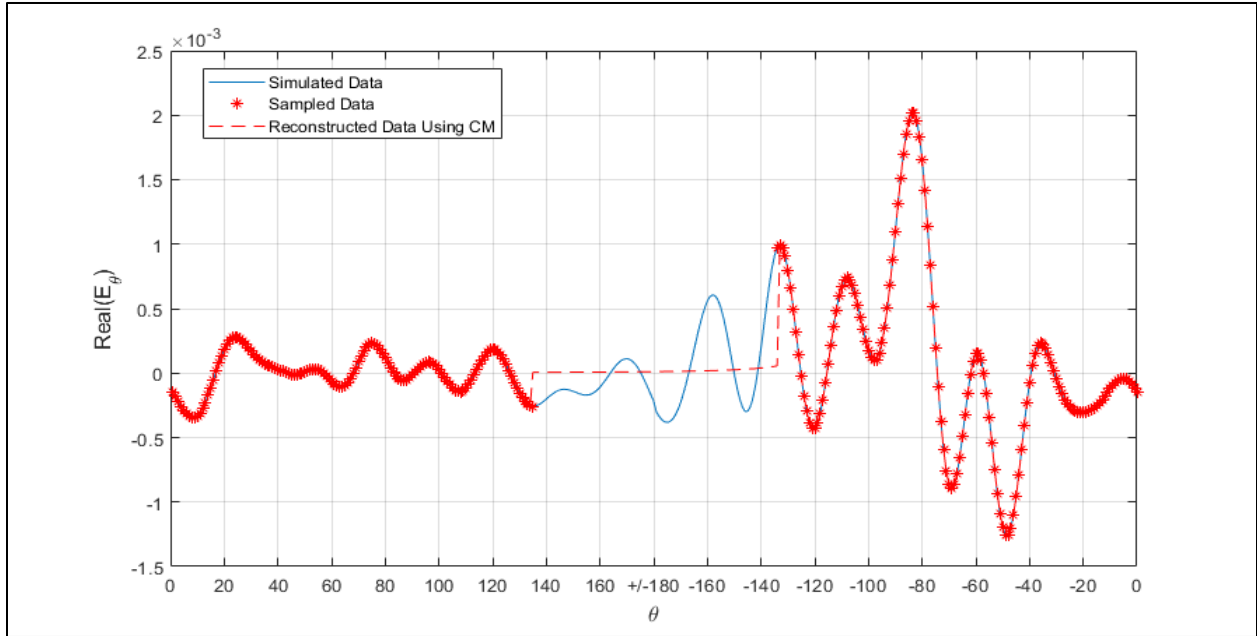


Figure 5.30. Interpolation of the real part of E_θ at $\varphi = 90$ degrees

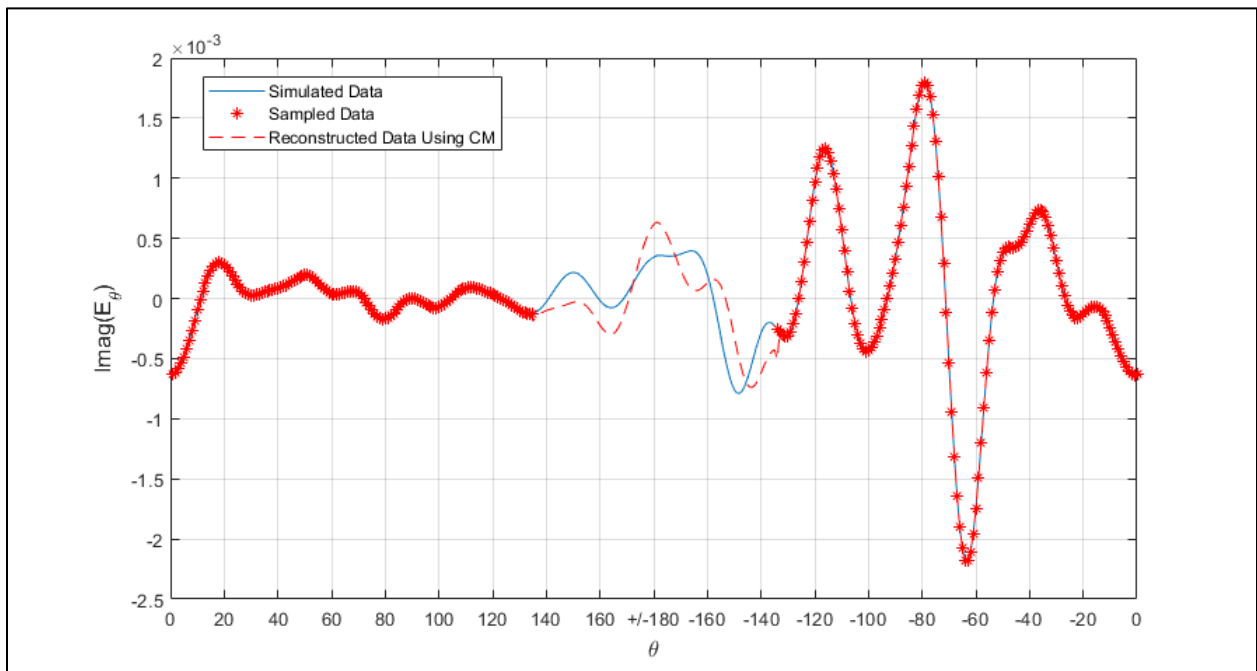


Figure 5.31. Interpolation of the imaginary part of E_θ at $\varphi = 90$ degrees

Due to the fact that the amplitude of the near-field at $\varphi = 90$ degrees is so small, these errors did not contribute significantly to the overall error of the far-field after the spherical near-field to far-

field transformation was applied. The MSE of the interpolation of the real part of E_θ was calculated to be 1.0748 and for the imaginary part it was calculated to be 0.6006.

The estimation of the real and imaginary parts of E_φ at the $\varphi = 0$ degree cut is shown next. The optimal rank, determined by the distribution of the singular values, was determined to be 63 for the real part of E_φ and 27 for the imaginary part. From the optimal rank of the input data matrix, the optimal order of the numerator polynomial was calculated to be 31 and 32 for the denominator polynomial for the real part of E_φ . The optimal order of the numerator and denominator polynomials of the imaginary part of E_φ was calculated to be 13 and 14 respectively. Figures 5.32 and 5.33 shows the interpolation results of the real and imaginary parts of E_φ respectively.

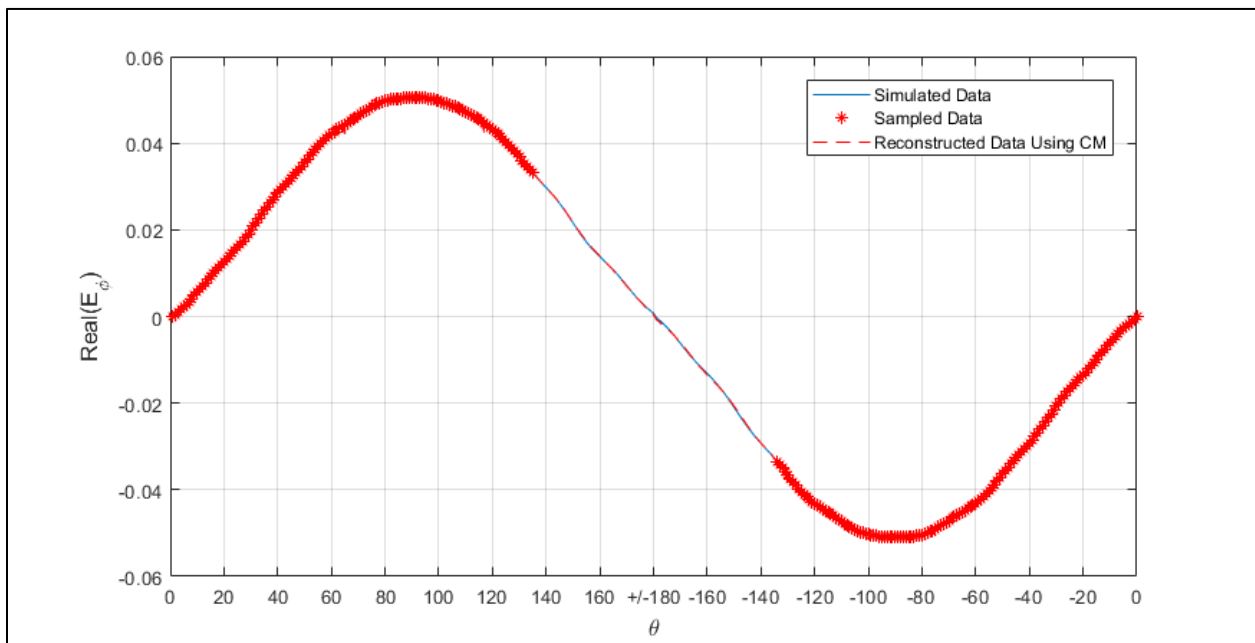


Figure 5.32. Interpolation of the real part of E_φ at $\varphi = 0$ degrees

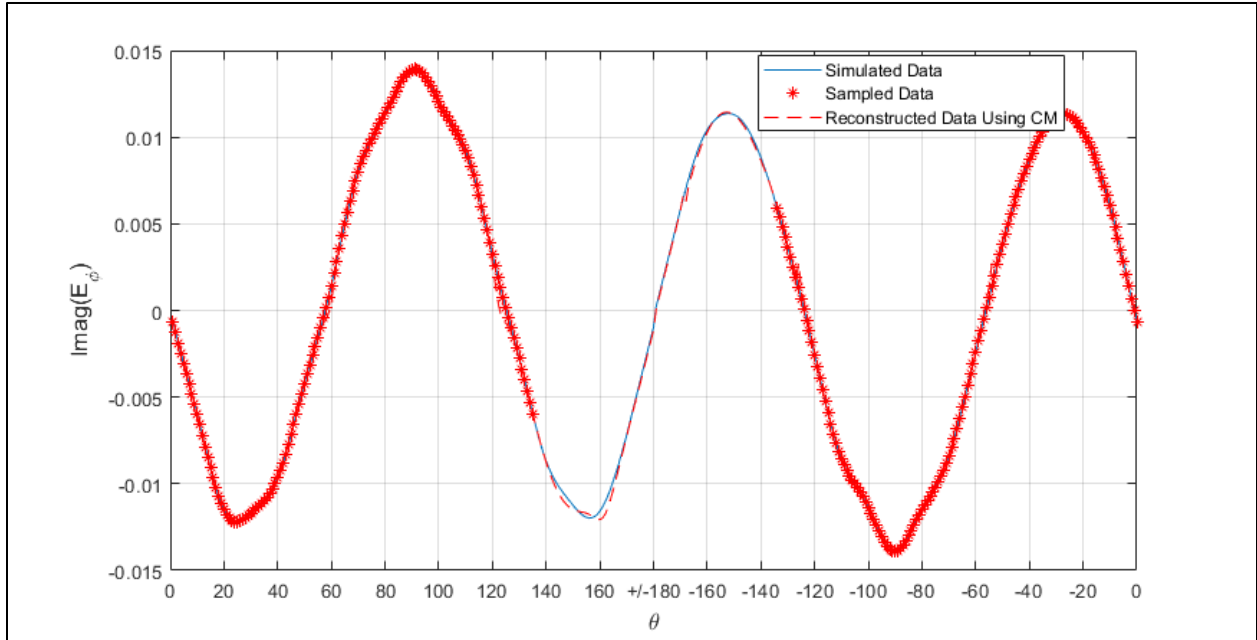


Figure 5.33. Interpolation of the imaginary part of E_φ at $\varphi = 0$ degrees

The interpolation of the real part of E_φ had an MSE of 0.0075 and the interpolation of the imaginary part had an MSE of 0.0304.

For the last set of plots, we will look at the interpolation of the real and imaginary parts of E_φ at the phi cut of 90 degrees. The optimal number of singular values and hence the optimal rank of the input data matrix was determined to be 53 for the real part and 47 for the imaginary part. With these values, the optimal orders of the numerator and denominator polynomials were calculated to be 26 and 27 respectively for the real part and 23 and 24 for the imaginary part. Figures 5.34 and 5.35 show the results of the interpolation of the real and imaginary part of E_φ at $\varphi = 90$ degrees respectively.

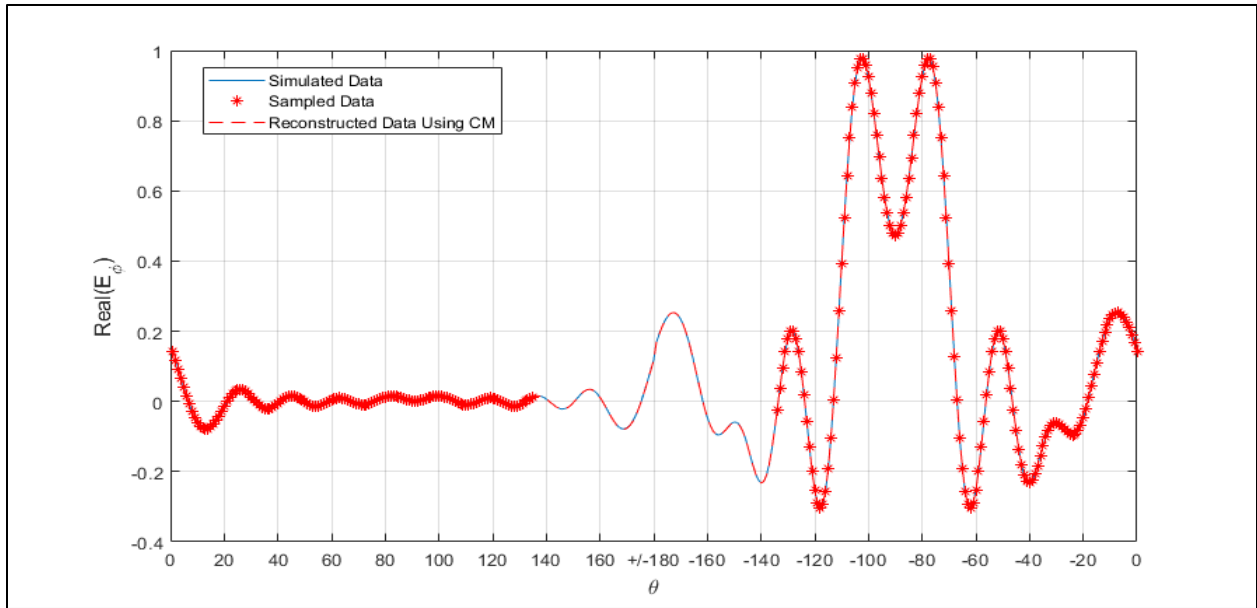


Figure 5.34. Interpolation of the real part of E_φ at $\varphi = 90$ degrees

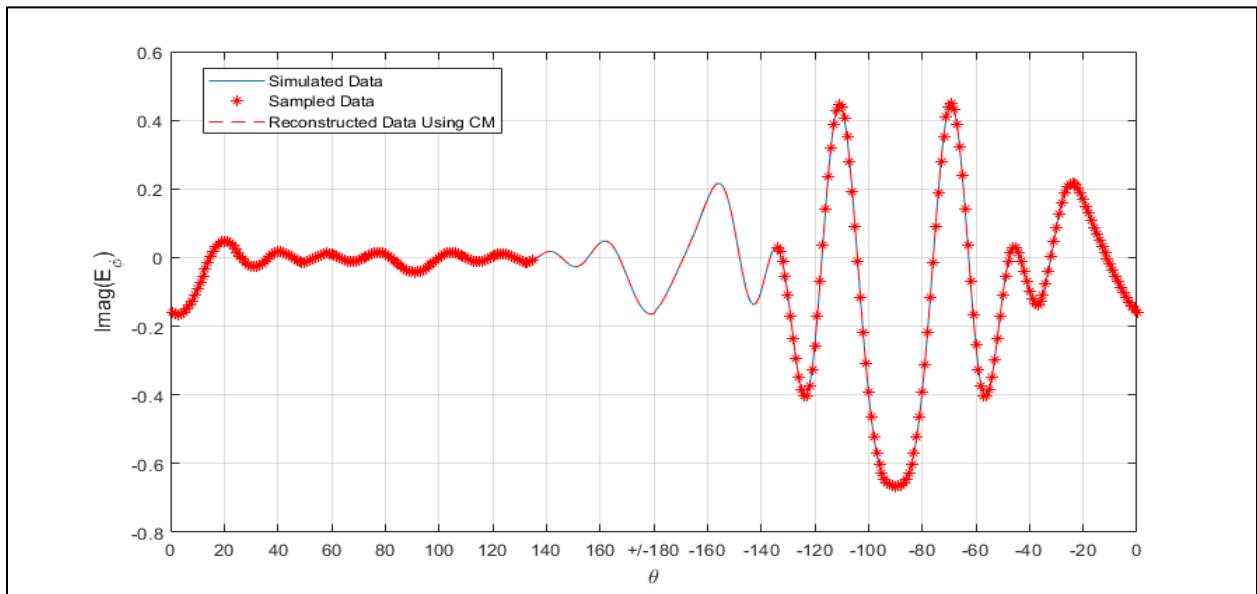


Figure 5.35. Interpolation of the imaginary part of E_φ at $\varphi = 90$ degrees

The MSE of the interpolation of the real part was calculated to be $9.5767e-04$ and 0.0015 for the imaginary part.

After the real and imaginary parts of the theta and phi components of the near-field at each cut of phi were interpolated, the data was then used in a spherical near-field to far-field transformation. Figure 5.36 shows the resulting far-field at $\varphi = 0$ degrees.

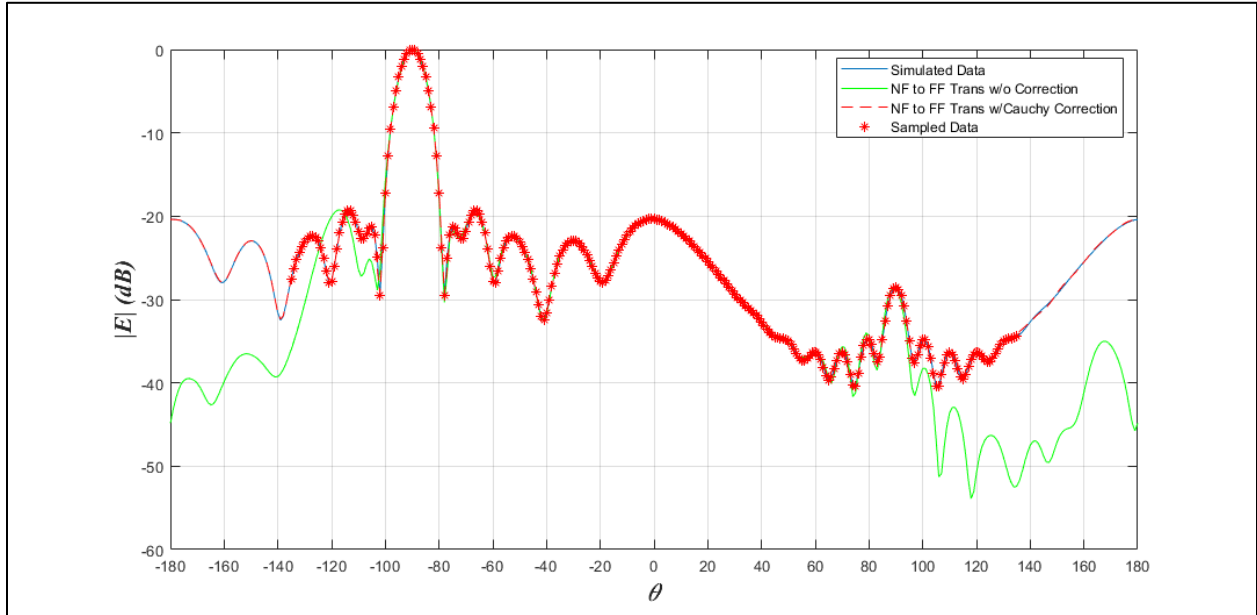


Figure 5.36. Comparison between original far-field and interpolated far-field

From figure 5.36, the solid blue line represents the simulated far-field, the dashed red line represents the result of transforming the near-field with the hole interpolated to the far-field, and the red asterisks represent the sampled data. The solid green line shows the result of the near-field to far-field transformation if the hole of the near-field was replaced with zeroes and then transformed. It can be easily shown that interpolating the missing data of the near-field using the Cauchy method before the transformation is much more accurate than just replacing the unknown data with zeroes. The overall MSE of the far-field using the interpolated near-field data was calculated to be 0.0080. If we were to replace the hole of missing near-field data with zeroes, then the MSE would increase to 0.3197.

Comparing the accuracy of the Cauchy method in interpolating the near-field of the zenith-directed and rotated parabolic reflector antenna's, it is obvious that the it performed much

better with the rotated antenna. We were even able to expand the hole of missing from 50 degrees to 90 degrees in theta for the rotated reflector case. If we take a look at the complexity of the missing data in both figures 5.26 and 5.36 we can see that the rotated case does not have as many peaks and nulls as the zenith-directed case. The individual near-field components are also much more complex in the zenith-directed case than the rotated case.

5.2 Matrix Pencil Method

5.2.1 $\lambda/2$ Dipole Antenna

The first example that we will be applying the Matrix Pencil method to is the same $\lambda/2$ dipole antenna that was introduced in section 5.1. The Matrix Pencil method approximates a function by first estimating the poles and residues and then forming a sum of complex exponentials. Throughout the study of the Matrix Pencil method, it was determined that this method performs best when the problem is of extrapolation. That is, the unknown data to be approximated is outside the range of the known data. Once again, this $\lambda/2$ dipole was designed to operate at a center frequency, f_c of 300 MHz. It was designed and simulated using HOBBIES electromagnetic solver software and the far-field data was exported to MATLAB where the Matrix Pencil method code was written. The dipole was simulated from -90 degrees to +90 degrees in theta and 0 to 360 degrees in phi, although only the $\varphi = 0$ degree cut was used for this extrapolation. Please refer to figure 5.1 for the geometry of the dipole.

Once the data was imported into MATLAB, the real and imaginary parts of the far-field were combined to form the complex far-field. This data was then sampled from -90 degrees to 0 degrees at three degree increments for a total of 31 samples ($N = 31$). We will choose the pencil parameter to be equal to $N/2 - 1$, which for 31 samples would be 14. From (4.5), the number of

singular values will be equal to $L + 1$. Figure 5.37 shows the distribution of singular values of the input sampled data.

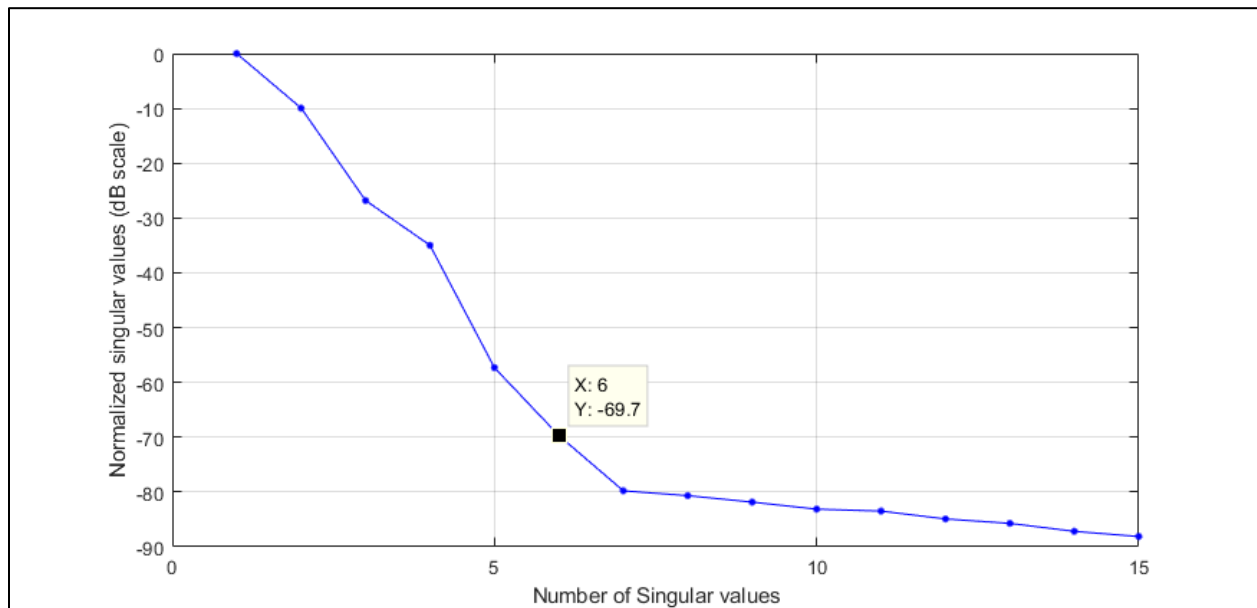


Figure 5.37. Distribution of singular values of the input data matrix $[Y]$

Since the number of accurate significant digits is equal to seven, we want the optimal number of singular values M to be closest to -70 dB. From figure 5.37 we can see that six singular values would satisfy this requirement. With the optimal number of singular values M now identified, we can use (4.17) through (4.23) to solve for the poles and residues of the system and therefore extrapolate the missing far-field data. Figure 5.38 shows the magnitude of the far-field along with the result of the extrapolation

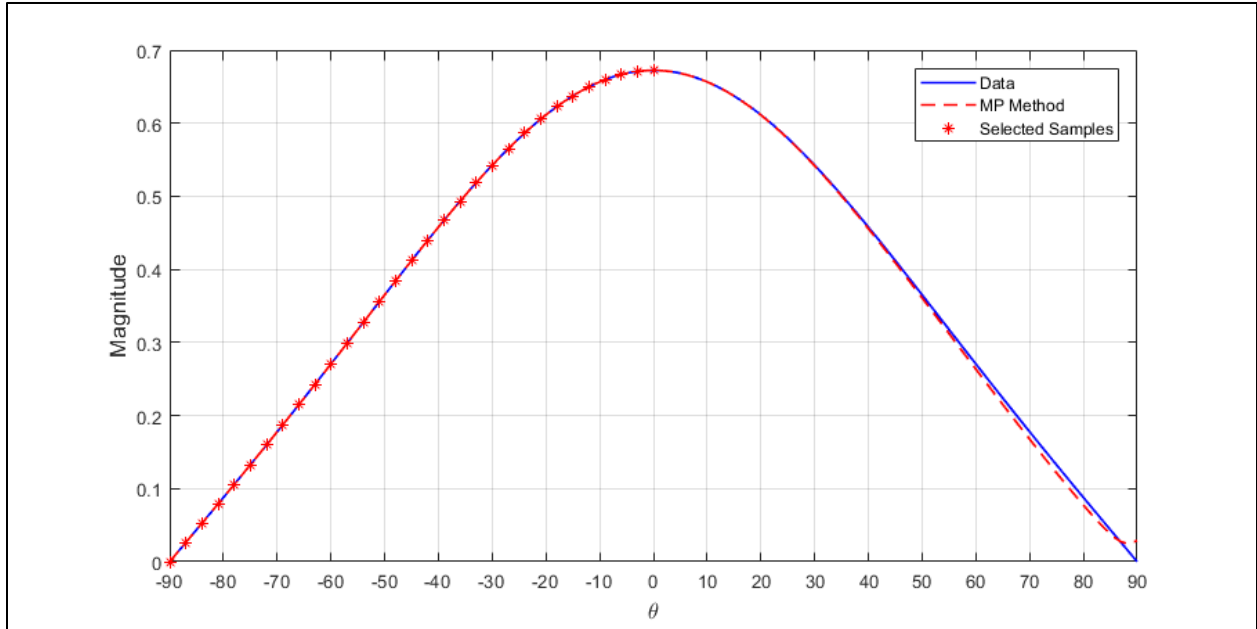


Figure 5.38. Result of extrapolating far-field of dipole antenna using MPM

We can quantify the accuracy of the Matrix Pencil method extrapolation by calculating the mean squared error (MSE) between the simulated and extrapolated data. The MSE was calculated to be 0.0106. Comparing these results to the Cauchy method results is a bit difficult because the Matrix Pencil method was unsuccessful in interpolating this data like the Cauchy method while the Cauchy method was unsuccessful in extrapolating the data like the Matrix Pencil method. However, we can say that the Cauchy method interpolation produced more accurate results with a smaller amount of sampled data. With that said, the Matrix Pencil method was still able to sufficiently extrapolate the data.

5.2.2 10x10 Linear $\lambda/2$ Dipole Array With λ Spacing

Next, we will look at the same 10x10 linear dipole array that was shown in section 5.1.2. Please refer to figure 5.4 for the geometry of the dipole array. All of the dimensions and simulation parameters are the same. After simulation the real and imaginary far-field data was

exported to MATLAB where it was extrapolated. The real and imaginary parts of the far-field were combined to create the complex far-field since the Matrix Pencil method performs best with complex data. The far-field was divided into two sections before being extrapolated. The first section included the far-field ranging from 0 degrees to 90 degrees in theta and the second section included the range from 0 degrees to -90 degrees in theta. However, since this far-field pattern is symmetric, similar performance is expected for both extrapolations. The extrapolation was first attempted by sampling the data from 0 degrees to +55 degrees for the first section and 0 to -55 degrees for the second section at every one degree, similar to that of the Cauchy method. The only difference being that this was set up to be an extrapolation problem instead of an interpolation problem like for the Cauchy method.

First, we will look at the singular value distribution of the input data matrix $[Y]$. Since we have 56 samples, the pencil parameter is 27 ($L = N/2 - 1$). Figure 5.39 shows the distribution of the 28 singular values ($L + 1$) when we sample from 0 degrees to +/- 55 degrees.

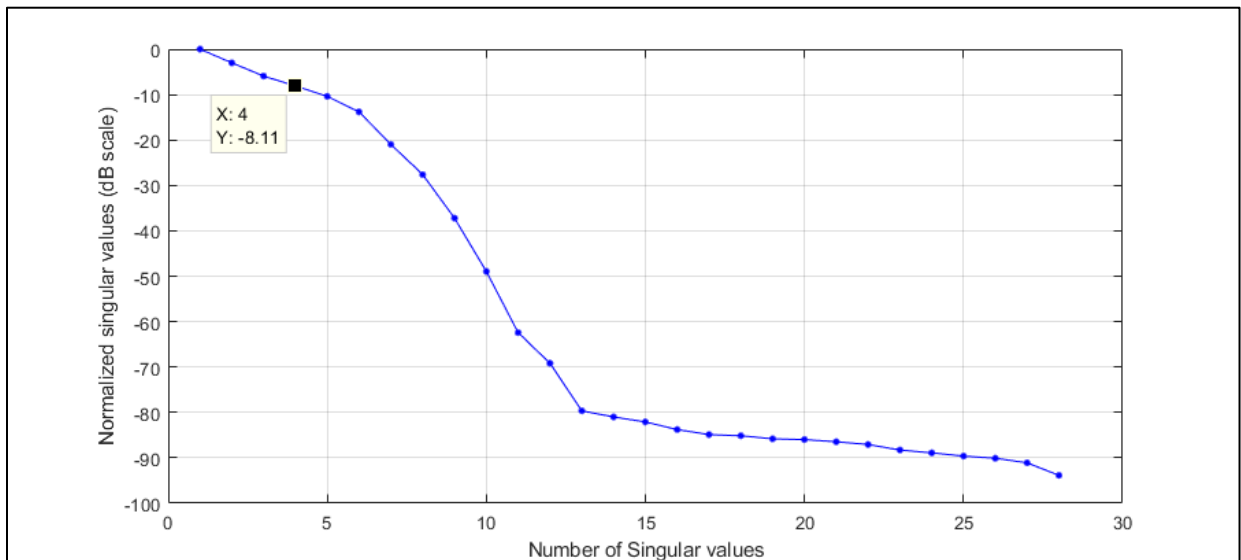


Figure 5.39. Singular value distribution of dipole array

As we can see from figure 5.39, the singular values do not decrease to the level needed for double precision data (-160 dB). In fact, using only 4 singular values led to the best performance of the extrapolation. However as will see in the result, the accuracy of extrapolation was poor compared to the accuracy of the interpolation using the Cauchy method. So, by setting M equal to the optimal number of singular values which is this case was 4, the extrapolation was performed. Figure 5.40 shows the result of the extrapolation with both sections of the extrapolation included.

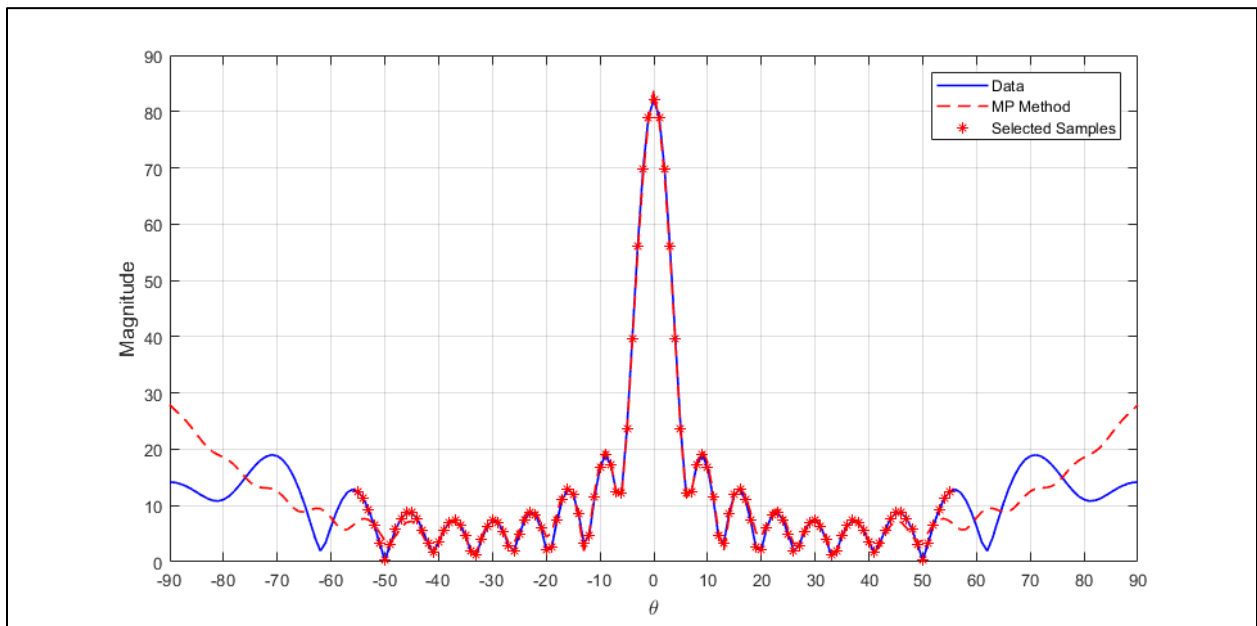


Figure 5.40. Comparison between original far-field and extrapolated far-field

Figure 5.41 shows the same extrapolation but of the normalized magnitude in dB scale.

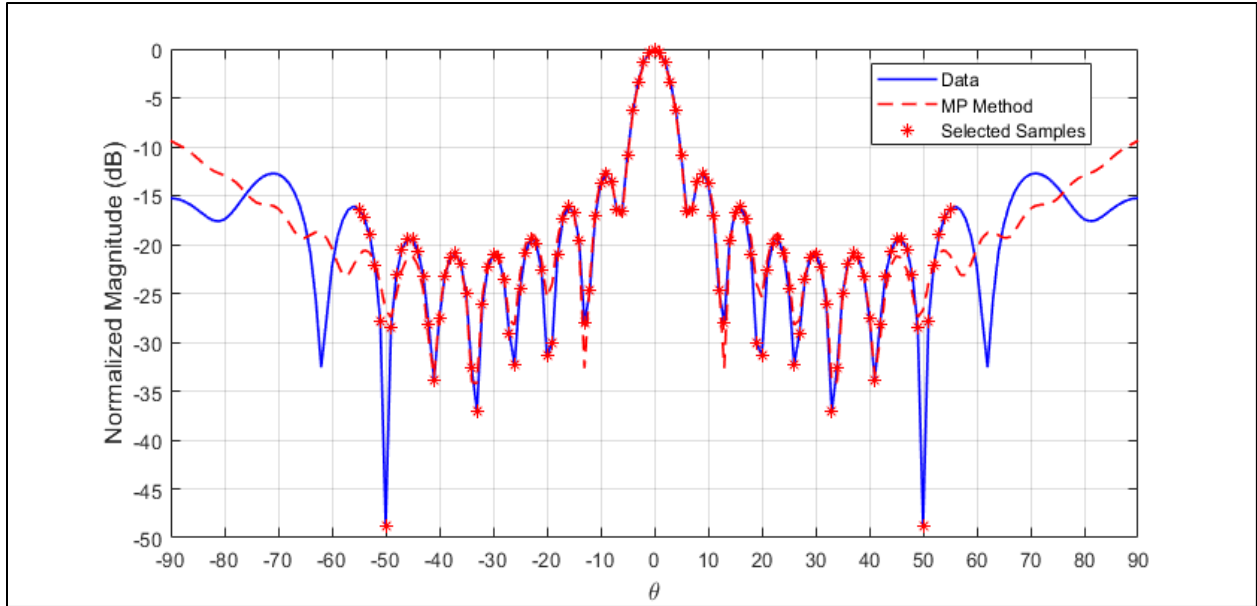


Figure 5.41. Comparison between original far-field and extrapolated far-field (dB)

From figures 5.40 and 5.41 we can see that the extrapolation performance is poor when the far-field is sampled from 0 to ± 55 degrees. The MSE of the extrapolation was calculated to be 0.2428 which is significantly worse than the Cauchy method interpolation MSE of 0.0126.

To improve the performance of the extrapolation, the number of samples had to be increased as well as the range of theta. The sampled data range was increased from 0 to ± 55 ($N = 56$) degrees to 0 to ± 75 degrees ($N = 76$). The far-field was then extrapolated from ± 76 degrees to ± 90 degrees. Figure 5.42 shows the result of the extrapolation with the increased number of samples.

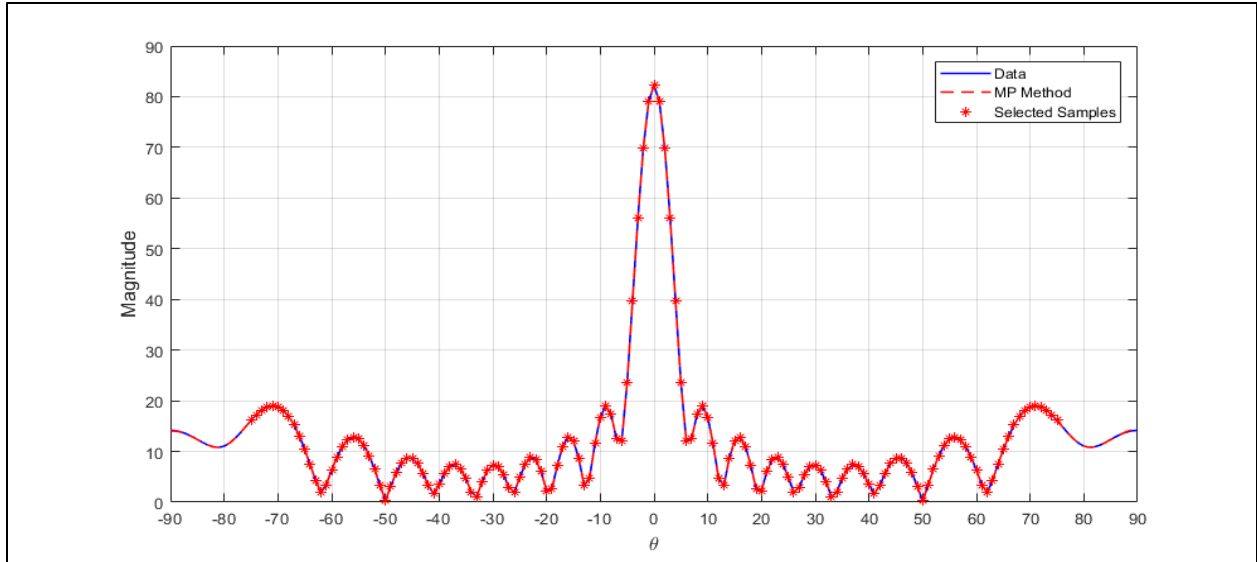


Figure 5.42. Comparison between original far-field and extrapolated far-field

Figure 5.43 shows the same extrapolation but of the normalized magnitude in dB scale.

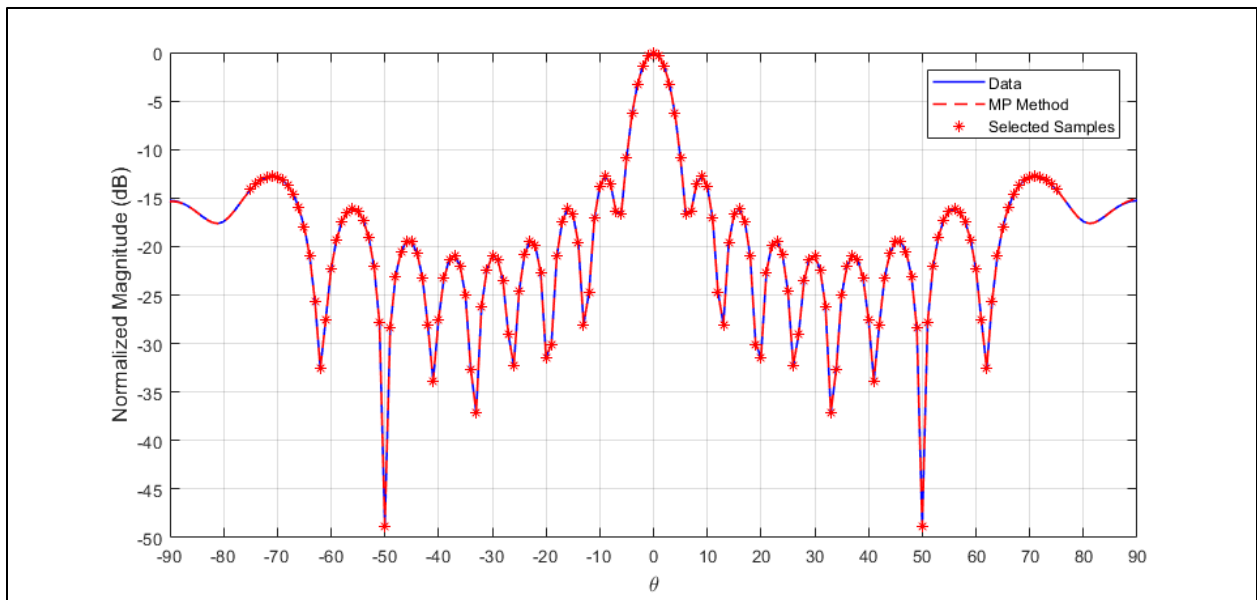


Figure 5.43. Comparison between original far-field and extrapolated far-field (dB)

The overall MSE of the extrapolation once the range of sampled data was increased, decreased to an acceptable level of 0.0106.

5.2.3 Near-Field to Far-Field Transformation of a Zenith-Directed Parabolic Reflector

We are now going to look again at the zenith-directed parabolic reflector that was introduced in section 5.1.3 with the Cauchy method. Similar to the previous Matrix Pencil method sections, we will be turning each approximation into one of extrapolation instead of interpolation. The simulation parameters and antenna geometry are exactly the same as described in section 5.1.3 and once again was designed and simulated using FEKO. Please refer to figure 5.17 for the design and orientation of the parabolic reflector antenna. In addition to changing the method of approximation from an interpolation to an extrapolation, we also must change the method of sampling to achieve the best performance with the Matrix Pencil method. For the Cauchy method, we sampled from 0 degrees to +/- 155 degrees. For the matrix pencil method, we will be sampling from +/-90 degrees to +/-135 degrees and extrapolating from +/- 135 degrees to +/-180 degrees ($N = 46$ samples).

Since there are over 720 pieces of data that make up the entire complex near-field of the simulated antenna, we will not be looking at every cut of phi. Just like for what was shown for the Cauchy method, we will be looking at the real and imaginary parts of E_θ and E_ϕ for the phi cuts of 0 and 90 degrees. Please note that while we will be looking at the real and imaginary parts separately, the algorithm of the Matrix Pencil method actually extrapolates the complex near-field, that is the real and imaginary parts combined. For ease of comparison to the results of the Cauchy method, the real and imaginary parts of near-field were extracted from the final extrapolation result.

First, we will look at the extrapolation results for the real and imaginary parts of E_θ at $\phi = 0$ degrees. Since the number of samples N is 46, the pencil parameter L is 22 ($L = N/2 - 1$). The optimal number of singular values M was determined to be 12 for the extrapolation of the

complex near-field of E_θ . Figure 5.44 and 5.45 show the resulting real and imaginary parts of the complex near-field of E_θ at $\varphi = 0$ degrees.

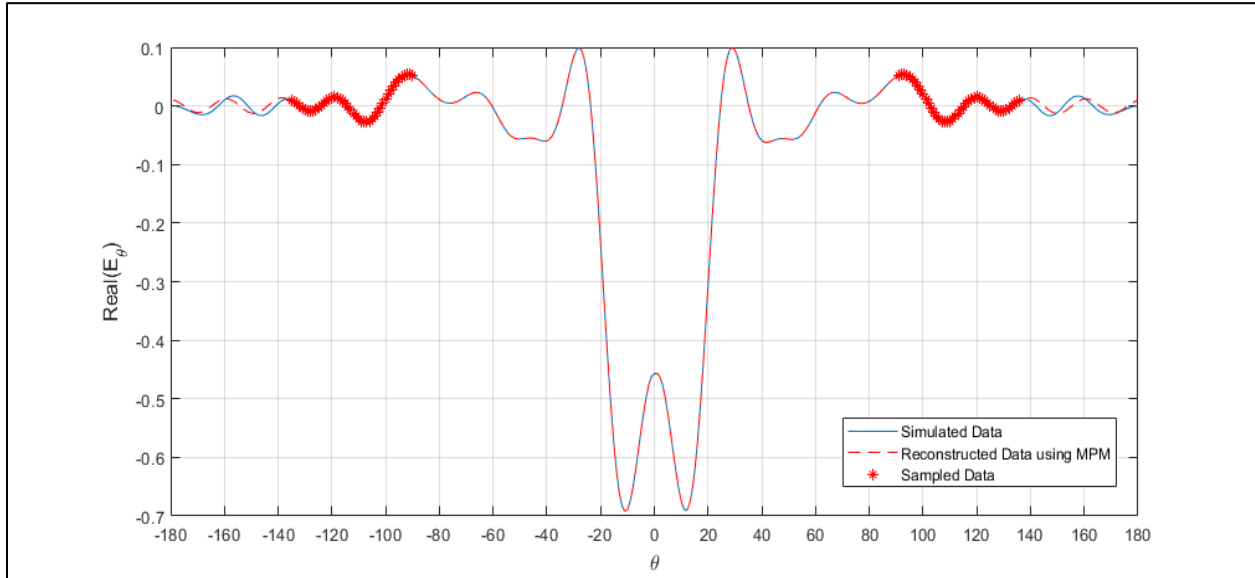


Figure 5.44. Extrapolation of the real part of E_θ at $\varphi = 0$ degrees

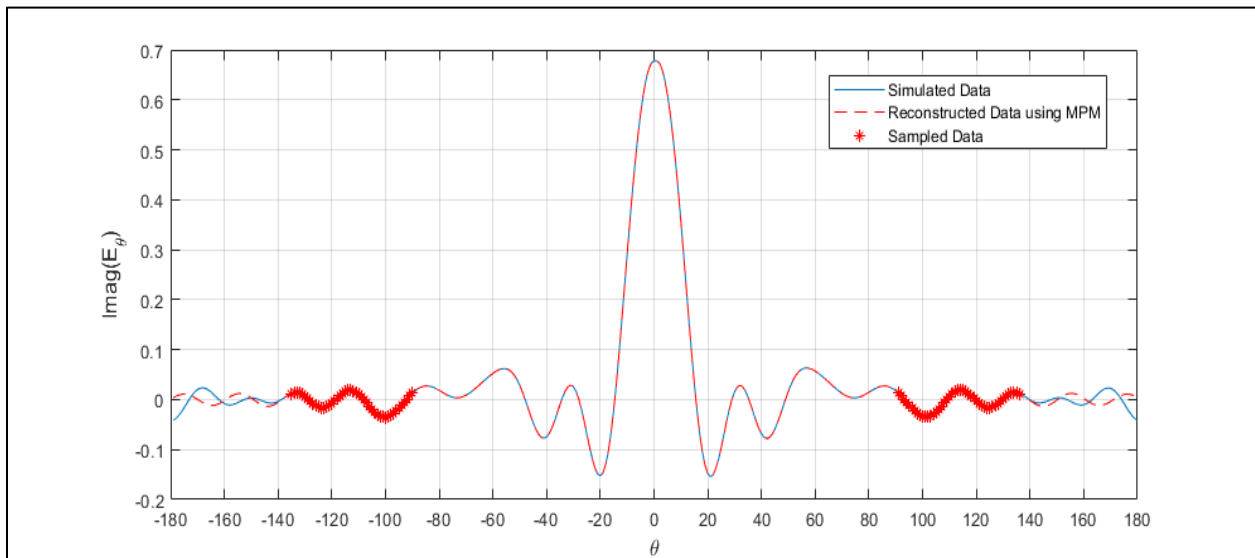


Figure 5.45. Extrapolation of the Imaginary part of E_θ at $\varphi = 0$ degrees

The MSE of the extrapolation of the real and imaginary parts of E_θ at $\varphi = 0$ degrees was calculated to be 0.0206 and 0.0694. While the error is higher using the Matrix Pencil method compared to the interpolation of the same fields using the Cauchy method, keep in mind that we

are only using 92 samples (46 samples for each half of the near-field versus 155 samples used in the Cauchy method) and we are extrapolating a larger range in theta (45 degrees on each side versus 25 with the Cauchy method).

Let us look at the extrapolation results for the real and imaginary parts of E_θ at $\varphi = 90$ degrees. The optimal number of singular values M was determined to be 6. Figure 5.46 and 5.47 show the resulting real and imaginary parts of the complex near-field of E_θ at $\varphi = 90$ degrees respectively.

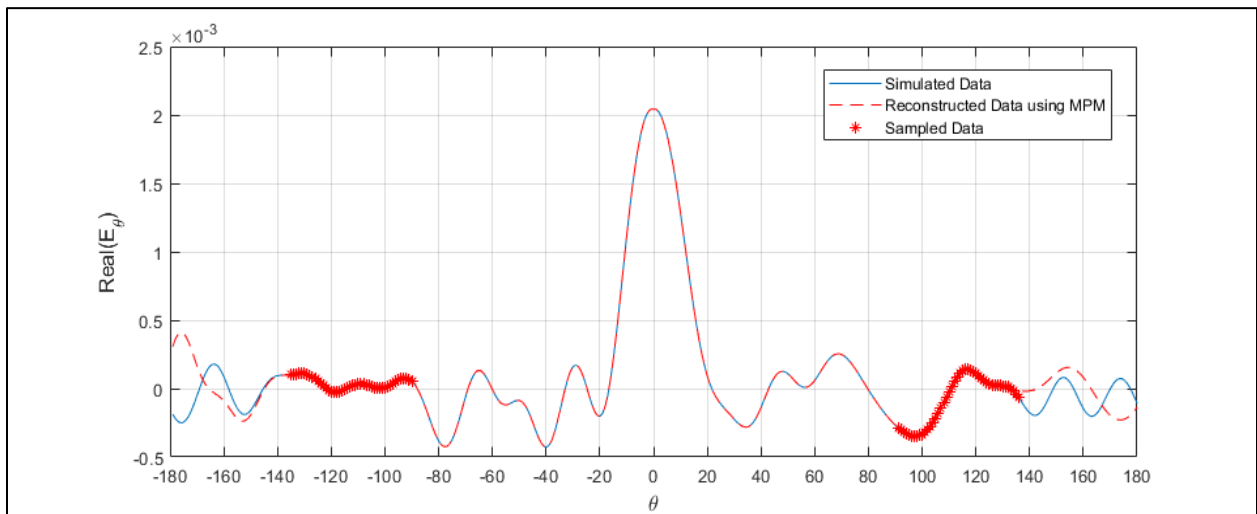


Figure 5.46. Extrapolation of the real part of E_θ at $\varphi = 90$ degrees

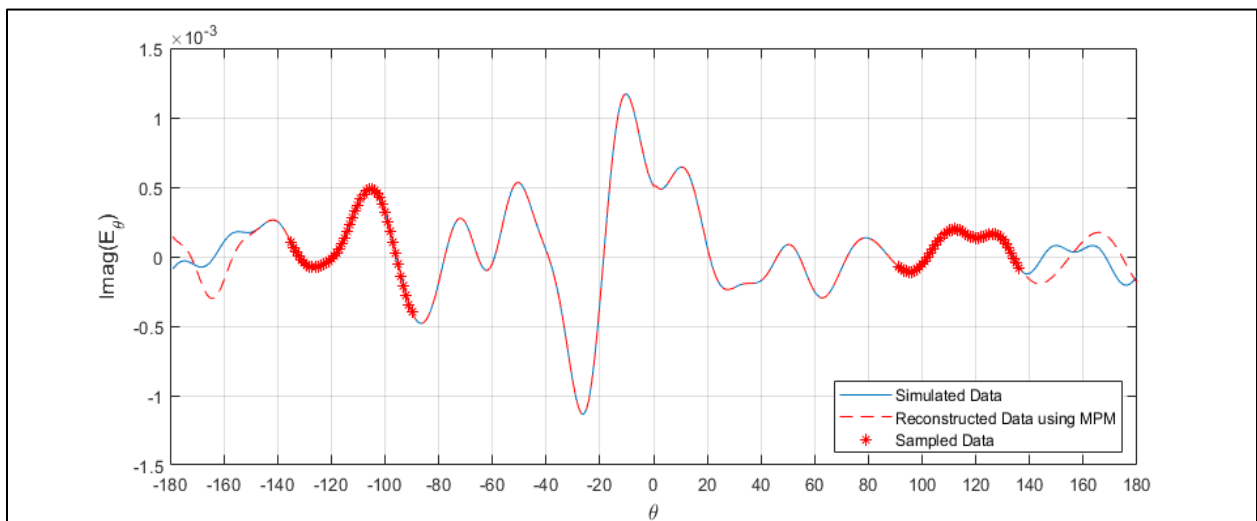


Figure 5.47. Extrapolation of the imaginary part of E_θ at $\varphi = 90$ degrees

The MSE's of the real and imaginary near-field approximations as a result of extrapolating the complex near-field were found to be 0.2378 and 0.2052 respectively.

Next, we will look at the extrapolation of the real and imaginary parts of E_φ at $\varphi = 0$ degrees. The optimal number of singular values M was determined to be 6. Figures 5.48 and 5.49 show the real and imaginary parts of E_φ at $\varphi = 0$ degrees as a result of the extrapolation of the complex near-field.

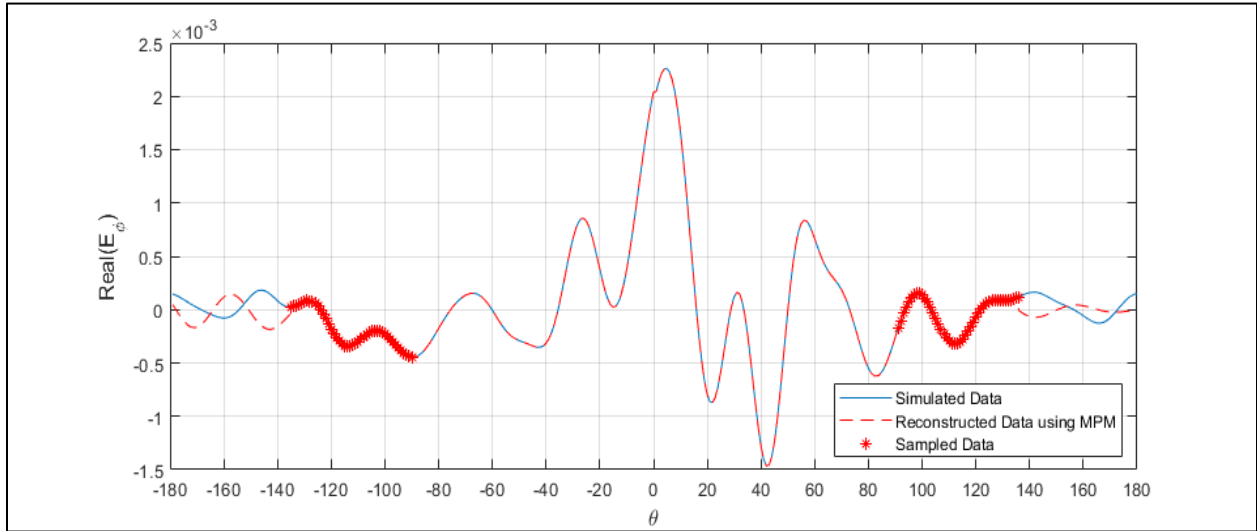


Figure 5.48. Extrapolation of the real part of E_φ at $\varphi = 0$ degrees

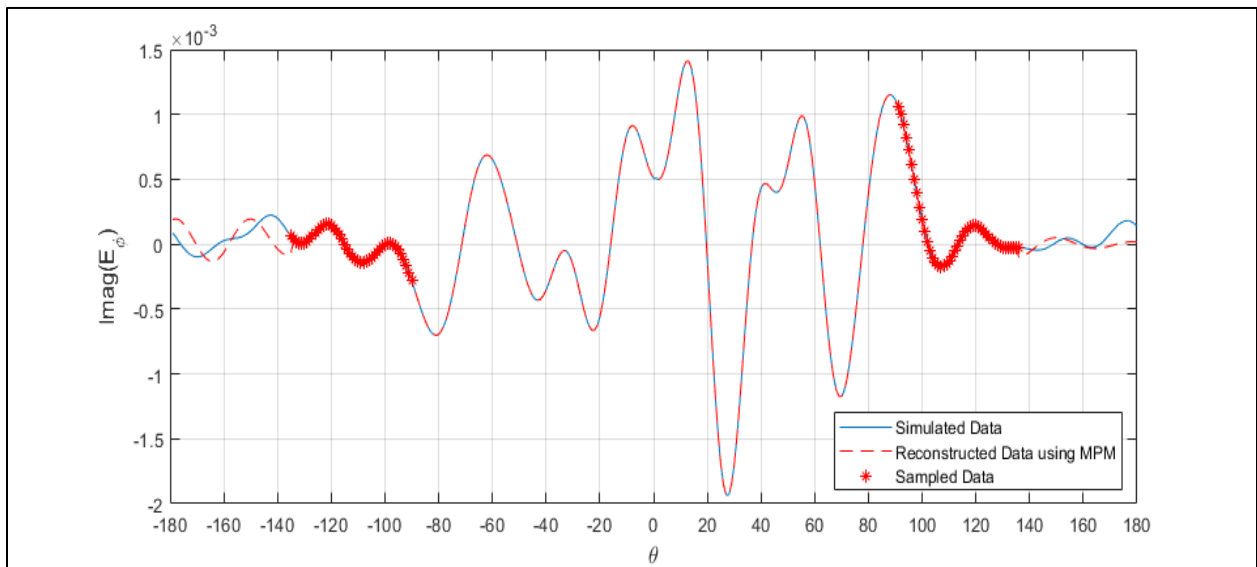


Figure 5.49. Extrapolation of the imaginary part of E_φ at $\varphi = 0$ degrees

The MSE's of the extrapolation of the real and imaginary part of E_φ at $\varphi = 0$ degrees were calculated to be 0.1474 and 0.0985 respectively.

For the final two plots, we will look at the real and imaginary parts of E_φ at $\varphi = 90$ degrees as a result of the extrapolation of the complex near-field. The optimal number of singular values M was determined to be 16. Figure 5.50 and 5.51 show the extrapolation results of the real and imaginary parts of E_φ at $\varphi = 90$ degrees.

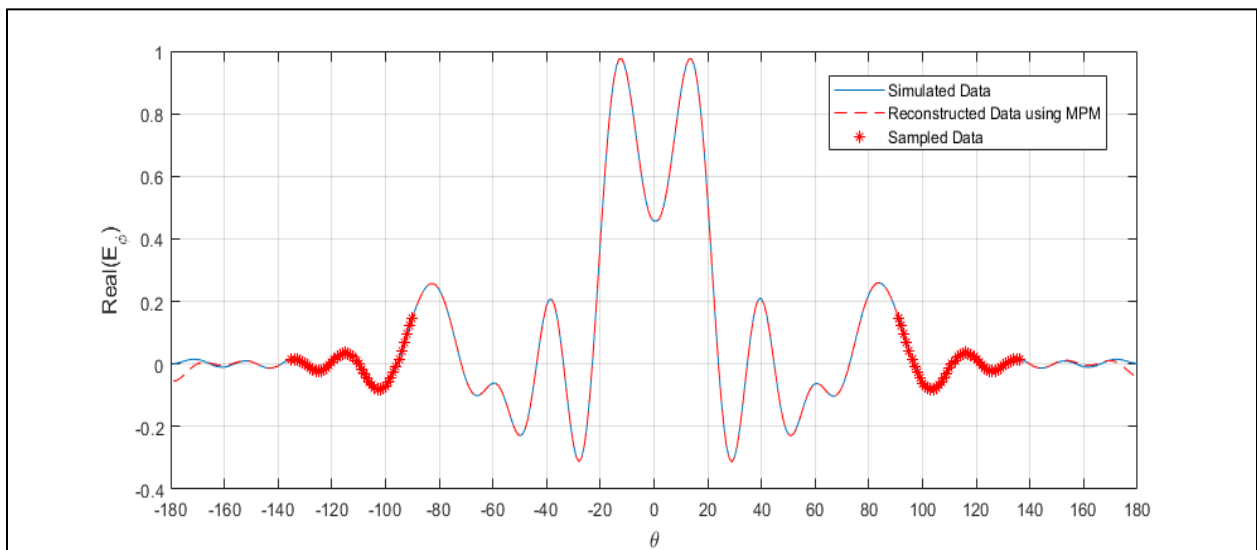


Figure 5.50. Extrapolation of the real part of E_φ at $\varphi = 90$ degrees

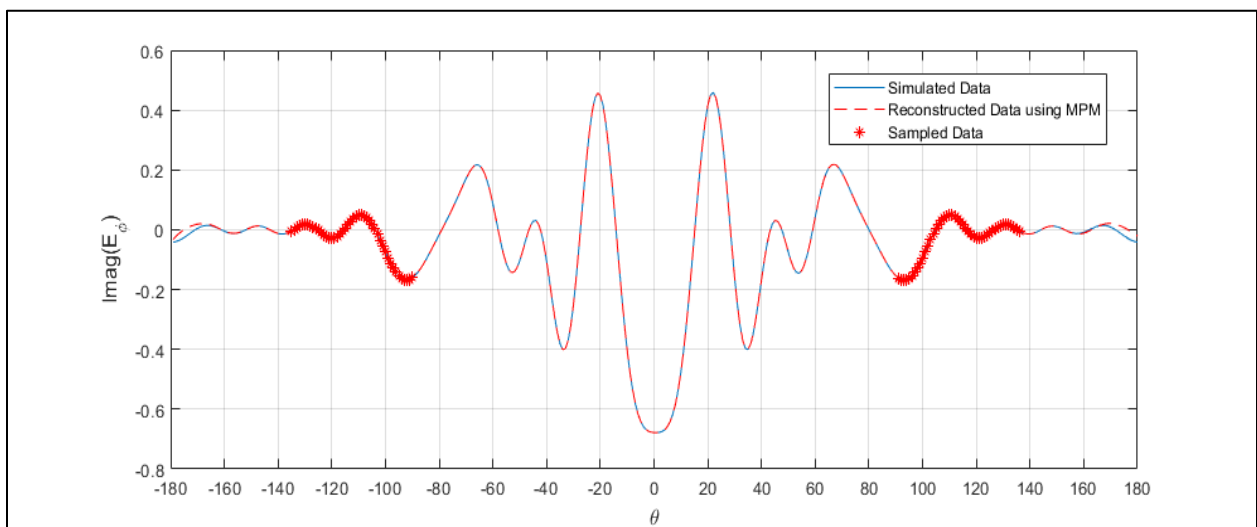


Figure 5.51. Extrapolation of the imaginary part of E_φ at $\varphi = 90$ degrees

The MSE's of the real and imaginary part as a result of the extrapolation of the complex near-field were calculated to be 0.0301 and 0.0268.

Once all of the near-field data was extrapolated, the data was then exported to perform a spherical near-field to far-field transformation. The larger errors seen in the extrapolation of E_θ at $\varphi = 90$ degrees and E_φ at $\varphi = 0$ degrees did not have a negative impact on the final far-field result, due to the fact that those fields were at smaller amplitudes. Figure 5.52 shows the result of the near-field to far-field transformation.

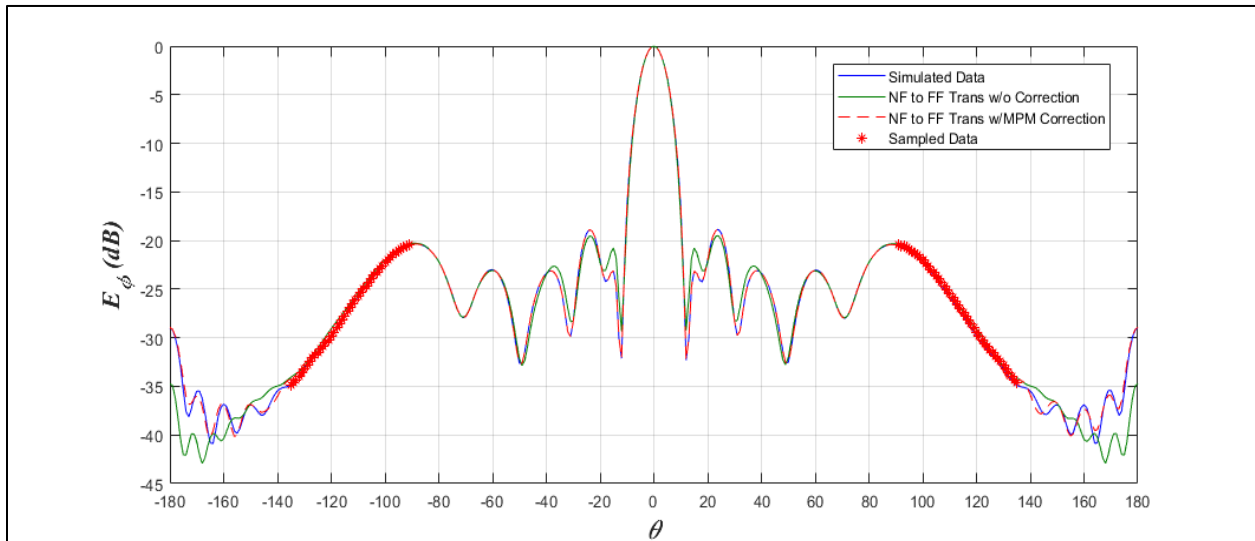


Figure 5.52. Comparison between the original far-field and extrapolated far-field

From figure 5.52, the solid blue line represents the simulated far-field, the dashed red line represents the result of transforming the extrapolated near-field to the far-field, and the red asterisks represent the sampled data. The solid green line shows the result of the near-field to far-field transformation if the hole of the near-field was replaced with zeroes and then transformed. It can be easily shown that extrapolating the missing data of the near-field using the Matrix Pencil method before the transformation is much more accurate than just replacing the unknown data with zeroes. The overall MSE of the far-field using the interpolated near-field data was

calculated to be 0.0104. If we were to replace the hole of missing near-field data with zeroes, then the MSE would increase to 0.0644.

While the Cauchy method had better accuracy interpolating the near-field and subsequently the far-field, the Matrix Pencil method was able to sufficiently extrapolate the near-field using less samples and it was also able to extrapolate over a larger range in theta.

5.2.4 Near-Field to Far-Field Transformation of a Rotated Parabolic Reflector

For the last example, we will be looking at the same rotated parabolic reflector antenna as was introduced in section 5.1.4. The rotated reflector antenna was simulated using FEKO and the near-field data was exported to MATLAB. The rotated case proved to be difficult to get accurate results unless the hole of missing data was reduced to 60 degrees (30 degrees on each side of the pattern), much like the zenith-directed case using the Cauchy method. So, the data was sampled from 90 degrees to +/-150 degrees ($N = 61$ samples) and extrapolated from +/-151 degrees to +/-180 degrees. Like in the previous section, we will be looking at the real and imaginary parts of E_θ and E_ϕ at the phi cuts of 0 degrees and 90 degrees.

First, we will look at the results of the extrapolation of E_θ at $\phi = 0$ degrees. Since the number of samples we are using for the input data matrix $[Y]$ is equal to 61, the pencil parameter L is equal to 29. From the singular value distribution along with error analysis, the optimal number of singular values M for the extrapolation of the complex near-field E_θ was determined to be 13. Using (4.17) through (4.23) we can estimate the poles and residues of the near-field. Figures 5.53 and 5.54 show the result of the extrapolation.

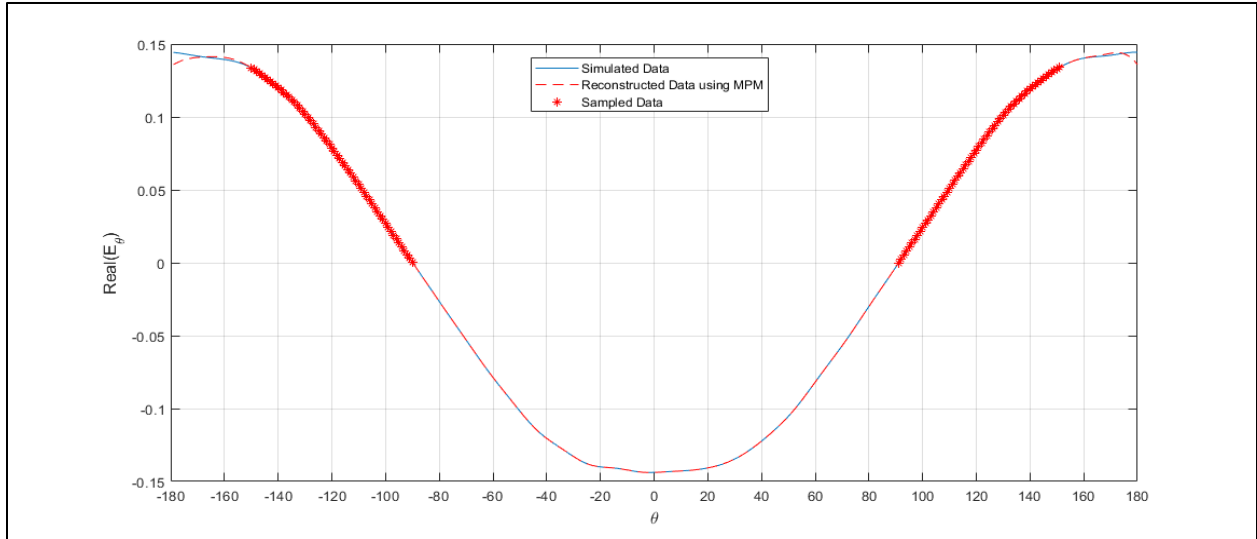


Figure 5.53. Extrapolation of the real part of E_θ at $\varphi = 0$ degrees

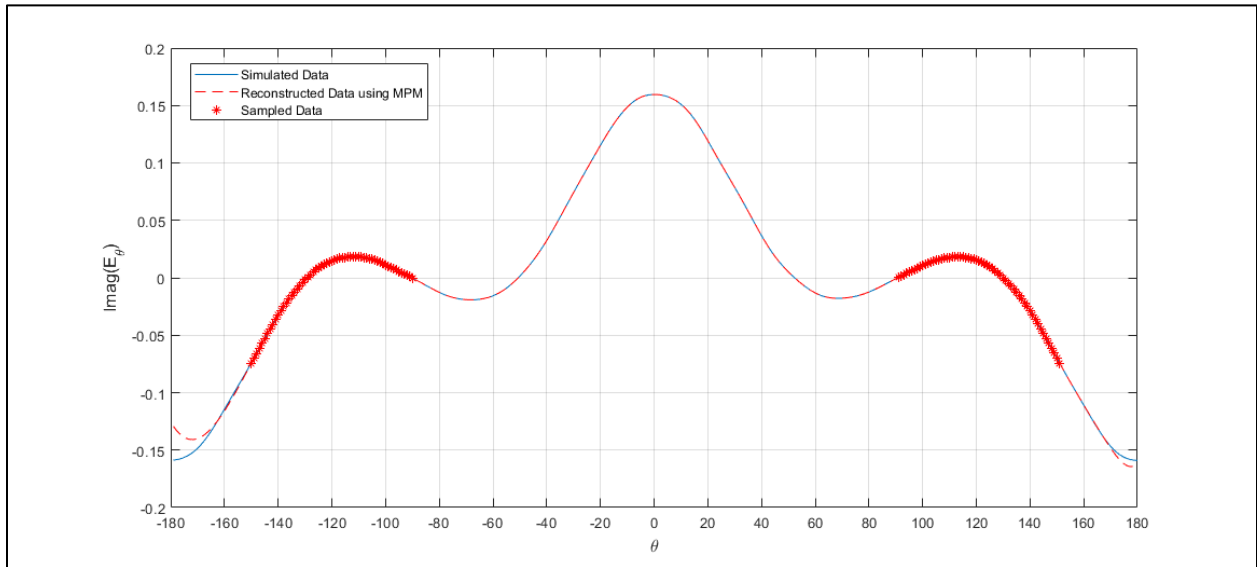


Figure 5.54. Extrapolation of the imaginary part of E_θ at $\varphi = 0$ degrees

The MSE of the extrapolation of the real part of E_θ was calculated to be 0.0097 and 0.0419 for the imaginary part.

Next, the extrapolation of the real and imaginary part of E_θ at $\varphi = 90$ degrees is presented. From the singular values distribution, the optimal number of singular values for the extrapolation

was determined to be 18. Figure 5.55 and 5.56 both show the result of the extrapolation of the real and imaginary parts of E_θ at $\varphi = 90$ degrees.

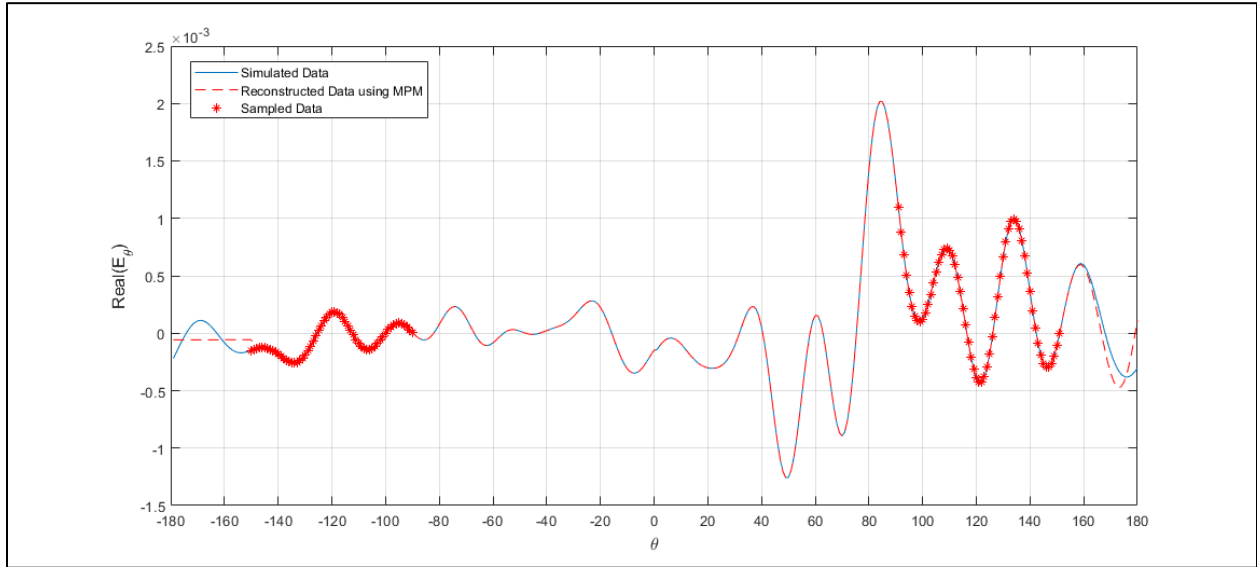


Figure 5.55. Extrapolation of the real part of E_θ at $\varphi = 90$ degrees

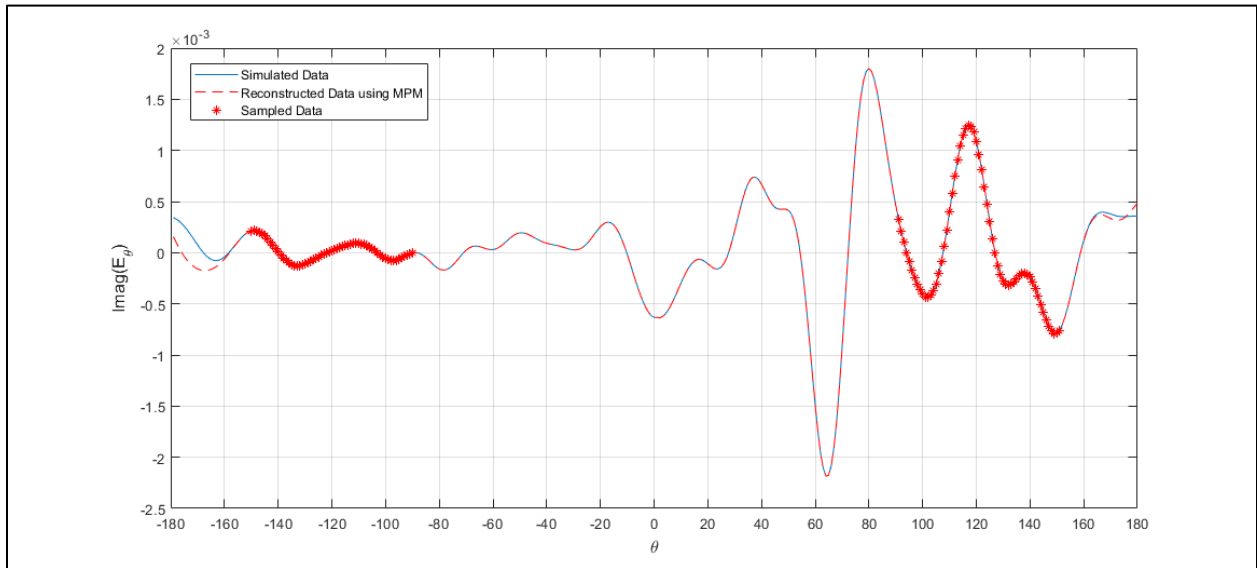


Figure 5.56. Extrapolation of the imaginary part of E_θ at $\varphi = 90$ degrees

The MSE for the extrapolation of the real and imaginary part of E_θ at 90 degrees was calculated to be 0.1070 and 0.0898 respectively. We are seeing higher error here most likely due to the

complexity of the near-field pattern. Notice that we are dealing with a highly un-symmetric pattern.

We will now move on the phi component of the near-field next at the phi cut of 0 degrees. The optimal number of singular values M was determined to be 11. Figures 5.57 and 5.58 show the resulting real and imaginary parts of E_φ from the extrapolation of the complex near-field.

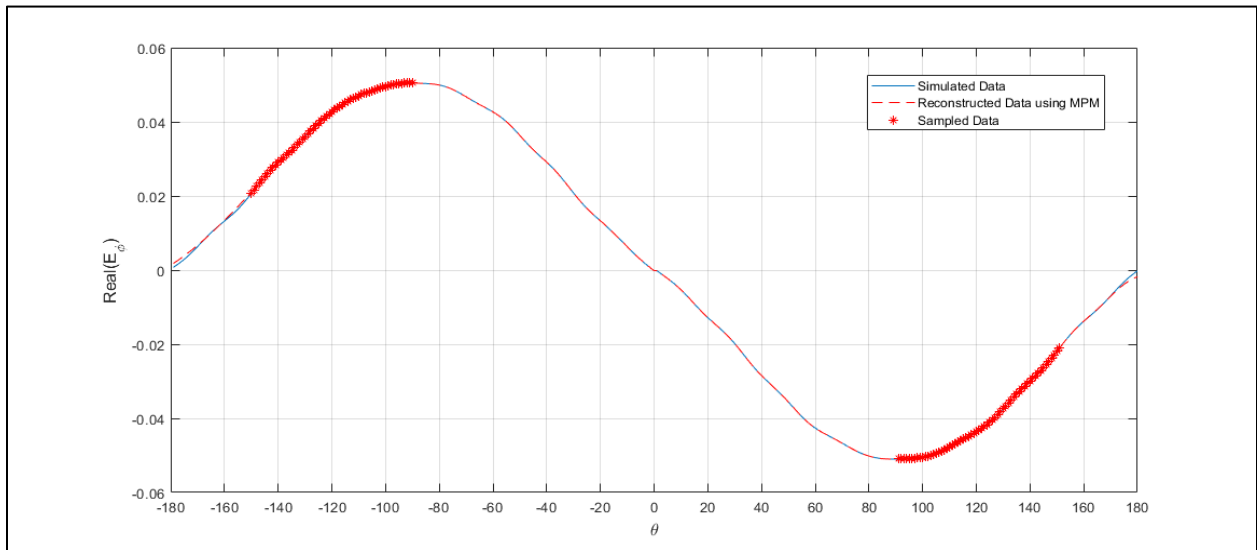


Figure 5.57. Extrapolation of the real part of E_φ at $\varphi = 0$ degrees

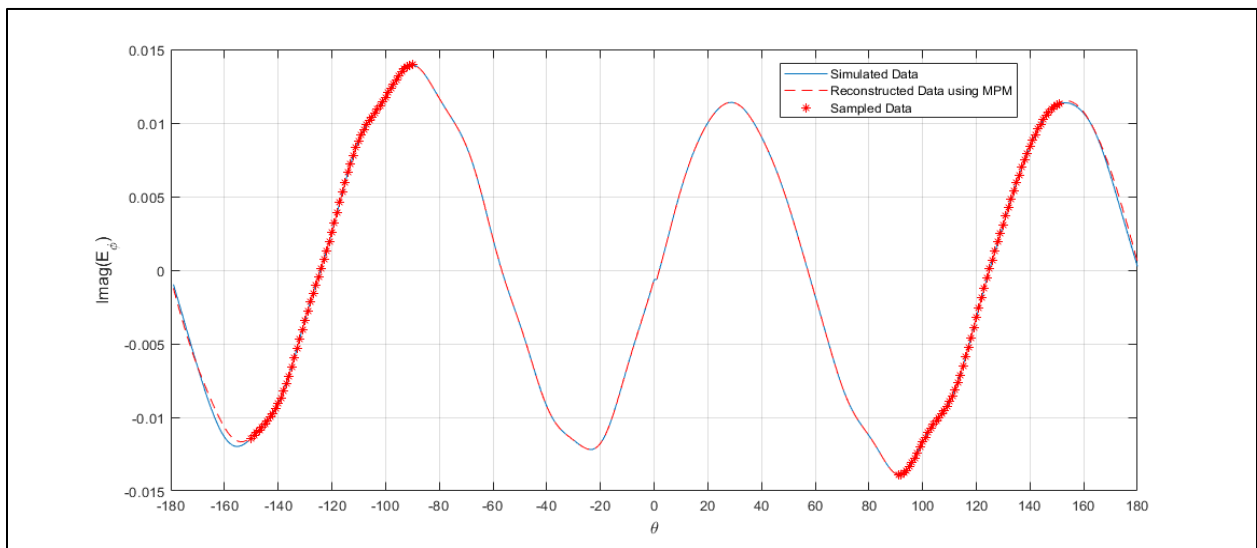


Figure 5.58. Extrapolation of the imaginary part of E_φ at $\varphi = 0$ degrees

The MSE of this extrapolation was calculated to be 0.0067 for the real part and 0.0167 for the imaginary part.

Finally, we will look at the result of the extrapolation for the real and imaginary parts of E_φ at $\varphi = 90$ degrees. The optimal number of singular values was determined to be 24. Figures 5.59 and 5.60 show the result of this extrapolation of the real and imaginary part of E_φ at $\varphi = 90$ degrees.

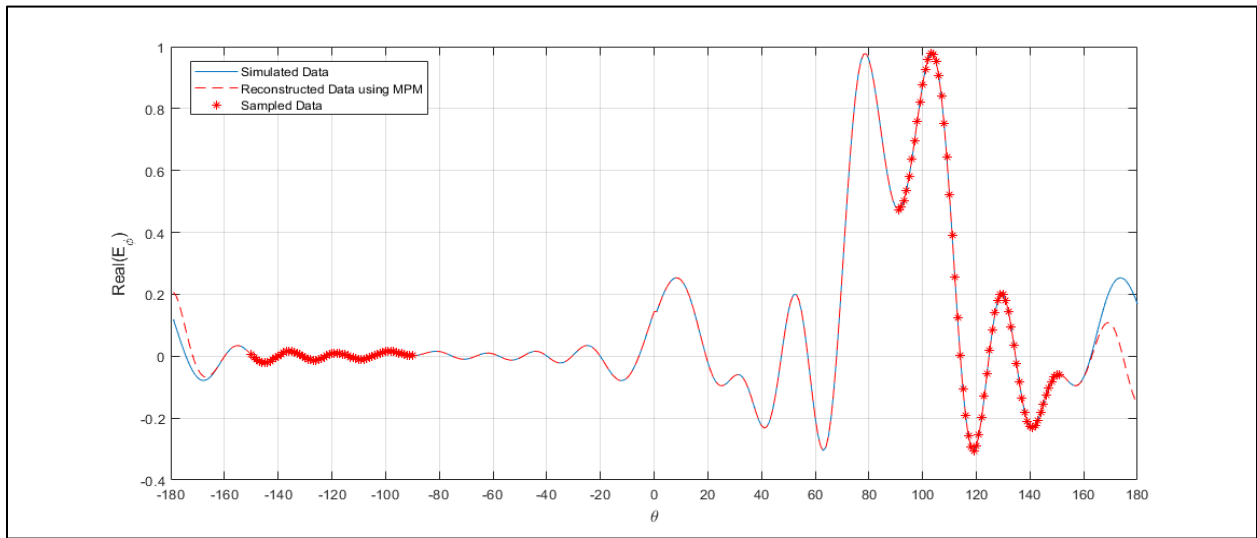


Figure 5.59. Extrapolation of the real part of E_φ at $\varphi = 90$ degrees

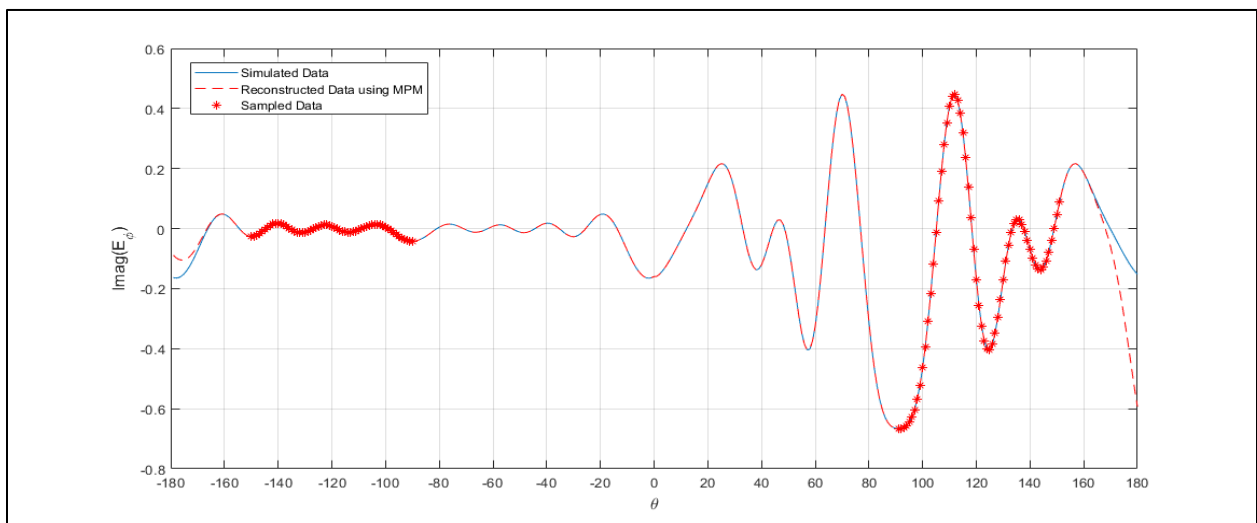


Figure 5.60. Extrapolation of the imaginary part of E_φ at $\varphi = 90$ degrees

The MSE of the extrapolation of the real and imaginary part of E_ϕ at $\phi = 90$ degrees was calculated to be 0.1719 and 0.2296 respectively.

Once all of the near-field patterns were extrapolated at each cut of phi, the data was exported and used in a spherical near-field to far-field transformation, just as in previous sections. Figure 5.61 shows the normalized far-field which resulted from the transformation of the extrapolated near-field patterns.

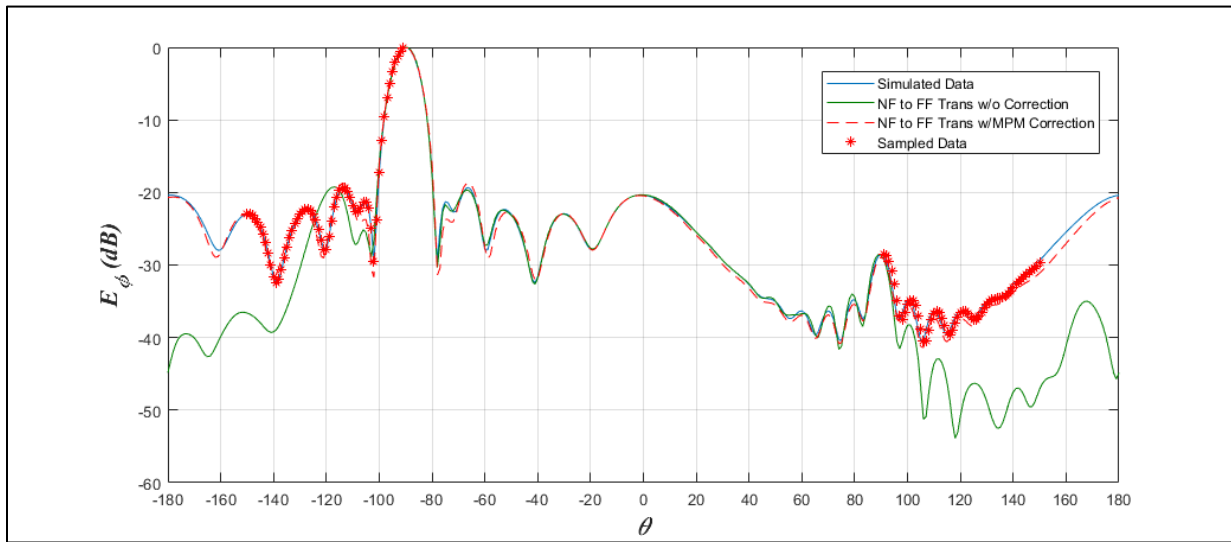


Figure 5.61. Comparison between original and extrapolated far-field

Once again, the solid blue line represents the simulated far-field, the dashed red line represents the far-field that resulted from the near-field to far-field transformation with the hole of missing data extrapolated, and the red asterisks represent the sampled data points. The solid green line is the far-field result if instead of extrapolating the missing data, zeroes were inserted. The MSE between the far-field that resulted from the near-field to far-field transformation with the missing data extrapolated and the simulated far-field was calculated to be 0.0345. The MSE between the transformed far-field without the Matrix Pencil method correction and the simulated far-field was calculated to be 0.3197.

While the extrapolation of the near-field of the rotated parabolic reflector antenna using the Matrix Pencil method was not as accurate as the interpolation of the same near-fields using the Cauchy method, the end result after the near-field to far-field transformation is sufficient. The Matrix Pencil method also could not properly extrapolate the near-field when the gap of missing data was increased to 90 degrees, for which the Cauchy method performed very well. However, the accuracy of the extrapolation and resulting far-field is much better than that of the far-field without the near-fields extrapolated.

CHAPTER 6

CONCLUSION AND FUTURE RESEARCH

6. Conclusion and Future Research

6.1 Conclusion

In modern computational electromagnetics, the problems, solutions, and therefore the computations tend to be very large, consuming a lot of time and computational power. Two different methods of interpolation and extrapolation were explored in this thesis. By estimating parameters of interest using sparsely sampled data, we are able to reduce the computational time and power.

The Cauchy method assumes that the parameter of interest (i.e., system transfer function, radiation pattern, etc.) can be approximated by a ratio of two polynomials. A QR decomposition is used to pre-process the data as it has better noise handling capability and computational stability. A singular value decomposition implementation of the method of total least squares is employed to solve for the coefficients of the polynomial. Once the coefficients of the polynomials are evaluated, the parameter of interest can be interpolated or extrapolated. This thesis explored the application of the Cauchy method on antenna near-field and far-field patterns. It was shown that the Cauchy method is more accurate when the problem is one of interpolation instead of extrapolation. The Cauchy method was able to successfully interpolate the far-field patterns of a single dipole antenna as well as a 10x10 linear dipole antenna array which had a much more complex pattern. We were also able to show that the Cauchy method could accurately interpolate a measurement gap that commonly occurs in real world near-field data. Using a simulated parabolic reflector antenna, it was shown that the measurement gap could span up to 50 degrees in theta when the reflector was directed towards zenith and up to 90 degrees in theta when the reflector was rotated 90 degrees counter-clockwise from zenith. Using a near-

field to far-field transformation, we were able to prove that the Cauchy method could interpolate all 720 segments of near-field data, resulting in an accurate far-field after transformation.

The Matrix pencil method is a model-based parameter estimation technique that approximates the residues and poles of an electromagnetic signal response using a sum of complex exponentials. Unlike the Cauchy method, the Matrix Pencil method excelled in approximation by the way of extrapolation. The same antenna far-field and near-field patterns that were interpolated by the Cauchy method were extrapolated by the Matrix Pencil method. It was shown that the Matrix Pencil method could not accurately extrapolate a larger gap of missing data than the Cauchy method when it came to the single dipole and 10x10 dipole array. However, we were able to accurately extrapolate a 90 degree span of near-field data for the zenith-directed reflector antenna while the Cauchy method could only accurately interpolate 50 degrees. When it came to the rotated reflector antenna, the Matrix Pencil method could only extrapolate 60 degrees of near-field data while the Cauchy method could interpolate 90 degrees.

6.2 Future Research

While both the Cauchy method and Matrix Pencil method were able to accurately interpolate or extrapolate missing antenna data, they both were very sensitive to what the sampled data was. Because of this, neither method is very versatile when it comes to estimating antenna radiation data such as far-field and near-field patterns. We are currently looking at modifying the Cauchy method so that the ratio of polynomials are replaced by a ratio of Legendre polynomials. Some initial work that has been done is showing promise in accurately interpolating a parabolic reflector antenna in several spatial configurations (i.e. zenith, rotated 45

degrees, rotated 60 degrees, rotated 90 degrees, etc.) with the measurement gap spanning 90 degrees for all configurations.

Another area of future research is determining why the Cauchy method sometimes had several solutions depending on the choice of the number of singular values and why there was not always one unique solution. The rule of selecting the number of singular values based on the number of accurate significant digits of the sampled data did not always lead to the best solution.

Finally, applying these methods to different types of antennas is another area of research to explore. Not only would it be interesting to look at simulated antennas but also actual physical antennas that were measured in the real-world.

References

- [1] T. K. Sarkar, P. Petre, A. Taaghola, and R. F. Harrington, "An Alternative Spherical near Field to Far Field Transformation," *Progress In Electromagnetics Research*, vol. 16, pp. 269–284, 1997.
- [2] G. Strang, *Introduction to linear algebra*, vol. 4. Wellesley, MA: Wellesley - Cambridge Press, 2016.
- [3] H. P. Gavin, "Total Least Squares," in *CEE 629. System Information*.
- [4] A. L. Cauchy, "Sur la formule de Lagrange relative a l'interpolation", *Analyse Algebrique*, Paris, 1821
- [5] K. Kottapalli, T. K. Sarkar, Y. Hua, E. Miller, and G. Burke, "Accurate computation of wide-band response of electromagnetic systems utilizing narrow-band information," *IEEE Transactions on Microwave Theory and Techniques*, vol. 39, no. 4, pp. 682–687, Apr. 1991.
- [6] R. S. Adve and T. K. Sarkar, "Generation of accurate broadband information from narrowband data using the Cauchy method," *Microw. Optical Technol. Lett.*, vol. 6, no. 10, pp. 569–573, Aug. 1993.
- [7] R. S. Adve and T. K. Sarkar, "The effect of noise in the data on the Cauchy method," *Microw. Optical Technol. Lett.*, vol. 7, no. 5, pp. 242–247, Apr. 1994.
- [8] R. S. Adve, T. K. Sarkar, S. Rao, E. Miller, and D. Pflug, "Application of the Cauchy method for extrapolating/interpolating narrowband system responses," *IEEE Transactions on Microwave Theory and Techniques*, vol. 45, no. 5, pp. 837–845, May 1997.
- [9] J. Yang and T. K. Sarkar, "Interpolation/Extrapolation of Radar Cross-Section (RCS) Data in the Frequency Domain Using the Cauchy Method," *IEEE Transactions on Antennas and Propagation*, vol. 55, no. 10, pp. 2844–2851, Oct. 2007.
- [10] A. V. Oppenheim and R. W. Schaffer, *Discrete-time signal processing*, 3rd ed. Upper Saddle River, NJ: Pearson, 2010.
- [11] D. S. Watkins, *Fundamentals of matrix computation*, 3rd ed. Hoboken, NJ: Wiley, 2010
- [12] T. K. Sarkar, M. C. Wicks, M. Salazar-Palma, and R. J. Bonneau, *Smart antennas*. New York: Wiley-Interscience, 2003.
- [13] Y. Hua and T. K. Sarkar, "Generalized pencil-of-function method for extracting poles of an EM system from its transient response," *IEEE Transactions on Antennas and Propagation*, vol. 37, no. 2, pp. 229–234, Feb. 1989.

- [14] Y. Hua and T. K. Sarkar, "Matrix pencil method for estimating parameters of exponentially damped/undamped sinusoids in noise," *IEEE Transactions on Acoustics, Speech, and Signal Processing*, vol. 38, no. 5, pp. 814–824, May 1990.
- [15] Y. Hua and T. K. Sarkar, "On SVD for estimating generalized eigenvalues of singular matrix pencil in noise," *IEEE Trans. Signal Process.*, vol. 39, no. 4, pp. 892–900, Apr. 1991.
- [16] T. K. Sarkar and O. M. Pereira, "Using the matrix pencil method to estimate the parameters of a sum of complex exponentials," *IEEE Antennas and Propagation Magazine*, vol. 37, no. 1, pp. 48–55, Feb. 1995.
- [17] R. S. Adve, T. K. Sarkar, O. M. Pereira-Filho, and S. M. Rao, "Extrapolation of time-domain responses from three-dimensional conducting objects utilizing the matrix pencil technique," *IEEE Transactions on Antennas and Propagation*, vol. 45, no. 1, pp. 147–156, Jan. 1997.
- [18] Y. Zhang, T. K. Sarkar, X. Zhao, D. Garcia-Donoro, W. Zhao, M. Salazar-Palma, and S. Ting, *Higher Order Basis Based Integral Equation Solver (HOBBIES)*. Hoboken, NJ: John Wiley & Sons Inc., 2012.

NICOLAS REGINELLI

369 Genesee Street • Oneida, NY 13421 • (315) 941-3306 • nfr3725@rit.edu

EDUCATION

Syracuse University

M.S. in Electrical Engineering, GPA: 3.59/4.0

Syracuse, NY
Expected August 2018

- M.S. Thesis: Interpolating and Extrapolating Missing Antenna Measurement Datasets Using the Cauchy and Matrix Pencil Method
- Relevant Coursework: Electromagnetics, Antenna Design, Computational Electromagnetics, Microwave Filter Design, Digital Signal Processing, Digital Communications
- Awards: Anaren Gerst-Hair Graduate Fellowship recipient

Rochester Institute of Technology

B.S. in Electrical Engineering, GPA: 3.42/4.0

Rochester, NY
August 2015

- Concentration in Electromagnetics
- Relevant coursework: Microwave Circuit Theory, Antenna Theory, Electromagnetics, Optics, Signal Processing, Communication Systems, Control Systems

EXPERIENCE

Syracuse University

Research Assistant, Computational Electromagnetics Lab

Syracuse, NY
August 2017 – Present

- Conducted research on methods of interpolation and extrapolation applied to missing datasets of electromagnetic systems such as microwave filters, radar cross-sections, and near-field and far-field radiation patterns of various antennas.
- Publication accepted into the IEEE IMS 2018 conference: "*Interpolation and Extrapolation of S-Parameter Data of Microwave Filters in the Frequency Domain Using the Cauchy Method*".
- Publication accepted into the EuMW 2018 conference: "*Interpolation of Missing Antenna Measurements or RCS Data Using the Matrix Pencil Method*"

Anaren

RF Engineering Co-op

Syracuse, NY
May 2017 – August 2017

- Designed several microstrip bandpass filters
- Carried out testing on a beamforming network to be used in satellite communication applications.
 - Testing included collecting s-parameter data, intermodulation, gain compression, AM/PM, EMC, noise figure, harmonics, spurious signals and beam-hopping. Testing was also conducted over several temperatures.
 - Created several Excel spreadsheets using VBA that reduced thousands of data points and organized the data into plots and tables.
 - Characterized coaxial connectors used in the testing of the beamformer to remove the loss and phase from the data.
 - Created PowerPoint presentations for the customer that included test descriptions and results.

Anaren

Electrical Engineer I

Syracuse, NY
December 2015 – August 2016

- Aided in the testing of a Variable Attenuation and Phase module to be used in a beamforming network.
 - Prepared the Source Control Drawing used in the manufacturing and testing of the VAP module.
 - Wrote test procedures and created test setup diagrams.
 - Designed several test harnesses.
 - Procured the test equipment required and setup test bench area.
 - Carried out testing of the VAP including s-parameters, intermodulation, gain compression, AM/PM, harmonics, and spurious signals over several temperatures.
 - Created Excel spreadsheets using VBA that reduced the data into plots and tables.
 - Created PowerPoints presentations that summarized the results of the testing that would be sent to the customer for review.
- Investigated the electrical qualities and durability of several off-the-shelf RF chip resistors and bonding materials.
 - Collected s-parameter data to compare the microwave performance of the different resistors.
 - Completed several environmental tests such as pulsed power testing, temperature testing and vibration testing to determine the durability of each resistor and bonding material.
 - Compiled the results into Excel and PowerPoint which were shared with the customer.

SKILLS

- Software: MATLAB, LabView, C, Python, FORTRAN, Ansys HFSS, Ansys Designer, ADS, Genesys, Sonnet
- Hardware: Network Analyzer, Signal Analyzer, RF Signal Generator, Oscilloscope, Power Meter